International School for Advanced Studies
(SISSA)

PhD Thesis:

Exploring Hund's correlated metals: charge instabilities and effect of selective interactions

Candidate: **Maja Berovic**
Supervisor: Massimo Capone

Trieste
October, 2018

To my family

Contents

1 Introduction

One of the greatest scientific adventures of the last decades has been the search for an understanding of high-temperature superconductivity. This fight is nowadays strongly entangled with the field of strongly correlated electron systems. This thesis finds its place in this framework and, despite we will not address directly the physics of superconductors, it is motivated by the properties of these materials, and in particular by the iron-based family.

Though it has been more than thirty years since the great discovery of high-temperature superconductors in copper-oxides [1–3], even nowadays we are lacking a generally recognized understanding of this phenomenon and a recipe to increase the critical temperature. The discovery of high-temperature superconductivity in iron-based compounds [4] about a decade ago stimulated the search for common features between these two different families, iron- and copper-based compounds, in order to get some general picture of the possible mechanism for superconducting pairing in these systems.

At first glance a similarity between the doping-temperature phase diagram of iron-based parent compounds and the celebrated one for the cuprates is evident, as reported in Fig. 1.1. The striking point is a long range antiferromagnetic ordering arising in proximity of the superconducting (SC) state. At least in the perspective of this thesis, the main difference is that the magnetic state of the the cuprates is a Mott insulator, while the parent compounds of the iron-based superconductors are metallic despite the spin-density wave ordering. Moreover, it is believed that the superconductivity appears in the neighborhood of other competing phases, once these phases are suppressed. Typically doping or pressure drives the system out of this low-T regime of the parent compounds, suppressing the present magnetism, and leading the system to the superconductive phase [5]. Furthermore, both families consist of the layers composed by the transition-metal atom (Fe and Cu, respectively), with ligand atoms alternating in the neighboring layers.

Indeed, in the last years Fe-based superconductors (FeSC) were sintetized in different shapes, structure and composition. Nonetheless, they all share a couple of common robust characteristics: an atomic layers with Fe in square lattice, and a pnictogen (P/As) or a chalcogen (S/Se/Te) [1] positioned above or below the center of each square of iron ions, forming this way the interlayers between the Fe planes, as shown in Fig. 1.2 (a). The formed structure has tetragonal symmetry,

[1] This is were the popular names for these compounds "pnictides" and "chalcogenides" come from.

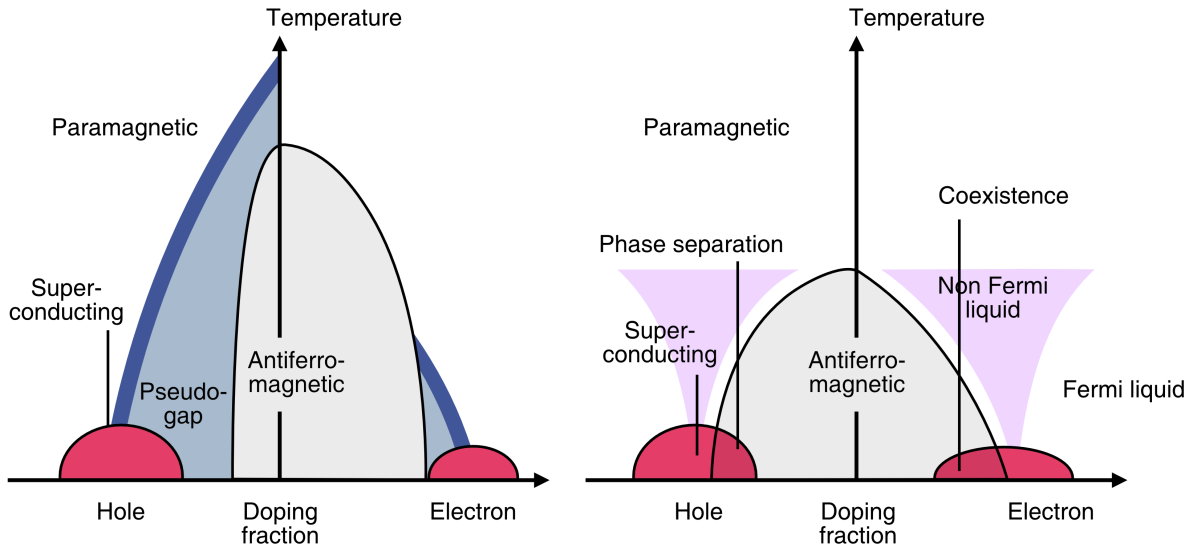

Figure 1.1: Schematic phase diagrams of copper- and 122 family of iron-based high-temperature superconductors [6]: both electron doping and hole doping suppress the magnetism of the parent compounds and induce superconductivity under the characteristic superconducting dome. The blue lines between the paramagnetic and pseudogap phases (blue shading) in the copper-based case represent crossover transitions, black lines between paramagnetic and antiferromagnetic phases are well-defined transitions. The non Fermi liquid behavior (purple shade) is present for the same doping where one observes the superconducing phase, for larger values of temperature.

which undergoes a structural transition in some parts of the phase diagram [7].

However, the major difference between the two families of superconductors is evident already at the level of electronic structure. Though in both of the families the major role is played by transition-metal atom, with bands arising from $3d$-orbitals crossing the Fermi level and dictating the physical properties of the system, the different number of electrons in the d-shell and the different crystal-field splitting lead to two different pictures. In the cuprates, only one band (arising from $d_{x^2-y^2}$ orbital) crosses the Fermi level, leading to theoretical descriptions based on the single-band Hubbard model or related models. On another hand, in FeSC the crystal-field splitting is typically quite small with respect to the other energy scales, meaning that in such case almost all five d-orbitals have to be taken into consideration while constructing the effective model. At the very least, a three-orbital modeling for the so-called t_{2g} orbitals is necessary to reasonably account for the electronic structure of these compounds, but for some phenomena it is necessary to consider the whole five-fold manifold. In principle, this could provide a very basic argument for the metallic character of the undoped FeSC, since Mott localization is much harder to get in multi-orbital systems due to the higher number of kinetic energy channels. In the rest of the thesis we will discuss these arguments, showing that the picture is quite more complicated, rich and interesting. Nonetheless, correlation effects have been observed in all the various families of FeSC (in increasing order): 1111 pnictides (such as LaFeAsO), 122 (such as $BaFe_2As_2$), 111 (such as LiFeAs) and, at the more strongly correlated end [8], the 11 chalcogenides (FeSe, FeTe). We will not list the numerous experimental evidences, but let us show, as depicted in Fig. 1.2 (b), the DFT+DMFT results for the mass enhancement m^*/m as a measure of the correlations of the system of the iron $3d$-orbitals in the paramagnetic state, together with the results obtained from optical spectroscopy experiments and (angle-resolved) photoemission spectroscopy experiments [9]. It is still under debate, however, whether this different degree of correlations arises due to the structural difference [9] or an increase of the interactions [10–12].

The importance of the multi-orbital nature of FeSC in determining the strength and the nature of correlations in FeSC is stressed in countless theoretical studies [11, 13–16]. Accounting for the presence of more than one relevant orbital, one needs to take into consideration also the effect of the inter-orbital interactions which are richer than the pure Hubbard repulsion. In particular, one has to deal with the Hund's exchange coupling, which favors high spin configurations. In the presence of the Hund's coupling, the effective interaction that electron "feels" depends on the orbital character of d-orbitals and spin alignment (which are in accordance with the Hund's rules in an isolated atoms) [16]. This energy scale is sizable in atomic Fe [17] and it leads to the remarkable effects which represent both the motivation and the topic of the present thesis. Intuitively, one expects that the Hund's rule coupling enhances the electron-electron correlation effects, owing to the suppression of atomic configurations that do not maximize the local magnetic moment. We will see that the interplay between Mott localization and the Hund's coupling is however more involved than this simple expectation.

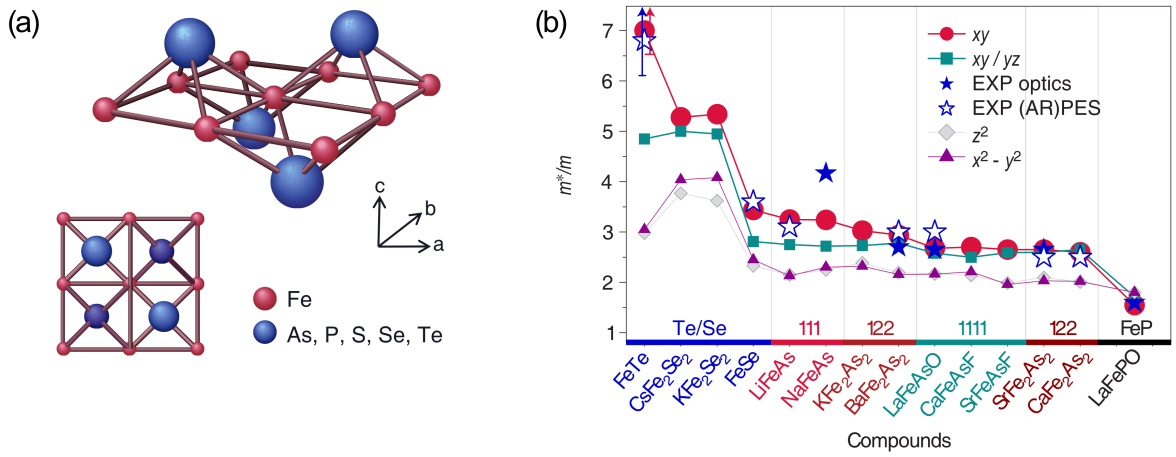

Figure 1.2: (a) Structural motif of the FeSC. Inset: Top view of the FeX trilayer, where X=As,P,S,Se,Te. The triad (a, b, and c) demonstrates the three crystallographic directions. (b) The DFT+DMFT-calculated mass enhancement m^*/m of the iron $3d$-orbitals in the paramagnetic state and the low-energy effective mass enhancement obtained from optical spectroscopy experiments and (angle-resolved) photoemission spectroscopy experiments [9].

Many direct consequences of this physics have been identified. The main concept arising from these studies has been the 'Hund's metal', a metallic phase displaying strong correlations and resisting to the Mott localization up to very large values of the interaction. It is important to stress that this phenomenology has been found for integer fillings different from half-filling (for example two electrons in three orbitals), including the case of six electrons in five orbitals which is a characteristic of undoped iron-based superconductors. In this regime one finds a particular sensitivity of the observables to the strength of the Hund's coupling J, an anomalous magnetic response [18] connected to a finite-temperature spin-freezing [19], an effective decoupling between the orbitals [14, 17, 20] and other anomalies that we will address in this thesis. In recent works [17, 21], the crossover between a regular metal and the Hund's metal has been connected to the Mott transition for the half-filled system [11, 12, 14, 22, 23], identifying a density-dependent crossover which seems to host the main anomalies we have listed above, plus an enhancement or even a divergence of the charge compressibility [21].

One of the most important observations is the relation between the Hund's coupling and

the so-called orbital selectivity, namely the realization of different physics for electrons with different orbital index. As we mentioned above, one of the effects of the Hund's coupling is to favor an effective low-energy decoupling between the different orbitals, measured by vanishing inter-orbital charge correlations. Once the orbitals are decoupled, even small differences in the bandstructure parameters are strongly emphasized when correlations are increased. This gives rise to orbital-selective physics, which is realized by the combination of electronic-structure effects (which split the degeneracy) and a sizable Hund's coupling. This can lead either to an orbital-selective Mott transition, where some orbitals are Mott localized and others are not [24], but also to a strong differentiation in the effective masses within the same metallic state [14, 25], found in earlier studies [9, 10, 27].

In this thesis we tackle some important questions raised by the above mentioned studies and in general by the physics of iron-based superconductors and other materials with an important effect of the Hund's coupling. We will focus on the origin of the interaction-resilient Hund's metal and present a new picture of the stabilization of this phase, which connects the Hund's metal with charge-disproportionation instabilities.

After introductory sections, where we will introduce the physics of strong correlations with a particular emphasis on the effect of multi-orbital character and the Hund's coupling, we will present the theoretical approach which we used in our original investigations, the Gutzwiller approximation.

The new results of this thesis will be presented in Chapters 5, 6 and 7. In Chapter 5 we will revisit the phase diagram of a three-orbital Kanamori model by drawing its phase diagram in the full U-J plane, considering even regimes which are usually discarded. In this way we will show that the Hund's metal state can be seen as a sort of superposition between two strongly correlated insulators: a high-spin Mott insulator and a disproportionated Hund insulator where the spatial charge distribution is not homogeneous. The mixed-valence nature of the metallic state can survive up to the large values of U and J if those are such to make the two insulating solutions degenerate (or nearly degenerate). The picture is confirmed by comparing it with the global half-filling case, where no Hund's metal can be found, and the case where the Hund's coupling is negative, which can be realized if a Jahn-Teller electron-phonon coupling exceeds the Coulomb exchange integral. Also in this case we find a correlation-resilient metal when disproportionated insulating solutions are degenerate with the Mott insulator and a more standard Mott transition when there is only one insulating solution which is simultaneously stabilized by U and J.

In Chapter 6 we discuss the effect of non-uniform Coulomb interactions on the physics of strong correlations, a topic which is directly connected with the possible orbital selectivity and it is motivated by realistic calculations of interaction parameters, which are typically not symmetric.

In Chapter 7 we study the charge compressibility of multi-orbital models with full orbital-rotation invariance, comparing Ising and Kanamori interactions and different values of the orbital degeneracy. In all cases we find a phase separation instability for interactions slightly larger than the critical U for the Mott transition in the half-filled system. The phase separation boundary extends in doping and U in different ways, according to the number of orbitals and the interaction form. While the precise results seem to be strongly dependent on the "details" of the model, an enhancement of the compressibility appears as a generic feature, which can be connected with many aspects of the phase diagram of the iron-based superconductors and other materials.

2 Strong electronic correlations

2.1 The band theory of solids

Band theory was the first theory that had a huge success in explaining the electronic properties of solids (electronic conductivity, optical response etc.). It was able to predict, by simple means, whether a system was expected to be metallic or insulating [28]. Consequently, this theory was considered some sort of "standard model" of the solid state.

The band theory of solids is based indeed on a rather strong approximation, namely assuming that the electrons behave as non-interacting. This means that adding or extracting one electron from the system will not leave any consequences on any other electron, since they, electrons, do not 'feel' the mutual presence. From a mathematical point of view, the band theory assumes that the Coulomb interaction between electrons can be approximated by an effective single-particle potential which adds to the interaction with the lattice. This approximation may appear rude because the energy scales associated with the Coulomb repulsion are quite large and they can not be neglected. Nevertheless, the band theory turned out to be valid in many solid systems since a large number of compounds have the screened Coulomb interaction. The rationale for this success is that the electronic properties are mainly controlled by the valence electrons whose interaction is screened by core electrons leading to a weaker effective interaction. The connection between the low-energy properties of interacting electrons and a sea of non-interacting electrons is the basis of the Landau theory of normal Fermi liquids, a phenomenological theory based on the idea that the excitations of a system of interacting fermions have the same nature of those of a non-interacting gas provided that some effective parameters are used.

Within the band theory the electronic spectrum is constituted by a number of energy bands separated by forbidden energy regions called gaps. The very existence of bands and gaps is a consequence of the periodic potential provided by the ionic lattice. Therefore one can construct the many-body state of the system by populating all the possible single-particle energy levels while respecting the Pauli principle. imposing that two electrons can not have the same quantum numbers. The last occupied energy level is usually called Fermi energy or Fermi level ε_F. The last populated band, commonly called valence band, can be partially or completely filled. When the valence band is partially filled, the system is metallic, and the electrons in this band give rise to the electrical conduction and to most electronic properties. Since there are free electronic

states just above the Fermi level, the electrons can be excited with no energetic cost. On the another hand, in order to have an insulator, the number of electrons must be such to completely fill the last, valence band, separated by a gap from the next, empty, band. In this latter case we have a situation where in order to add or excite one of the existing electrons would require an energy cost of the energy gap between the lower exactly filled valence band and upper empty conduction band. We say that the system has the gap at the Fermi level. Hence in this situation the insulator is inert to the applied external field, meaning that it can not cause the flow of the carriers.

Within this scheme, the only way to have a phase transition between a metal and an insulator would be to modify the electronic population of the valence band. This can be done by chemical doping or by electrostatic gating.

The above picture can easily be connected with the chemical character of the material: each atom in the solids contains an integer number of electrons. It is clear, due to the spin degeneracy, that having an even number of electrons per unit cell will mean having the full band hence an insulator. Within the band theory this is an necessary but not sufficient condition to have a gap at the Fermi level. Accordingly, systems with an odd number will end up having partially filled band driving the system to the metallic state.

2.2 Fermi liquid theory

A challenge to obtain the theoretical descriptions of interacting many-body systems gave rise to many different theoretical approaches. Capturing the effects of Coulomb interactions between many electrons in a lattice was greatly simplified by the Fermi liquid theory [29–31], an approximative approach introduced by Landau in 1956. As a phenomenological description of weakly interacting fermionic systems, the Landau theory of normal Fermi liquids provides description of many properties of metals, explaining why some properties of an interacting fermion system are very similar to those of the Fermi gas (i.e. non-interacting fermions), and why other properties differ. Moreover it is even able to describe some superconducting state, which was noticed in many metallic systems at low temperatures.

In fact, the basic assumption of this phenomenological theory is that the low-energy and low-temperature elementary excitation of a system of interacting fermions, so called quasiparticles, are in one-to-one correspondence with the excitations of a system of non-interacting particles. This can be realized starting from the single-particle excitations and "turning on" adiabatically the interaction without changing the character of the excitations. Therefore the quasiparticle states (thought not being a true state of the interacting Hamiltonian) can be labeled with the same quantum numbers (particle number, spin, and momentum) as the non-interacting fermionic states. This correspondence is valid only for weak excitations at low-energy, meaning that the excitation spectrum remains close to the Fermi surface. In general a quasiparticle excitation has a finite lifetime at low energy, as opposed to non-interacting particle.

At this point we can say that most of the low energy properties of a Fermi liquid can be interpreted as the ones of an ideal gas but rather with renormalized parameters. One of the main characteristics of the Fermi liquids is the quasiparticles effective mass m^*, which, comparing to the bare non-interacting electron mass m, has a larger value, owing to the presence of the interactions (between the quasiparticles). The bare band mass m of an electron is defined, within the band theory, as a result of the movement of an electron in a periodic potential, which makes its motion different with respect to the free-electron one. Accordingly one can see the effective mass m^*, within the Fermi liquid theory, as the reduction of the mobility of the electron as a consequence of the interactions between the particles. Hence, it comes naturally to take the two

masses, m^*/m, as the measure of the degree of correlation of a system under the consideration.

Previously described phenomenological idea of Landau Fermi liquid theory was later developed by Abrikosov and Kalatnikov [32], who gave a formal derivation using diagrammatic perturbative expansion of the interaction. Therefore, in order to give an insight in m^*/m ratio, let us consider the self-energy $\Sigma(\mathbf{k}, \omega)$ that represents the contribution ("correction") to the single particle energy (or effective mass) due to interactions between the particle and the rest of the system. Let us then focusing on the zero-temperature behavior, up to order ω, where the self-energy is purely real and can be expanded as

$$\Sigma(\mathbf{k}, \omega) \simeq \Sigma'(\mathbf{k}, 0) + \omega \frac{\partial \Sigma'(\mathbf{k}, \omega)}{\partial \omega}\bigg|_0 , \tag{2.1}$$

where we denoted the real part of the self-energy as $\Sigma'(\mathbf{k}, \omega)$. Here we have neglected the imaginary part of the self-energy, that corresponds to the decay of quasiparticles, since we assumes that the decay rate of quasiparticles in much smaller than their energy. This is justified at energies and temperatures much lower than ϵ_F. If we further expand the self-energy and the dispersion around the Fermi momentum $\mathbf{k}_F$, we obtain the expression for the effective mass

$$\frac{m}{m^*} = \frac{1 - \frac{\partial \Sigma'(\mathbf{k},0)}{\partial k}\Big|_{k_F}}{1 - \frac{\partial \Sigma'(\mathbf{k}_F,\omega)}{\partial \omega}\Big|_0} . \tag{2.2}$$

Since the self-energy does not depend on momentum in the mean-field approaches we will be dealing with in the present work, the numerator of Eq. (2.2) becomes 1 giving

$$\frac{m^*}{m} = \left(1 - \frac{\partial \Sigma'(\mathbf{k}_F, \omega)}{\partial \omega}\bigg|_0\right)^{-1} = \frac{1}{Z} , \tag{2.3}$$

where Z represents the quasiparticle weight, which plays the role in renormalizing the quasiparticle energy. Eq. (2.3) shows that the effective mass is given simply by the inverse of the quasiparticle weight. Starting from the metallic phase with $Z = 1$, decrease of Z can be related to an increased effect of correlation, and consequently a metal-insulator transition will occur when Z vanishes or, following Eq. (2.3) the effective mass diverges. This means that at the moment of transition the electrons do not move anymore, they localize, hence one should expect the huge enhancement of the effective mass comparing to the non-interacting value. Consequently, the effective mass carries the main description of the correlation effects as long as the system remains in a Fermi liquid state. In another words, the quasiparticle picture of Fermi liquid theory can be taken as a correct description of the metallic states of the systems of interest, breaking down at the moment of transition to insulator phase.

On another side, the Landau theory that holds for the weakly interacting electrons fails to describe the system as soon as the interactions become sufficiently large to drive a phase transition to an insulator, or possibly to a novel non Fermi liquid metals characterized by anomalous properties. This scenario occurs in materials with open d- or f-electron shells, whose orbitals are localized and the bands are narrow. In these materials the effect of the Coulomb repulsion between electrons is very pronounced, meaning that the mean-field theories can not be applied anymore.

2.3 Mott insulators

Despite its huge success, the band theory of solids failed to describe the behavior of some materials with open d- or f-electron shells, such as transition-metal oxides. In spite of having an odd number of electrons per unit cell, already in the late 30's of the twentieth century experiments [33] have shown unambiguously that these materials behave as insulators. Since this insulating behavior clearly contrasts with the band theory of solids, we are facing a new class of insulators, different from those predicted by the band theory, which are usually referred to as band insulators.

Mott and Peierls [34] suggested that this might be the result of the presence of strong Coulomb repulsion between electrons, which, in case of transition-metal oxides, are relevant and must be treated with equal footing with the kinetic energy of the electrons. Seemingly, this is the point where the mean-field treatment of the electron-electron interaction within the band theory fails, since this theory can hold just for the weakly interacting systems that can be represented with this independent particle picture. The reason why the effect of the screened Coulomb interaction can not be neglected is because d-orbitals of transition-metal oxides are very localized and the electronic bands are quite narrow due to the small overlap of the two adjacent d-orbitals.

The physical picture proposed by Mott can be described in terms of a tight-binding model where the electrons experience a screened Coulomb repulsion U when two electrons with opposite spin are on the same lattice site (corresponding to an ion in the crystal). As we shall see, this is precisely the famous Hubbard model. Let us consider a system with the same number of electrons as lattice sites, which corresponds to a half-filled band in the non-interacting limit.

Within this simple framework we can not only understand the existence of Mott insulators, but also a new kind of transition connecting a metal to an insulator without changing the number of carriers or, equivalently, the Fermi level.

We can theoretically imagine to tune the interaction strength. At $U = 0$ the system obviously describes a metal because we have a half-filled band. When we increase the interaction, we have a competition between the kinetic energy, which favors delocalization of the electronic wave-function, and the interaction, which imposes constraints to the motion of the electrons. It is easy to be convinced that, when U becomes much larger than the kinetic energy, the ground state of the system is given by one electron localized on each lattice sites. Every hopping starting from a similar state necessarily creates a doubly occupied site, which is energetically unfavored by the Coulomb repulsion. In this way the electrons stay on their sites, ie. they localize and the material becomes an insulator, or more specifically - the Mott insulator [35].

From this description we can easily see that, in a Mott insulator, the behavior of each electron depends on the state of the others, which is exactly what the adjective correlated means. The correlations between electrons can not, obviously, be captured by the mean-field treatment of the band theory. For this reason the materials where the interactions are so strong to give rise to violations or even the breakdown of the band theory of solids are called strongly correlated systems.

We remind that Mott localization can happen only when the number of electrons is equal to the number of sites, for this particular case, or, for more generic picture when dealing with multi-orbital systems, at any commensurate filling when we have an integer number of electrons per site. Otherwise doping the Mott insulator with either holes or electrons the system becomes metallic; the correlations between the electrons still remain, but without possibility to drive the system up to the Mott insulating state in the absence of any spatial symmetry breaking.

It is important to stress that Mott insulators are usually characterized by a long-range ordering of the spin (and orbital for more general models) of the localized electrons. It is natural

that some residual interaction emerges between the spins, leading to real-space ordering. For the single-band Hubbard model, one finds a Heisenberg interaction with antiferromagnetic coupling which gives rise to an antiferromagnetic ordering on bipartite lattice or in the absence of substantial frustration. Nevertheless, in this work we focus on paramagnetic solutions, where we inhibit any magnetic or orbital ordering to focus on the intrinsic correlation effects induced by the interactions. This solution is also representative of the finite-temperature behavior above the ordering temperature in actual materials.

The main reason for the interest in Mott insulators and Mott metal-insulator transitions is that many remarkable phenomena happen "close" to Mott transitions, i.e., with little changes of control parameters like doping, pressure, magnetic field or others. Among these phenomena the appearance of high-T_c superconductivity by doping a copper oxide is certainly one of the most fascinating and speculated one. In general terms, one can rationalize the proliferation of interesting phenomena in terms of the fragility of the strongly correlated metallic state in proximity of Mott localization.

2.4 Single-orbital Hubbard model

As we anticipated in the previous section, the basic ideas behind Mott insulators can be described in terms of a simple tight-binding model which includes a screened short-range Coulomb repulsion. Even if the valence bands of most correlated materials have d or f character, which would imply a multi-orbital description, we can picture the physics within a model where only one orbital is considered on every lattice site. This situation is also relevant for the high-temperature superconducting cuprates, where every copper atom has nine electrons in the d-shell: eight out of nine electrons will fill those levels which are substantially below (and do not affect the physics of the system), and the only band that crosses the Fermi level is the $d_{x^2-y^2}$ with one electron per orbital.

For simplicity we only consider near-neighbor hopping on a square or cubic lattice experiencing an on-site Coulomb repulsion U between two electrons on the same site (obviously with opposite spin in order to fulfill the Pauli principle). The Hamiltonian reads

$$\hat{H} = -t \sum_{\langle ij \rangle \sigma} c^{\dagger}_{i\sigma} c_{j\sigma} + U \sum_{i} \hat{n}_{i\uparrow} \hat{n}_{i\downarrow} \,, \tag{2.4}$$

where $c^{\dagger}_{i\sigma}$ is the creation and $c_{j\sigma}$ is the annihilation operator on two different lattice sites i and j, respectively, hence the first term, together with the hopping amplitude t (an overlap of the two neighboring Wannier orbitals with dependence on the lattice constant a), represents the hoppings between the neighboring sites. The second term contains the local U Coulomb repulsion between the electrons, knowing that $\hat{n}_{i\sigma} = c^{\dagger}_{i\sigma} c_{i\sigma}$ is the number operator.

For $U = 0$ we have a standard tight-binding approximation for independent electrons which can be diagonalized in momentum space giving rise to a single band of width $W = 2td$, where d is dimentionality, and it is proportional to the hopping amplitude t. On the other hand, for $t = 0$ the model reduces to a collection of isolated sites, each hosting one localized electron. If we do not allow for any magnetic ordering, the spins of the electrons are disordered and we have a trivial paramagnetic insulator, where the electronic motion is impossible because of the absence of hopping processes. These two trivial limits, where the system is respectively a metal and an insulator, must be connected by some transition. If we consider the model at fixed density, it contains only two energy scales, therefore the whole physics must be controlled by the ratio U/W.

Despite the simplicity the model can not be solved exactly, except for the two limiting case of one and infinite spatial dimensions where the Dynamical mean-field theory becomes exact, thus the search for a characterization of the Mott transition is still a serious challenge.

The main reason for this is that the transition is expected to occur for intermediate $U/W \sim 1$, where no perturbative approach is possible, and that the competition between the two terms is a very fierce one. The kinetic term tends to produce delocalized solutions, while the interaction terms wants to localize the electrons in real space. For these reasons, the study of the Hubbard model, especially in two dimensions, has been based on numerical approaches or approximate analytical methods.

As stressed before, one can take a quasiparticle spectral weight Z as a measure of metallicity, which is equal to 1 in metallic case. Increasing the value of U/W ratio Z starts to decrease. When the local interaction, ie. the Hubbard repulsion between the electrons U overcomes the energy scale of the kinetic energy which is defined by the bandwidth W, the quasiparticle spectral weight becomes suppressed, reaching the zero value at the transition.

In this thesis we do not attempt to review all the different approaches focusing on the various aspects of the Hubbard model, and we focus on a class of studies devoted to the Mott transition and focusing on the metallic side, where a strongly correlated metal emerges by increasing the interaction strength.

Mott insulator is characterized by the two bands, lower and upper Hubbard band, separated with the gap of the order U, that can be pictured as shown in the last panel of Fig. 2.1. Upper Hubbard band includes those states where we have the double occupied site and represents the energy cost, in contrast to the lower Hubbard band. When the strength of the interaction overcomes the bandwidth, the gap opens and the metal-insulator transition occurs.

Let us try to describe schematically the Mott transition. Let us recall (2.4) and rewrite the Hamiltonian $\hat{H} - \mu\hat{n}$ it in a slightly different way, for the later convenience

$$\hat{H} = -t \sum_{\langle ij\rangle\sigma} c^{\dagger}_{i\sigma} c_{j\sigma} + \frac{U}{2} \sum_{i} \left(\sum_{\sigma} \left(\hat{n}_{i\sigma} - \frac{1}{2} \right) \right)^2 . \tag{2.5}$$

This form comes from rescaling the chemical potential such that at half-filling $\mu = 0$ and the particle-hole symmetry is evident. If we now consider a system at half-filling, the density of states at large U ($U > W$) can be represented [36] as two peaks centered around $\epsilon_F \pm \frac{U}{2}$, so-called upper and lower Hubbard bands, both with bandwidth W and the gap between them. This picture describes in the appropriate way the Mott insulating state, and the distance U between them represents the energy cost for having double occupied state in the upper Hubbard band. Further, decreasing U means that the gap between these two peaks is decreasing (the overlap between the atomic orbitals starts to increase as well as the tendency of the electrons to delocalize) and finally vanishes at a critical value of the interaction strength $U_c = W$, signalizing the Mott insulator-metal transition in the single-orbital case [36, 37]. This "atomic-limit" description will be discussed in more details in Sec. 3.4.1.

2.5 DMFT

So far we have seen that the correlation driven Mott metal-insulator transition, as one of the most intriguing phenomena in condensed matter physics, has been widely examined in numerous studies, particularly the single-orbital model (2.4) at half-filling [36, 38–41]. The Brinkman-Rice picture [42] of the transition (within the frameworks of Gutzwiller approach [43] - see Chapter 4) gives a good description of the quasiparticle spectral weight in the metallic regime,

with no possibility of reproducing the upper and lower Hubbard bands. The disappearance of the quasiparticle peak signalizes the metal-insulator transition. On the other side, Hubbard's picture describes metal-insulator transition in terms of continuous splitting of metallic band into an upper and lower Hubbard band defining this way an insulating state. Apparently, this description does not give any information about the quasiparticle spectral weight. Dynamical mean-field theory represents the theoretical approach that was the first to unify the Mott and Brinkman-Rice picture and therefore describe the transition from both insulating and metallic side.

The initial point for constructing Dynamical mean-field theory (DMFT) [44–47] comes from the study of Metzner and Vollhardt [48] and shortly after Müller-Hartmann [49, 50], who realized that the diagrammatic perturbation expansions of expectation values (related to a Hamiltonian under the consideration) simplify in the limit of infinite lattice coordination number z. Keeping only the zeroth order term of such expansion gives a simplified theory that is exact in the limit $z \to \infty$. An important point in this limit is that one has to scale properly the hopping parameter $t \to \frac{t}{\sqrt{z}}$ to get a non-trivial solution for the physical properties of the system [48]. Moreover, within the limit $z \to \infty$ all non-local contributions to the self-energy vanish, recovering the momentum-independence of the self-energy $\Sigma(\mathbf{k}, \omega) \overset{z\to\infty}{=} \Sigma(\omega)$. The self-energy, though momentum independent, retains the full many-body dynamics, and can thus describe genuine correlation effects.

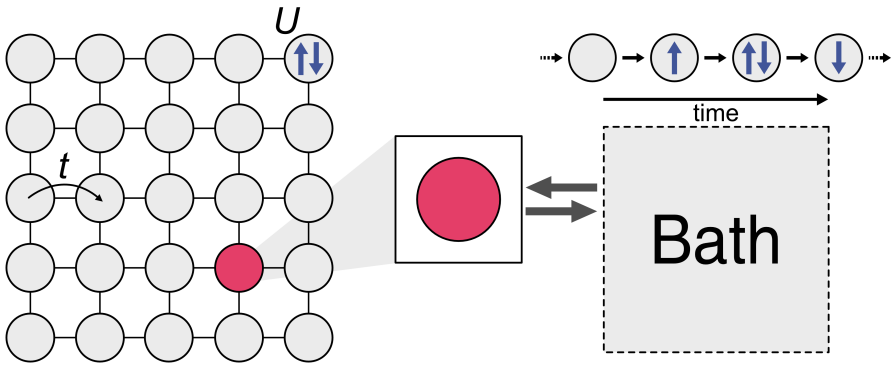

Figure 2.1: In the limit $z \to \infty$ the original Hubbard model reduces to a dynamical single-site problem, which may be viewed as an impurity atom embedded in a dynamical mean-field. Electrons may hop from this atom to the mean-field and back, whereas the on-site interact is as in the original model.

The second important step for the realization of this method lies in the following simplification suggested by Georges and Kotliar [51]: the lattice model, such as the single-orbital Hubbard one that we have previously introduced, is mapped onto a purely local impurity model, which is described with an atom embedded in a non-interacting bath [44, 52, 53], as represented in Fig. 2.2. The bath represents the effective medium and it contains all the information about the intra-atomic interactions. It is coupled to the impurity atom through a hybridization function $\Delta(\omega)$ via exchange of an electron. The local configuration on the chosen atom will essentially fluctuate between all the possible local configurations, giving an information about the quantum evolution of the atom. Moreover, the impurity self-energy becomes equal to the lattice self-energy. Having self-energy local gives the self-consistency condition and the crucial advantage of DMFT approach.

Starting with an arbitrary choice of the self-energy of the system, one solves the corresponding impurity problem in order to get a new self-energy. This must be repeated until the self-energy does not change anymore. From the converged self-energy $\Sigma(\omega)$ it is possible to

compute the full spectral function $A(\omega)$ of the impurity. Since the spectral function is related to the density of electron states, its evolution with respect to increasing interaction U can provide us an information about the emergence of the Mott transition at a specific critical value U_c. In Fig. 2.2 we show the schematic evolution of the density of states while increasing the interaction strength U, which summarizes up the results of many different studies from Ref. [44, 54–56].

At $U = 0$ the system is represented by the free-electron density of states, with a bare bandwidth W. As soon as we start increasing the interaction, we can observe the coherent quasiparticle peak, but slightly different from the one expected from the Brinkman-Rice picture (dashed region in Fig. 2.2), due to the appearance of the symmetric spectral weight broadening. These two broad peaks are considered to be a precursor of the lower and upper Hubbard bands previously introduced in the Hubbard picture [36, 41]. They belong to the incoherent part of the spectral function and represent the high-energy excitations caused by electron-electron interactions. At this point we can observe the dual nature of electrons, having both localized character at high energies and metallic behavior with the formation of itinerant quasiparticles at low energies. Increasing further U/W the two peaks tend to move further apart, while the low-energy peak gets reduced. Close to the Mott transition ($U \lesssim U_c$), this three peak structure gets more pronounced. The quasiparticle peak becomes narrower, keeping the height at ϵ_F unchanged. Suddenly it vanishes at a critical coupling U_c, signalizing the Mott transition, and leaving on another side Mott gap between the lower and upper Hubbard band developed around $\epsilon_F \pm U/2$.

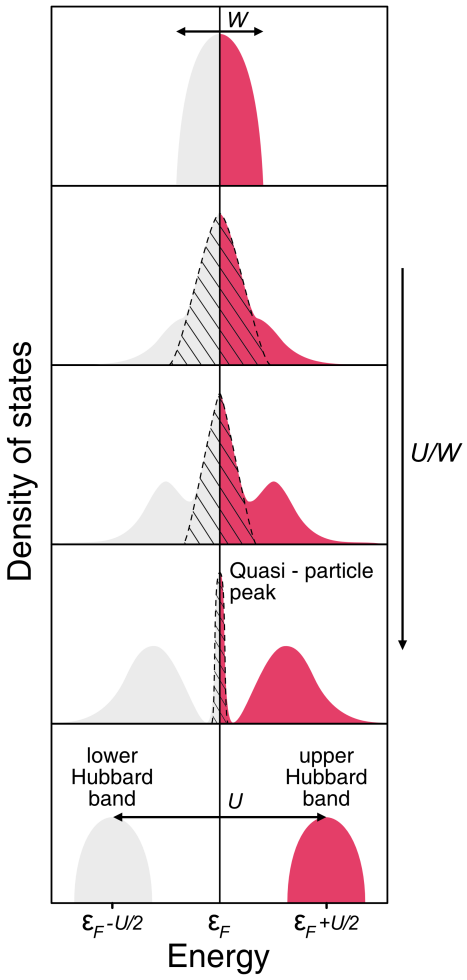

Figure 2.2: Schematic plots of the evolution of the density of states with respect to increasing interaction. This scheme is made particularly for the case of half-filled Hubbard model in the paramagnetic case, in scope of comparing different theoretical approaches. The value of U is increasing from top to bottom. The first four plots with a finite spectral weight refer to the metallic phase. The very last plots refer to the insulating phase. The Hubbard peaks, as a precursor of the Hubbard bands, are visible already in the metallic phase.

The low-energy physics can be described, to some extent, in terms of Fermi liquid theory. Using the fact that, within DMFT, the self-energy $\Sigma(\omega)$ describes the local correlations as momentum-independent, we can conclude that the width of the peak that is proportional to the quasiparticle weight $Z \equiv (1 - \partial\Sigma/\partial\omega)^{-1}$ coincides with the effective mass enhancement, ie. $m/m^* = Z^{-1} = 1 - \partial\Sigma/\partial\omega|_{\omega=0}$. This means that for vanishing quasiparticle spectral weight the Mott transition occurs through a divergence of the effective mass associated with the localization of the electrons. Hence we can interpret the metal-insulator Mott transition as a delocalization-localization transition, demonstrating the wave-particle duality of electrons. The factor Z will be later on introduced within the Gutzwiller approximation described in Chapter 4, which reproduces qualitatively in a correct way the DMFT picture of the coherent peak.

In this chapter we gave a very brief insight to Dynamical mean-field theory, focusing on the relevant aspects that will be important for understanding the results of the Gutzwiller

approximation that we will mainly use within this work. As stressed, Gutzwiller approach is sufficient if considering the metallic side of the transition. However, the Gutzwiller approximation picture can be compared, confirmed and eventually improved by DMFT study, which provides the exact properties not only of metallic but also insulating many-body state in infinite lattice coordination.

So far we have considered the single-orbital Hubbard model, but similar picture can be generalized for the multi-orbital one. However, DMFT must be taken as an approximation for real materials. Nevertheless, calculations showed that within DMFT a large amount of physical properties of among all transition-metal based materials can be analyzed and later compared with experiments [55, 57, 58]. Information about the lattice structure appears in the DMFT equation only through the local density of states. Seemingly, more realistic (and less symmetric) density of states do account for the different competitions between interactions and hence different results in the various phenomena of this picture. Hence DMFT is a good starting point for analyzing this many-body problem.

Solving the impurity model in a self-consistent way, one gets the solution of the initial many-body problem. Yet, this approach, thought a simplification comparing to the original lattice model, still requires different numerical methods for its handling. Solutions of the general DMFT self-consistency equations require extensive numerical methods, in particular Quantum Monte Carlo techniques [44, 59–62], the Numerical renormalization group [54, 63–65], Exact diagonalization [66], and other techniques. All of these approaches use the fact that in the limit of infinite spatial dimensions $z \to \infty$ the Hubbard model effectively reduces to a dynamical single-site problem with the self-consistency condition (Fig. 2.1). In this sense, the only approximation in DMFT is the negligence of spatial fluctuations. However, it takes full account of quantum fluctuations, so that it becomes a good approximation in the case where the spatial fluctuations are not important, as for example in the systems with large coordination numbers.

3

Multi-orbital models and Hund's physics

The single-band Hubbard model is the paradigmatic model to understand the physics of electron-electron correlations and the Mott transition in their simplest realization. However, in a vast majority of compounds the electronic structure can not be approximated with a single band crossing the Fermi level and a description in terms of the single-band model is questionable. This observation is not surprising because the typical example of strongly correlated materials are based on transition-metal atoms, in which the $3d$-orbitals are partially occupied with different number of electrons according to the atomic species of interest. The five d-orbitals lead in principle to five bands in the solid (or even more if oxygen degrees of freedom are included and/or spatial symmetry breaking leads to a larger unit cell). While in some special situation, like the cuprates, the combination of a splitting of the bands and a particular filling leads to a single-band description, in the most general case, the electronic structure requires the explicit inclusion of a given number of orbitals.

The change from one to more orbitals turns out to be far from trivial, leading us to quote (with a slight abuse) Phil Anderson and his famous phrase "More is different". A number of recent studies shows indeed that Mott physics reveals surprising new phenomena when we take into account more than one orbitals and the consequent richer form of the electron-electron interaction.

As a matter of fact, the properties of multi-orbital systems are very rich and they depend crucially on different parameters, like the number of electrons and orbitals, the energy splitting between orbitals and the exchange coupling J. This can give rise to a variety of metallic, insulating, or bad metallic regimes, leading to the richness of phenomena that we can designate generally as Hund's physics. In this chapter we review the main aspects of the modeling of multi-orbital materials and some very important results which represent the starting point of the original investigations reported in this thesis.

3.1 d-orbitals in transition-metal oxides

Transition-metal atoms are characterize by a partially filled $3d$-orbitals. This level is five-fold degenerate due to angular momentum $\ell = 2$, which implies that the z-component can assume the values $\ell_z = -2, -1, 0, 1, 2$. When the atom is included into a lattice, the neighboring atoms,

which can be other transition-metals or ligands (like oxygen in oxides) induce a crystal-field that lifts (partially) the degeneracy of these d-orbitals. Depending on the different coordination (thetrahedral, ochtahedral, square planar etc.), the crystal-field can have different effects, hence d-orbitals can be split in different way. This point is of the crucial importance because it allows us to understand which are the active orbitals that have to be taken into account when defining the model.

In some materials where the degeneracy is totally lifted, such as in the case of copper-oxides, it can happen (if the bands are narrower than the crystal-field splitting) that only one band with a precise orbital character crosses the Fermi level, meaning that the single-orbital Hubbard model is sufficiently good choice for a description of the low-energy physics. In this case just two control parameters, interaction strength U and the bandwidth W, are enough for understanding the important effects of the system.

We discuss now, as a notable example, the case of a cubic crystal-field splitting, generated by a configuration where the transition-metal atom is surrounded by ligand ions with negative charge at the same distance along the three coordinate axes, $\hat{x}, \hat{y}, \hat{z}$.

In Fig. 3.1 we show the typical structure of the atomic energy levels in this situation. The cubic crystal-field elevates the energy of $d_{x^2-y^2}$ and $d_{3z^2-r^2}$ orbitals, which are extending in the direction towards the ligand ions, with respect to d_{xy}, d_{yz} and d_{xz} orbitals, which are extending in directions between the surrounding ligand ions. Hence the five d-orbitals split into a two-fold degenerate subset, $e_g \equiv \left\{d_{x^2-y^2}, d_{3z^2-r^2}\right\}$, and a three-fold degenerate subset, $t_{2g} \equiv \left\{d_{xy}, d_{yz}, d_{xz}\right\}$, as demonstrated in Fig. 3.1. Since this splitting is usually quite large, only one of the subsets, e_g or t_{2g}, crosses the Fermi energy. However, for example, in iron-based superconductors, where the ligand atoms are either pnictogen or chalcogen atoms, the separation between e_g and t_{2g} is small and all the five d-orbitals are relevant for the description of the low-energy physics. Therefore we can have situations where the effective low-energy manifold is composed by two, three or five orbitals. Moreover, there can be other perturbations that further lift the remaining degeneracies or modify this hierarchy.

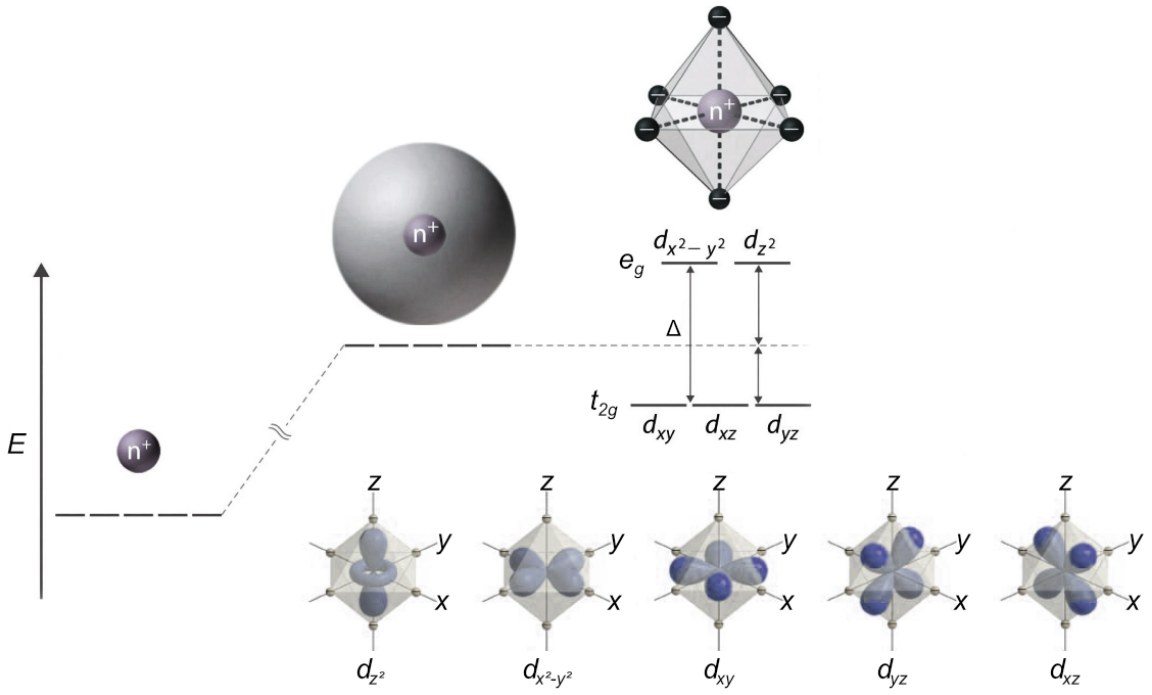

Figure 3.1: Crystal-field split of d-orbitals of transition-metal ion in a cubic crystal-field with an octahedral environment.

One can conclude that when several correlated orbitals contribute to the conduction bands, more parameters come into play, since the number of electron-electron interaction terms increases due to inclusion of orbital degrees of freedom. We will show that this leads to a rich phenomenology.

3.2 Multi-orbital Hubbard model

In the previous chapter we have considered the single-orbital Hubbard model. However, as stressed before, in more realistic materials one actually has to deal with more than just one single-orbital. This mean that, when we expand the Coulomb interaction on a basis of localized Wannier orbitals (or even simply atomic orbitals), we find a number of independent integrals which in turn correspond to different couplings appearing in the second quantization electron-electron interaction term (see Appendix A). This holds even if we limit ourselves to on-site interactions. The most general form of the local Coulomb interaction is obtained in Appendix A and is written as

$$U^{mm'm''m'''} = \int d\mathbf{r}d\mathbf{r'} w^*_m(\mathbf{r}) w^*_{m'}(\mathbf{r'}) \, , U(\mathbf{r}-\mathbf{r'}) w_{m''}(\mathbf{r'}) w_{m'''}(\mathbf{r}) \, . \tag{3.1}$$

If we take $m = m' = m'' = m'''$, we obtain a Coulomb integral which naturally generalizes the expression for the Hubbard U of the single-band model. This integral contains the product of two electron densities (squares of the Wannier orbital wave-function). If instead we take $m = m'$ and $m'' = m'''$, with $m \neq m''$, performing a change of variable label $m'' \rightarrow m'$, we define an independent integral associated with the overlap between the electron densities of two different Wannier orbitals. Assuming rotational invariance between the orbitals U and U' do not depend on the orbital indices and can be computed as

$$\begin{aligned} U &= \int d\mathbf{r}d\mathbf{r'} \, |w_m(\mathbf{r})|^2 \, U(\mathbf{r}-\mathbf{r'}) \, |w_m(\mathbf{r'})|^2 \\ U' &= \int d\mathbf{r}d\mathbf{r'} \, |w_m(\mathbf{r})|^2 \, U(\mathbf{r}-\mathbf{r'}) \, |w_{m'}(\mathbf{r'})|^2 \, . \end{aligned} \tag{3.2}$$

It is clear from Eq. (3.2) that $U > U'$ because the overlap between two different Wannier orbitals will always be smaller than the overlap of an orbital with itself. This reflects the natural expectation that the Coulomb interaction is stronger for electrons belonging to the same orbitals (therefore sharing the same portion of space) than for electrons in different orbitals, which avoid each other more effectively.

Eq. (3.1) defines also other Coulomb integrals, where m, m', m'', m''' assume different values that one can account also for some other independent integral, which rather depends of the choice of relevant orbitals and symmetry of the system. But let us, for the sake of simplicity, consider just U and U', with the possibility of having any number of the orbitals in the system (from five possible d-orbitals), and with no crystal splitting, in order to understand better the effect of inter-orbital Coulomb interaction U'. It is clear, though, that in more realistic treatment of the problem the Coulomb repulsion should be taken as orbital dependent, since, say, repulsion between the d_{xy} and the $d_{x^2-y^2}$ orbital is larger than the one between the d_{z^2} and the $d_{x^2-y^2}$ orbital. Nevertheless, at this point it is enough to consider the upper assumption of having equal U' between all different orbitals.

Assuming N orbitals, the interacting Hamiltonian gets the following form:

$$\hat{H}_{int} = U \sum_{i,m} \hat{n}_{im\uparrow}\hat{n}_{im\downarrow} + U' \sum_{i,m\neq m'} \hat{n}_{im\uparrow}\hat{n}_{im'\downarrow} + U' \sum_{i,m<m'\sigma} \hat{n}_{im\sigma}\hat{n}_{im'\sigma}\,, \tag{3.3}$$

where the first term represents the intra-orbital density-density interaction, while the second and third one stand for inter-orbital density-density interaction between anti-parallel and parallel spins, respectively. Considering the limit of isotropic $U' = U$, and adding the kinetic contribution and chemical potential shift to the interacting Hamiltonian (3.3), the total Hamiltonian becomes

$$\hat{H} = -\sum_{\langle ij\rangle}\sum_{m\sigma} t_{ij}^{m} c_{im\sigma}^{\dagger} c_{jm\sigma} + \frac{U}{2}\sum_{i}\left[\sum_{m\sigma}\left(\hat{n}_{im\sigma} - \frac{1}{2}\right)\right]^2 . \tag{3.4}$$

where we have considered just the intra-orbital hopping terms between the same orbitals m (see Appendix A). Introducing $1/2$ in the Hamiltonian (3.4) is just a convention for the chemical potential μ, in order to imply the particle-hole symmetry in half-filling case. The Hamiltonian considered here has a full $SU(2N)$ rotational symmetry with respect to spin and orbital degrees of freedom. Indeed, the form of (3.4) shows us that the second term depends just on the total charge since the only relevant term that remains (apart of constant shift) is proportional to $\hat{n} = \sum_{m\sigma} \hat{n}_{m\sigma}$. This indicates that any rotation in the local spin-orbital space leaves the interacting term invariant under these transformations hence independent of the choice of the local basis set.

One can anticipate the existence of the Mott transition for any integer filling of the system $x = n/2N$, where $n = 1, ..., 2N-1$. Indeed, for very large U, the situation where n electrons are localized on each site represents the ground state. Instead, the excited state where a charge excitation is created is separated from the ground state by a gap of order U. This generalizes the half-filling situation of the single-band model, where $n = 1$ is the only configuration which can lead to a Mott transition.

Several different studies [67–71] using different techniques have recovered and confirmed this result. Particularly interesting for our case is the one obtained with the Gutzwiller approach (see Chapter 4) in Ref. [67]. The authors demonstrated that the critical interaction strength U_c for which the metal-insulator transition occurs can be expressed as

$$U_c(N,n) = \frac{1}{(2N-n)\,n}\left(\sqrt{n(2N-n+1)} + \sqrt{(n+1)(2N-n)}\right)^2 |\bar{\epsilon}| \tag{3.5}$$

where $\bar{\epsilon}$ is the average energy per site in the uncorrelated case

$$\bar{\epsilon} = \sum_{\sigma}\int \epsilon D(\epsilon) d\epsilon = \sum_{\sigma} \bar{\epsilon}_{\sigma}\,, \tag{3.6}$$

and $D(\epsilon)$ represents the density of states. In our specific case we will assume the semi-circular density of states with half-bandwidth $D = 1$ and average energy per spin $\bar{\epsilon}_{\sigma} \simeq -0.2122$. Using Eq. (3.5) for this particular case, one can obtain the left panel of Fig. 3.2.

Obviously, U_c is a function of N and n. Same results were recovered numerically, using Gutzwiller variational approach, while studying the behavior of quasiparticle spectral weight Z as a function of interaction strength U, with the transition into a Mott phase for $U > U_c(n,N)$. Right panel of Fig. 3.2 essentially shows that if we analyze for instance case $N = 3$, the values of U_c coincide with the ones predicted with formula (3.5). Note that $U_c(n=1) = U_c(n=5)$ as well as $U_c(n=2) = U_c(n=4)$. This is a result of our choice of density of states which is symmetric in this specific case.

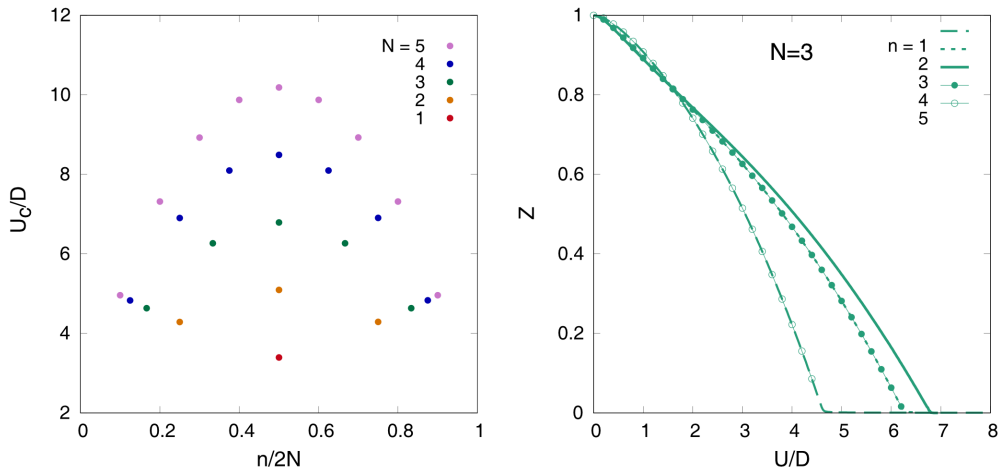

Figure 3.2: Left panel: Critical interaction U_c for different number of orbitals N and different fillings $n = 1, 2, ..., 2N - 1$, as a function of n. Right panel: Quasiparticle weight Z as a function of U/D, for three-orbital models at different fillings; results are obtained with Gutzwiller technique.

Let us now consider in particular the half-filling case. Recalling Eq. (3.5), imposing $n = N$, one obtains:

$$U_c(N) = 8(N + 1)|\bar{\epsilon}_\sigma| \tag{3.7}$$

which coincides with the result obtained analytically in Ref. [71] using the Slave-spin mean-field technique and performing a perturbative expansion[1] around the atomic limit. Ref. [71] points out that the critical interaction strength is a growing function of the atomic ground state degeneracy, meaning that U_c increases together with N. Another point is that U_c is the largest for the half-filling case for any number of orbitals.

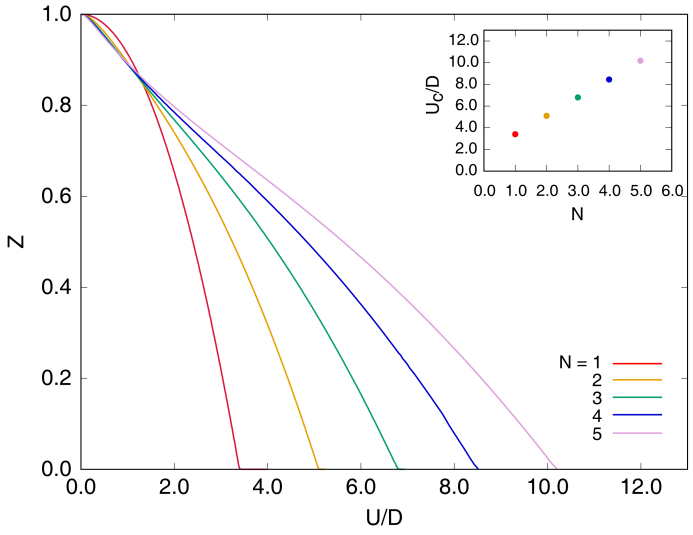

Figure 3.3: Quasiparticle weight Z as a function of interaction strength U/D (where D is a semi-circle with half-bandwidth), for the N-orbital Hubbard model at half-filling (with, from left to right: $N = 1, 2, 3, 4, 5$). The results are obtained with Gutzwiller variational approach and they show a perfect accordance with the Slave-spin mean-field [72]. Inset: Dependence of the critical interaction strength U_c on N.

[1] This can be performed only if the transition is of the second order, which is the case.

Fig. 3.3 displays numerical results for the quasiparticle weight Z together with values of the critical interaction U_c (inset), for different number of orbitals N, and confirms the predictions of Eq. (3.7). These results are obtained both using Gutzwiller and Slave-spin [72] approach.

Result (3.7) can be compared with more reliable DMFT approach in the limit of infinite lattice coordination and large N [68]. In this limit we get the exact large N behavior of the critical interaction $U_c(N)$ at half-filling, which is shown to be linear in N, ie.

$$U_c(N) = 8N|\bar{\epsilon}_\sigma|, \qquad \text{(at large N)} \tag{3.8}$$

It is evident that Eqs. (3.7) and (3.8) match in the limit of large N, meaning that the Gutzwiller approximation (and other slave-techniques) becomes more accurate with increasing N.

3.2.1 Anisotropic Coulomb interaction

When the Coulomb interaction is completely isotropic, i.e. $U = U'$, we find that the critical U_c scales proportionally to the number of orbitals N. However the assumption that the Coulomb repulsion between electrons in the same orbital is the same as for electrons in different orbitals is not likely to be realized in solids. We thus consider here the first and simplest generalization, in which we analyze the case where $U' \neq U$ [73, 74]. Indeed, the two Coulomb integrals presented with Eq. (3.2) do differ in real materials. Let us parameterize the different values defining α according to $U' = \alpha U$ and give an explicit example for the three-orbital case, though the following argument holds for any multi-orbital model. We present our results using the Gutzwiller approximation which agrees with previous slave-particle approaches [73, 74].

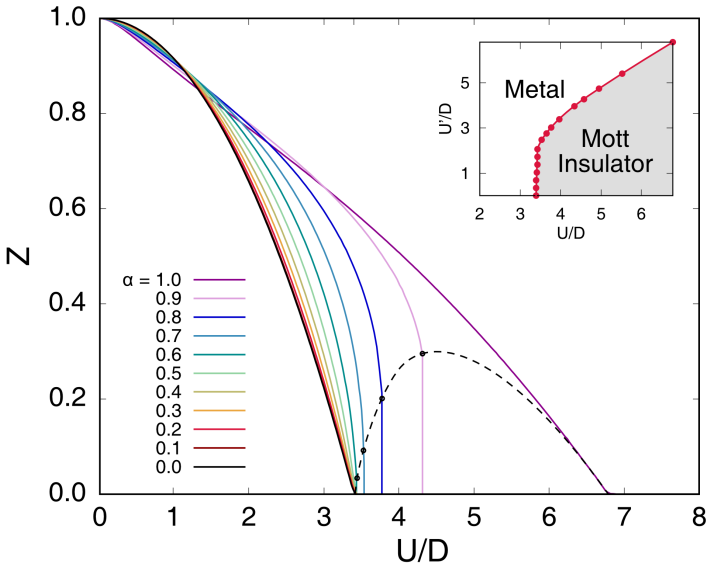

Figure 3.4: Quasiparticle weight Z as a function of interaction strength U/D (where D is a semi-circle with half-bandwidth), for fixed value of $U'/U = \alpha$. The results represent the three-orbital Hubbard model and they are obtained using the Gutzwiller variational technique, showing the perfect accordance with the RIBS results [74].

Fig. 3.4 shows the behavior of the quasiparticle weight Z as a function of the intra-orbital interaction U, for fixed values $\alpha = U'/U$ and at half-filling. U_c reaches a maximum $U' = U$, where we obviously recover the result discussed above, namely $U_c^{N=3}$. In the opposite limit $U' = 0$, the orbitals are completely decoupled and the system is reduced to three single-band Hubbard models, and therefore the transition occurs at $U_c^{N=1}$, which is much smaller than $U_c^{N=3}$

(see Fig. 3.3, for $n = N = 1$). Interestingly the connection between the two obvious limits does not appear smooth and regular, but it is extremely abrupt. Indeed, even for α very close to 1 we find a significant reduction of U_c which rapidly approaches small values. Already for $\alpha \approx 0.5$ we recover $U_c = U_c^{N=1}$ and the result remains unaltered all the way down to the decoupled value $\alpha = 0$ [73, 74].

We notice that the reduction of U_c is not associated with a smaller atomic gap (see also Sec. 3.4.1), since $\Delta_{at} = U$ regardless the value of α, but it is related to a complete quenching of the orbital fluctuations associated with the lifting of the degeneracy of the system for $U > U'$, as shown in Table 3.1. We will turn to this point in Chapter 6.

n	Degeneracy	Energy
0, [6]	$\boxed{1}$	$0\,,[3U + 12U']$
1, [5]	$\boxed{6}$	$0\,,[2U + 8U']$
2, [4]	$\boxed{12}$	$U'\,,[U + 5U']$
	3	$U\,,[2U + 4U']$
3	$\boxed{8}$	$3U'$
	12	$U + 2U'$

Table 3.1: Eigenstates and eigenvalues of the Hamiltonian (3.3) in the atomic limit. The boxed numbers denote the ground state degeneracies for $U > U'$.

3.3 Kanamori model

Besides the two independent integrals introduced by Eq. (3.2), which are associated to charge-charge interactions for intra-orbital and inter-orbital Coulomb interaction, one can account for the other two independent integrals that result from Eq. (3.1) (see Appendix A). These integrals are defined as

$$\begin{aligned} J &= \int d\mathbf{r}d\mathbf{r'} w^*_m(\mathbf{r}) w^*_{m'}(\mathbf{r'}) U(\mathbf{r} - \mathbf{r'}) w_m(\mathbf{r'}) w_{m'}(\mathbf{r})\,, \\ J' &= \int d\mathbf{r}d\mathbf{r'} w^*_m(\mathbf{r}) w^*_m(\mathbf{r'}) U(\mathbf{r} - \mathbf{r'}) w_{m'}(\mathbf{r}) w_{m'}(\mathbf{r'})\,, \end{aligned} \tag{3.9}$$

and they are related to the exchange integrals which are responsible for what we shall call Hund's physics. In fact, F. Hund formulated a set of rules that describe the effect of exchange interactions in degenerate atomic shells. These rules specify the ground state configuration of outer-shell electrons in isolated transition-metal atoms [75]: singly-occupied configurations in each orbitals are the first to be created, aligning as much as spins as possible in order to reach the configuration with the total spin S maximized (rule of 'maximum multiplicity'). Once given S, total angular momentum L should be maximized. When there are no single spin configurations left, the extra electrons are used to create doubly occupied configurations. Fig. 3.5 shows how the ground state configuration is built for the various atoms of the $3d$-block of the periodic table, dictated by the Hund's rules. These rules indeed arise simply from the exchange interaction associated to the couplings (3.9).

Eventually, recent works [17, 20, 76–78] have shown that the Hund's exchange coupling plays an important role in tuning the correlations in correlated metals. The main investigation in this thesis will be shaped following this idea. Hence, in order to understand better the effect of these rules on a physical systems that we are interested in, let us consider a convenient choice of

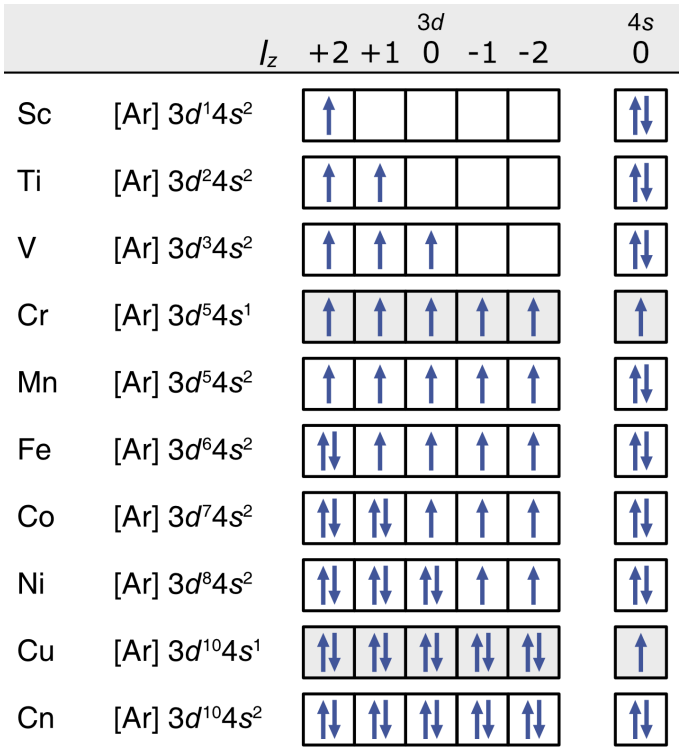

Figure 3.5: Ground state electron configurations and Hund's rules for $3d$-elements

a set of orbitals, where we can utilize corresponding spatial symmetries, that can simplify further the problem. For this purpose let us assume, as a specific case that will be of main interest in this work, d-orbitals of a transition-metal ion in a crystal-field with an octahedral environment. As we have already emphasized, the five d-orbitals are typically split into a two-fold degenerate e_g, and three-fold degenerate t_{2g} orbitals (see Fig. 3.1). Let us now consider the case where the t_{2g} triplet describes the low energy physics. Since wave-functions $w_m(r)$ can be chosen real, as it stands for d-orbitals, one gets that $J = J'$, which represents the further simplification and is convenient for the evaluation of the rotationally-invariant Kanamori Hamiltonian. All other integrals apart U, U' , and J are equal to zero due to the axial symmetry of d-orbitals. Since we want to understand what is the origin of the strong electron correlations in multi-orbital systems, it comes natural to try to understand the effect of each of these Coulomb integrals, (3.2) and (3.9).

The interacting Hamiltonian for the set of t_{2g} orbitals is first proposed by Kanamori [79] for describing ferromagnetic metals, though later on it turned out to be convenient for describing multi-orbital systems in general. It has the following form:

$$\begin{aligned}\hat{H}_{int} = &\sum_{m} U\hat{n}_{m\uparrow}\hat{n}_{m\downarrow} + \sum_{m\neq m'} U'\hat{n}_{m\uparrow}\hat{n}_{m'\downarrow} + \sum_{m<m'\sigma} (U'-J)\,\hat{n}_{m\sigma}\hat{n}_{m'\sigma} \\ &- J\sum_{m\neq m'} c^{\dagger}_{m\uparrow}c_{m\downarrow}c^{\dagger}_{m'\downarrow}c_{m'\uparrow} + J\sum_{m\neq m'} c^{\dagger}_{m\uparrow}c^{\dagger}_{m\downarrow}c_{m'\downarrow}c_{m'\uparrow}\,,\end{aligned} \tag{3.10}$$

with number operator $\hat{n}_{m\sigma} = \sum_{m\sigma} c^{\dagger}_{m\sigma}c_{m\sigma}$ that counts electrons on orbital $m = 1, 2, 3$ with spin σ. The first three terms of the Kanamori Hamiltonian (3.10) expresses density-density interactions: the intra-orbital Coulomb repulsion U and the inter-orbital one U' between two electrons with opposite spins, as well as the inter-orbital Coulomb interaction $U' - J$ between two electrons with aligned spins, respectively. The last one, $U' - J$, includes the z-component

of Hund's coupling J, and reflects Hund's first rule. If we present these density-density terms schematically, as in Fig. 3.6, it becomes obvious that the Coulomb repulsion U between two electrons occupying, say, orbital m (a) can be reduced placing one of the two electrons on a different orbital m' (b), since $U' < U$. Moreover, if the two electrons occupy two different orbitals, m and m', the Pauli principle does not prevent the electrons to have parallel spins along the quantization $\hat{z}$-axis (c). In such configuration the energy is further lowered by the Hund's coupling J, ie. it is equal to $U' - J$.

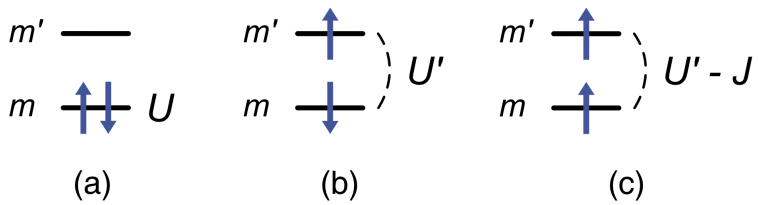

Figure 3.6: Electron-electron Coulomb interactions in multi-orbital systems: (a) intra-orbital, (b) inter-orbital with anti-parallel and (c) inter-orbital with parallel spins

The very last terms in Eq. (3.10) represent the spin-flip and pair-hopping interactions: the former is the x- and y-component of Hund's exchange and it flips the spins of two singly-occupied orbitals (Fig. 3.7 (a)), while the latter represents the two-electron transfers from a doubly-occupied to an empty orbital (Fig. 3.7 (b)). These two terms are needed in order to preserve the $SU(2)$ spin symmetry of Kanamori Hamiltonian, which is still not evident from the form of Eq. (3.10).

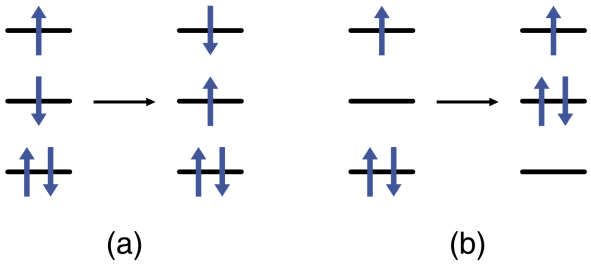

Figure 3.7: Hund's exchange processes: (a) spin-flip and (b) pair-exchange

Furthermore, in order to have the rotational invariance of the system, one needs to impose an additional constraint, ie.

$$U' = U - 2J\,. \tag{3.11}$$

This condition is exact in case of equivalent t_{2g} orbitals which actually are invariant under the rotations in real space. Obviously, this holds just when the crystal splitting is strong enough to push away e_g pair of orbitals, and if U, U' and J are calculated assuming a spherically symmetric interaction, as we have done so far.

The choice of t_{2g} orbitals is relevant for describing the transition-metal oxides with cubic symmetry. In the solid-state, however, in many different materials where we consider orbitals different that t_{2g} ones, the spherical symmetry of the screened Coulomb interaction $U(r - r')$ is not preserved, hence the Kanamori Hamiltonian (3.10) is not exact. Nevertheless, numerous studies applied the Kanamori interaction (3.10) to the full set of d-states. This choice is often considered to be a reasonable approximation so that $U' = U - 2J$ can be used in order to ease the numerical calculations and simplify the definition of the problem. However, for more

realistic treatment of screened interaction one should consider the full Coulomb interaction, which contains also different matrix elements, and/or realistic values of the parameters of the Hamiltonian, which can be obtained through constrained-RPA (Random-phase approximation) method [80].

The full rotational symmetry (ie. invariance under charge, spin and orbital gauge transformations, separately, denoted as $U(1)_C \otimes SU(2)_S \otimes SO(3)_O$ symmetry) becomes apparent if we rewrite the Kanamori Hamiltonian (3.10) in a slightly different way. This can be done by defining the local electron number, spin and orbital angular momentum operators, respectively:

$$\hat{n} = \sum_{m\sigma} c^\dagger_{m\sigma} c_{m\sigma}\,, \qquad \mathbf{S} = \frac{1}{2}\sum_{m,\sigma\sigma'} c^\dagger_{m\sigma}\hat{\boldsymbol{\sigma}}_{\sigma\sigma'} c_{m\sigma'}\,, \qquad \mathbf{L} = \sum_{mm',\sigma} c^\dagger_{m\sigma}\hat{\boldsymbol{\ell}}_{mm'} c_{m'\sigma}, \tag{3.12}$$

where $m, m' = 1, 2, 3$ labels the t_{2g} orbitals and $\sigma = \uparrow, \downarrow$ the spin components, whereas $\hat{\boldsymbol{\sigma}}_{\sigma\sigma'}$ are the Pauli matrices and $\hat{\boldsymbol{\ell}}^{(m)}_{m'm''} = -i\epsilon_{mm'm''}$ are the $O(3)$ group generators characterizing orbital rotations. Once done so, the Hamiltonian (3.10) becomes [78]

$$\hat{H}_{int} = (U - 3J)\frac{\hat{n}(\hat{n}-1)}{2} - J\left[2\,\mathbf{S}^2 + \frac{1}{2}\mathbf{L}^2\right] + \frac{5}{2}J\hat{n}\,. \tag{3.13}$$

The first term of Eq. (3.13), that depends on the total charge of the site and is proportional to the Hubbard U, can be interpreted as the overall Coulomb repulsion experienced by electrons on the same site. On another hand, the second term represents the Coulomb exchange mechanism responsible for Hund's rules, which favors, in following order, high spin and high orbital angular momentum configurations. Therefore, J tends to maximize $\mathbf{S}$ and $\mathbf{L}$ obeying the Hund's rules, in order to minimize the energy of the system, according to Eq. (3.13).

The spectrum of Hamiltonian (3.13) is given in Table 3.2:

n	ℓ	s	Degeneracy	Energy
0, [6]	0	0	$\boxed{1}$	$0\,, [15U - 30J]$
1, [5]	1	1/2	$\boxed{6}$	$0\,, [10U - 20J]$
2, [4]	1	1	$\boxed{9}$	$U - 3J\,, [6U - 13J]$
	2	0	5	$U - J\,, [6U - 11J]$
	0	0	1	$U + 2J\,, [6U - 8J]$
3	0	3/2	$\boxed{4}$	$3U - 9J$
	2	1/2	10	$3U - 6J$
	1	1/2	6	$3U - 4J$

Table 3.2: Eigenstates and eigenvalues of the t_{2g} Hamiltonian (3.13) in the atomic limit. The boxed numbers denote the ground state degeneracies for $J > 0$.

3.3.1 Ising form of Kanamori model

We pointed out that from the form of the multi-orbital Hubbard model (3.13) the $SU(2)$ symmetry of the Hund's spin-spin coupling $-2J\mathbf{S}^2$ is evident. However, it is quite common, for the practical reasons, to retain just the z-component of spin $\mathbf{S}$. This means that, starting from the Hamiltonian (3.10), one needs to keep just the first three density-density terms, omitting the off-diagonal ones, spin-flip and pair-exchange. In this way we obtain the "Ising type" of Hund's coupling, $-2JS_z^2$, which obviously does not preserve anymore the $SU(2)$ symmetry. This approximation turns out to be extremely useful both for numerical solutions (e.g. Continuous-Time Quantum

Monte Carlo as a solver for DMFT) and for the Slave-spin mean-field. Comparing the tables of eigenvalues and their degeneracies (see Table 3.2 and 3.3), one notices that the use of the Ising Hamiltonian does not destroy the main effect of the Hund's coupling, namely favoring high-spin state, but it reduces the degeneracy of the multiplets as a consequence of the broken spin-rotation invariance.

n	ℓ	s	Degeneracy	Energy
0, [6]	0	0	$\boxed{1}$	$0\,,[15U-30J]$
1, [5]	1	1/2	$\boxed{6}$	$0\,,[10U-20J]$
2, [4]	1	1	$\boxed{6}$	$U-3J\,,[6U-13J]$
	1	0	6	$U-2J\,,[6U-12J]$
	2	0	3	$U\,,[6U-10J]$
3	0	3/2	$\boxed{2}$	$3U-9J$
	1	1/2	6	$3U-7J$
	2	1/2	12	$3U-5J$

Table 3.3: Eigenstates and eigenvalues of density-density term of the t_{2g} Hamiltonian (3.13), or so-called "Ising" form of Kanamori model, in the atomic limit. The boxed numbers denote the ground state degeneracies for $J > 0$.

The main differences between the two models become obvious if we list, as done in Table 3.3, the eigenstates and eigenvalues of the Ising form of Hamiltonian (3.13), together with the corresponding degeneracy and quantum numbers. Customarily we set $U' = U - 2J$.

3.3.2 Ising vs. Kanamori model

Fig. 3.8 (left) shows the quasiparticle weight Z as a function of the interaction strength, for different ratios J/U in the half-filled system. Comparing the two forms of Hund's coupling, Kanamori and Ising, we want to check the importance of neglecting spin-flip and pair-hopping terms. The reduction of the critical interaction strength needed to obtain a Mott insulator U_c for increasing J/U is evident in both cases. However, the two models exhibit some differences. In particular the Ising model has always a larger Z, which reflects a more correlated state, for the same value of Hund's coupling and Hubbard repulsion.

Let us focus on the order of the transition. Even if for $J = 0$ the transition is continuous, as soon as J is switched on the transition becomes of first order in both cases. While for the Ising form the first-order character persists until the largest physical value $J/U = 1/3$ and is always stronger for monotonically growing J/U ratio, the rotationally-invariant Kanamori form shows rather a non-monotonous trend, where the jump at the first-order transition reduces in the large J region. Though for $J/U = 1/3$ the jump of Z is quite small, the transition remains first order within the present calculation. This agrees with previous calculations in Ref. [71, 81–83]. However, Ref. [63] suggested the occurrence of a continuous transition in the full Kanamori case within DMFT approach using the Numerical renormalization group as a solver.

We can get more insight about the two models and the differences that arise between them if we take a look at numerical results in Fig. 3.8 (b), showing the value of the local spin $\langle S_z^2 \rangle$ at half-filling. Typically, for strongly correlated metallic systems this quantity increases with U, as one can see from the plot, and at U_c it jumps to a finite value for any finite J, following the behavior of the quasiparticle weight which reaches zero value at that transition point.

However, one can notice a large discrepancy between the values of $\langle S_z^2 \rangle$ in the two models. Basically, this is the consequence of the main drawback of Ising model with respect to Kanamori

one, namely the negligence of quantum fluctuations of the spins. This is apparent once we compare Table 3.2 and Table 3.3, for Kanamori and Ising model, respectively. We can see, say when $n = 3$, that in the ground state we have the formation of quadruplet in Kanamori and doublet in Ising form. The same disagreement is present in the other n sectors (apart of $n = 0, 1$ electrons/holes, where Hund's coupling does not play a role - see Tables 3.2 and 3.3). This causes, to some extent, some differences in the low-energy physics, which will have some important consequences for the results we will present in the rest of this thesis.

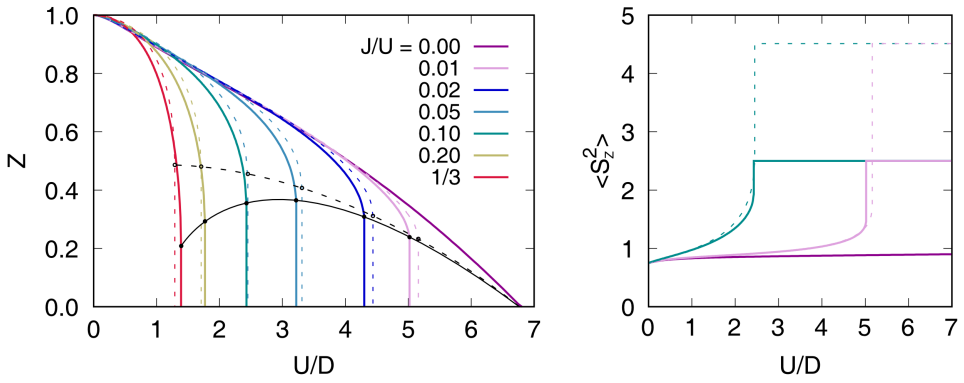

Figure 3.8: Left panel: The behavior of the quasiparticle weight Z with respect to U/D, where D is the bandwidth of semi-circular density of states, for different values of J/U ratio. Full lines are associated to the rotationally-invariant Kanamori form, whereas dashed lines correspond to the Ising form of Hamiltonian (3.13). For $J \neq 0$ the first order transition jump is noted, with a slightly different trend in the two approaches (see text). Black curves associate U_c-s for different J/U ratios. Right panel: $\langle S_z^2 \rangle$ behavior as a function of U for the corresponding values of Hund's coupling: $J = 0.0, 0.01, 0.1$. The expectation value $\langle S_z^2 \rangle$ in the Mott insulator differs within the two models. This is due to the negligence of the quantum fluctuations in the Ising-like form.

3.4 "Janus" effect of Hund's coupling

In this section we briefly introduce some important results about the effect of the Hund's coupling on the Mott transition for different integer fillings. We will elaborate more on these ideas in Chapter 5, where we will present an original analysis of this physics.

We focus on the three-orbital Hubbard-Kanamori model for three independent commensurate fillings ($n = 1, 2$ and 3). The results for Z are reported in Fig. 3.10. If we consider the system at half-filling, $n = N = 3$, we find that the effect of increasing J is to decrease the value of Z. Consequently, one finds the suppression of the value of the critical coupling U_c for which the quasiparticle spectral weight Z vanishes, reaching the Mott insulator state for $U > U_c$. In this case the correlation effects are increased by Hund's coupling for every value of U and J. Actually, this behavior might be considered as expected because Hund's J tends to align the spins in different orbitals, consequently constraining the electronic motion because hopping processes leading to low-spin configurations will be unfavored. We can picture this physics with a simplified sketch shown in Fig. 3.9: we can notice that reaching the double occupied configuration by simply hopping from site i to another, say j, is not energetically favorable (one pays the energy cost U (upper case in Fig. 3.9)), whereas, on another side, some of the hopping processes are excluded due to the Pauli exclusion principle (lower cases in Fig. 3.9). Hence this way there remain only those configurations where we have aligned spins, which maximize total spin, lowering in this way the energy of the system (see Eq. (3.13)).

On another hand, the case $n = 1$ is in contrast with respect to the previous one. Namely, the increase of J/U ratio drives system towards the larger values of the critical coupling U_c, giving rise to the enhancement of Z for the same fixed U value in the metallic phase. In this case the Hund's coupling does not introduce important constraint to the motion.

Actually, the most interesting case turns out to be the one with $n = 2$ electrons in three orbitals (or in more general case $1 < n < N$, where n is the integer number). Here one finds that the Hund's coupling has a rather surprising two-fold effect on the quasiparticle renormalization.

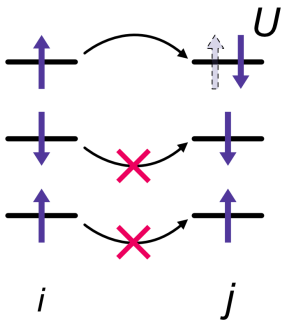

Figure 3.9: Allowed hopping processes between the two sites, in the presence of the Hund's coupling. The lower two are forbidden by the Pauli principle, whereas the upper one implies an energy cost U.

In the range of small values of J/U, Z is suppressed with respect to the case $J = 0$, similarly to the half-filled case. After a first rapid drop of Z we find, however, a novel behavior in which Z flattens and displays a long tail. In fact, for J/U large enough, Z retains a small but finite value and the system remains metallic. We have therefore a rather large windows of interactions in which Z is small and the electrons are strongly correlated but they are not even close to Mott localization, which occurs at much larger U. This correlation-resistant metal has been called Hund's metal and the two-phase effect of the Hund's coupling has been called Janus effect from the roman God Janus.

It is worth stressing that the tail of Janus phase becomes infinitely long when J/U becomes equal to $1/3$, meaning that for this particular case the system never encounters the Mott transition. In Chapter 5 we will discuss at length the physics along this special line and its effect on the properties of the metal also at different values of U and J.

These observations are robust and can be obtained by both DMFT [76] or some of the auxiliary-("slave") particle techniques [71], all giving the same qualitative behavior as the one we presented in Fig. 3.10, obtained by Gutzwiller methods. While the weak-coupling behavior can be understood in terms of the simple arguments we have given above, we can provide an argument for the resistance of the metal by estimating the Mott gap in the atomic limit.

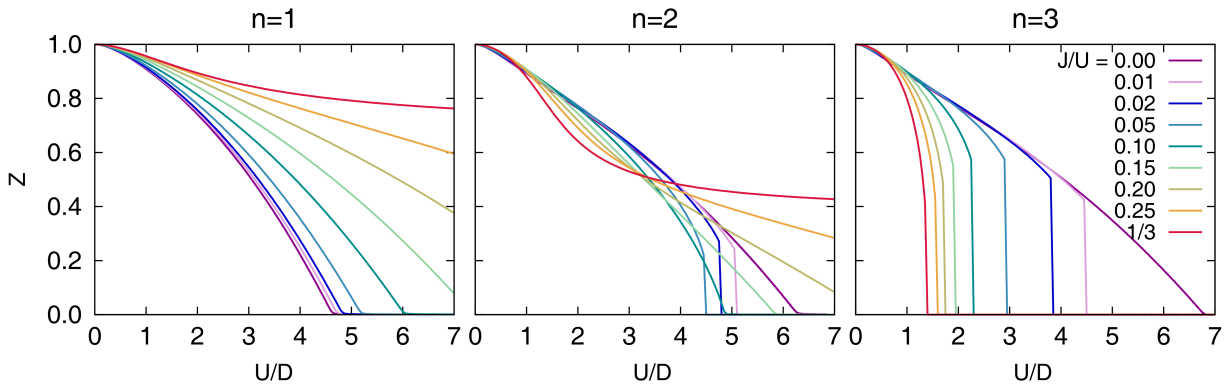

Figure 3.10: Quasiparticle weight Z as a function of Coulomb interaction U in a three-orbital degenerate Hubbard-Kanamori model, for different integer filling $n = 1, 2, 3$ and different J/U ratio. The presence of Hund's coupling J has different effect on these three cases, particularly $n = 2$, where one can observe the emergence of the Janus effect (see in the text).

3.4.1 Energetics of the Mott gap

In this section we discuss an argument to support our numerical results showing that the Mott transition is shifted to very large values of U in the presence of a sizable J when the filling is integer but not half-filling. A simple way to estimate the Mott transition is based on a cartoon of the Mott insulator which, however, nicely reproduces for example DMFT results. As shown in Fig. 3.11, in the Mott insulator the spectral weight is concentrated in two Hubbard bands. For a single-band Hubbard model the centers of the two bands are separated by U and they have a width of the order of the bare bandwidth W. We can rationalize this picture in terms of an atomic solution broadened by incoherent hopping processes.

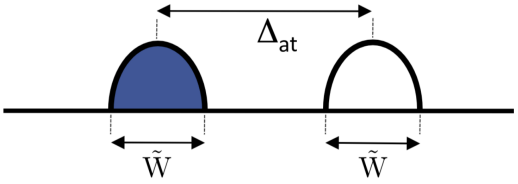

Figure 3.11: Hubbard bands emanating from the atomic excitation spectrum [17]. They are spread apart following the atomic Mott gap Δ_{at}, and are broadened by an effective bandwidth $\tilde{W}$. The blue color represents "filled states" (the extraction part of the spectrum).

We can generalize the estimate of the atomic Mott gap in a more involved multi-orbital model as

$$\Delta_{at} \equiv E_{at}(n+1) + E_{at}(n-1) - 2E_{at}(n)\,. \tag{3.14}$$

Fig. 3.11 gives a sketch of this strong-coupling argument [41], with the effective bandwidth $\tilde{W} = W$ for the half-filled single-orbital Hubbard model in the Mott insulating phase $U > U_c$. A crude estimate of the critical U_c would be obtained computing the value of U for which the Hubbard bands separate, obviously given by $U_c \simeq W$ within our simple atomic picture:

$$\Delta_{Mott} = U - W = 0 \;\rightarrow\; U_c = W\,. \tag{3.15}$$

This reflect the natural physical expectation that a Mott insulator is obtained when the Coulomb repulsion between the electrons overcomes the delocalization energy due to the hopping. When this cost is zero, the Mott insulator cannot exist, and a metal is obtained, which by definition is the state with delocalized excitations at vanishing energy.

In the case of multi-orbital models, one has to take into account the effect of the orbital degrees of freedom on the effective bandwidth $\tilde{W} \neq W$, yet still of the order of bare bandwidth W, defined above. Obviously, introducing N orbitals in a Hubbard model (3.3) increases the ground state degeneracy and the possible hopping channels, giving contribution to the effective kinetic energy. Owing to the orbital quantum fluctuations in the ground state, it has been estimated that the Hubbard bands disperse on an energy range $\tilde{W} \sim \sqrt{N}W$ [67, 68, 70].

Let us now use the same Hubbard criterion we have considered in the single-orbital case, where $\Delta_{at} = U$ holds also for the multi-orbital case. Therefore [77]

$$\Delta_{Mott} = \Delta_{at} - \tilde{W} = U - \sqrt{N}W = 0 \;\rightarrow\; U_c \simeq \sqrt{N}U_c^{N=1}\,, \tag{3.16}$$

and we find that U_c increases with orbital degeneracy N, as a result of wider Hubbard bands. If we compare this result (3.16) with the one obtained using DMFT (3.7) and in the Gutzwiller approximation, we notice that the atomic estimate appears to miss the functional dependence on N ($\sqrt{N}$ instead of linear behavior) which leads to a large underestimation of U_c for large N. However, this disagreement can be reconciled considering the scenario for the Mott transition in DMFT, where two critical interactions can be defined, usually called U_{c1} and U_{c2}. The two values

define a window $U_{c1} < U < U_{c2}$ in which two solutions, metallic and insulating, exist. Therefore U_{c2} is the largest interaction for which a metal exists, and U_{c1} is the smallest value for which an insulator exists. In this light, the critical U_c found in Gutzwiller is clearly an estimate for U_{c2} because the method only deals with metallic solutions, while our atomic estimate measures the instability of the insulator starting from the atomic limit, and therefore is an estimate for U_{c1}. Indeed in DMFT one finds exactly that U_{c2} scales with N, whereas U_{c1} scales with $\sqrt{N}$.

Once we include the Hund's coupling, the low-energy multiplets are those with high-spin. Using these values (see Sec. 3.3) we obtain [77, 78] that the atomic charge acquires the form

$$\Delta_{at}^{n} = \begin{cases} U + (N+1)J\,, & n = N\,, \\ U - 3J\,, & \forall n \neq N\,. \end{cases} \tag{3.17}$$

We can estimate the change of U_c once J included, obtaining [77]

$$\delta U_c^n \propto \begin{cases} -(N-1)J\,, & n = N\,, \\ 3J\,, & \forall n \neq N\,. \end{cases} \tag{3.18}$$

Consequently, the half-filled system shows the maximal gain in energy, favoring the opening of a Mott gap and the Mott insulating phase, simultaneously reducing U_c, whereas in all the other cases where $n \neq N$ we encounter the reduction of the Mott gap as a result of the presence of Hund's coupling, pushing U_c to very large values [77]. This is a first argument to support the results of the previous section, where we have indeed shown trends which qualitatively follow this picture, with a critical U_c for the Mott transition reduced by J for global half-filling and increased by the same coupling for any other filling.

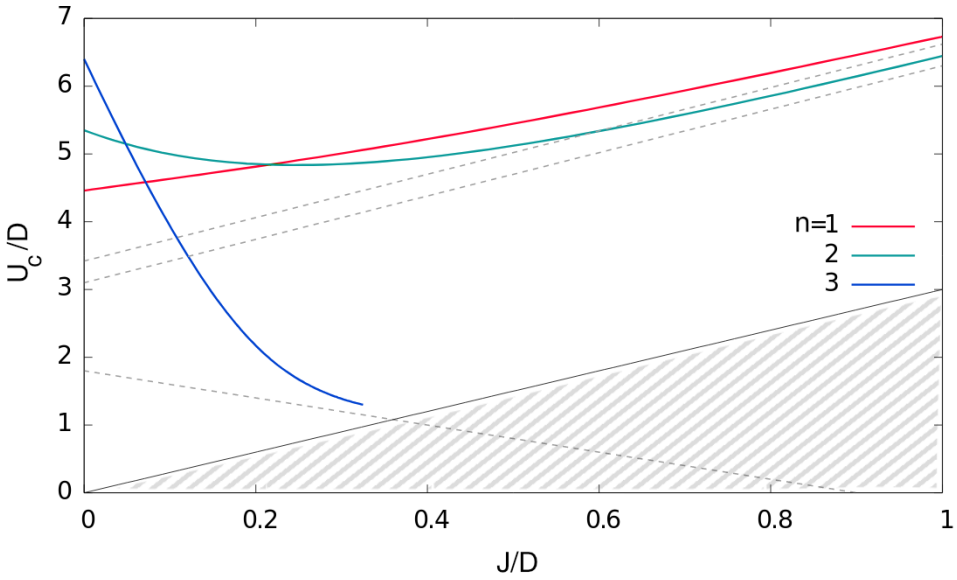

Figure 3.12: Critical interaction strength U_c for the Mott transition, as a function of Hund's coupling J, for a Hubbard-Kanamori model of three degenerate bands with one (red), two (green) and three (blue) electrons per site (identical results hold for $n > N$ due to the particle-hole symmetry). The model is solved with DMFT, with a semi-circular density of states of half-bandwidth D for each band. The dashed lines indicate the large J behavior calculated analytically in the atomic limit, Eq. (3.18). The shaded region corresponds to $U - 3J < 0$ ($J/U > 1/3$). See Ref. [77, 78].

In Fig. 3.12 we report the DMFT results for $U_c(J)$, comparing them with the results obtain in the atomic limit (3.18), for all integer fillings in the three-orbital Kanamori model. One can observe that the two results match at strong J, confirming that the simple Hubbard criterion and Eq. (3.18) capture perfectly the dependence of U_c on J [77]. However, large discrepancy is found for small values of Hund's coupling. We can understand this better if we evoke the $J = 0$ case. In this limit the hopping processes are not blocked by Hund's coupling, consequently giving rise to orbital fluctuations, which are the largest in the absence of J. This leads to a delocalizing effect which moves the critical U_c up to the higher values proportional to the band degeneracy [68] as we have discussed above.

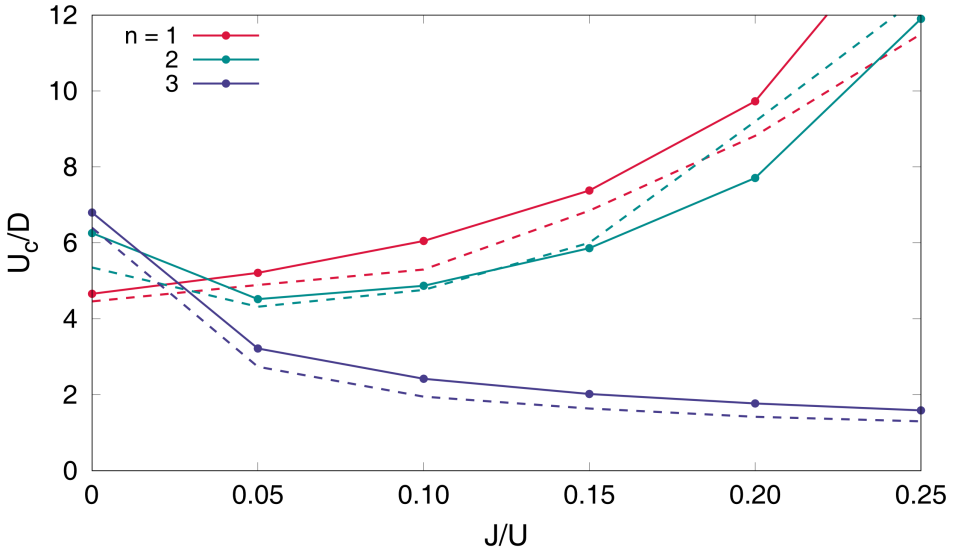

Figure 3.13: Gutzwiller and DMFT results for the metal-Mott insulator critical coupling U_c for the three-orbital degenerate Hubbard-Kanamori model as a function of the J/U ratio, at fillings $n \leq N$ (the ones for $n > N$ give identical results due to particle-hole symmetry). For half-filled cases (3 electrons in three orbitals) the Hunds coupling correlates the system and reduces the critical U_c/D. For all other fillings on the contrary U_c/D is strongly increased. The slight overestimation of U_c is a known issue of Gutzwiller (and slave-particle) approach. Nevertheless, the two techniques reveal the same qualitatively behavior.

Once we set $J \neq 0$ these orbital fluctuations get suppressed, which in turns blocks many of the hopping processes contributing to $\tilde{W}$, reflecting a fast reduction of U_c from the high values at $J = 0$. This is true for all cases but those in which the system is filled by one electron or one hole per site, $n = 1$, where the aforementioned scheme does not apply because the degeneracy of the atomic ground state is not split by the Hund's coupling. Eventually, it can be shown [71] that already at moderate values of J the orbital quenching is large enough to cause the effective width of the Hubbard bands $\tilde{W}$ to shrink to the single-orbital bandwidth W.

Accordingly, it is necessary to assume a J dependence of the width of the Hubbard bands, namely $\tilde{W} = \tilde{W}(J)$, to account for $U_c^n(J)$ behavior showed in Fig. 3.12. This leads to

$$U_c^n(J) \propto \begin{cases} \tilde{W}_{n,n}(J) - (N-1)J\,, & n = N\,, \\ \tilde{W}_{N,n}(J) + 3J, & \forall n \neq N\,, \end{cases} \tag{3.19}$$

where $\tilde{W}_{N,n}$ is an estimate of the available kinetic energy for n electrons hopping among N degenerate orbitals. Now becomes evident that at large J, where $\tilde{W}_{N,n} \sim W$, the Eq. (3.19) yields

a linear decrease of U_c at half-filling and a linear increase for $n \neq N$, as in the Hubbard criterion, which, actually, relies itself on assumption that J is already large enough [77, 78]. As a result, the atomic-limit argument is not able to explain a non-monotonous $U_c(J)$ at $n = 2$, which, on the another hand, is evident from Eq. (3.19). Namely, for generic commensurate filling $1 < n < N$, the reduction of $\tilde{W}_{N,n}(J)$ by orbital blocking is responsible for the decrease of U_c at small J, while the reduction of the atomic Δ^n_{at} (see Eq. (3.17)) is responsible for the increase of U_c at large J. The competition between these two effects gives the non-monotonous behavior in Fig. 3.12. We conclude that for $J = 0$, the largest value of U_c is obtained at half-filling $n = N$ and the smallest one for a single electron $n = 1$. This is reversed at moderate and large J, with U_c smallest for a half-filled shell. Once again, the insulating state is favored at half-filling. Indeed, most transition-metal oxides with a half-filled shell are insulators (some examples of relevant compounds shown in Fig. 3.14).

Finally, in Fig. 3.13 we present the results for the three-orbital degenerate Hubbard-Kanamori model obtained using the Gutzwiller method together with the DMFT results taken from Ref. [77, 78]. Apparently, DMFT fully confirms the reliability of the Gutzwiller method, despite the slight overestimation of U_c which is a known issue of Gutzwiller (and slave-particle) approach.

3.4.2 Density-dependence of the electron-electron correlations

We can now generalize our study to arbitrary densities. In Fig. 3.14 we show a color plot of the quasiparticle weight Z obtained in DMFT [76] for a fixed value $J/U = 0.15$ as a function of filling ($n = \langle \hat{n}_i \rangle$) and strength of the interaction U (normalized to the half-bandwidth D). The thick vertical bars are the regions where the system is a Mott insulator. The results at integer fillings are those presented in Fig. 3.10, with a very small critical U_c at global half-filling and a large value for the other integer fillings. The bottom region of small U is weakly correlated, and a clear and relatively sharp crossover takes place when the interaction is increased, leading to a large region of strongly correlated states (light color) which can be described as a bad metal. However, the onset of strong correlation effects as a function of U strongly depends on doping. In particular, the phase diagram appears to be to some extent controlled by the distance from the Mott transition point at half-filling. The plot in the full plane clearly shows one single region with small Z which origins around the Mott transition point for $n = 3$ and decays relatively slowly with doping, with a shape which is basically unaffected when we cross the other integer fillings.

Therefore, the region where the strongly correlated Hund's metal is found for integer fillings $n = 2$ and 4 does not appear to be connected to the Mott transition of that doping, which is pushed to large values of U, but rather it seems to be at least topologically connected with the half-filled Mott transition. For $n = 1$ the system clearly favors a good metallic behavior (except at large enough U/D value), meaning that the correlation strength is reduced, therefore U_c is enhanced. However, the low-energy physics of single-electron case is not affected by the presence of Hund's coupling, hence we will not discuss it in the following.

We notice that, in the absence of J, the same plots shows a series of correlated regions around the vertical bars marking the Mott insulators. Therefore, the effect of the Hund's coupling is to extend the impact of the half-filling Mott insulator in determining the degree of correlations. This effect has been noted, among the others in Ref. [11, 23], and it has been shown to be a crucial effect to understand the normal-state properties of iron-based superconductors in Ref. [14], where it has been linked to orbital selectivity and an orbital decoupling mechanism that we will address in the next section.

The observed particle-hole symmetry in Fig. 3.14 is a direct consequence of symmetric density of states. It is clear that considering some more realistic density of states will give

slightly asymmetric picture (see Ref. [78]). We remind that all these results are obtained in the paramagnetic state where no symmetry breaking is allowed. In this light the results can be seen as representative of the normal-state of real materials, above the ordering temperature.

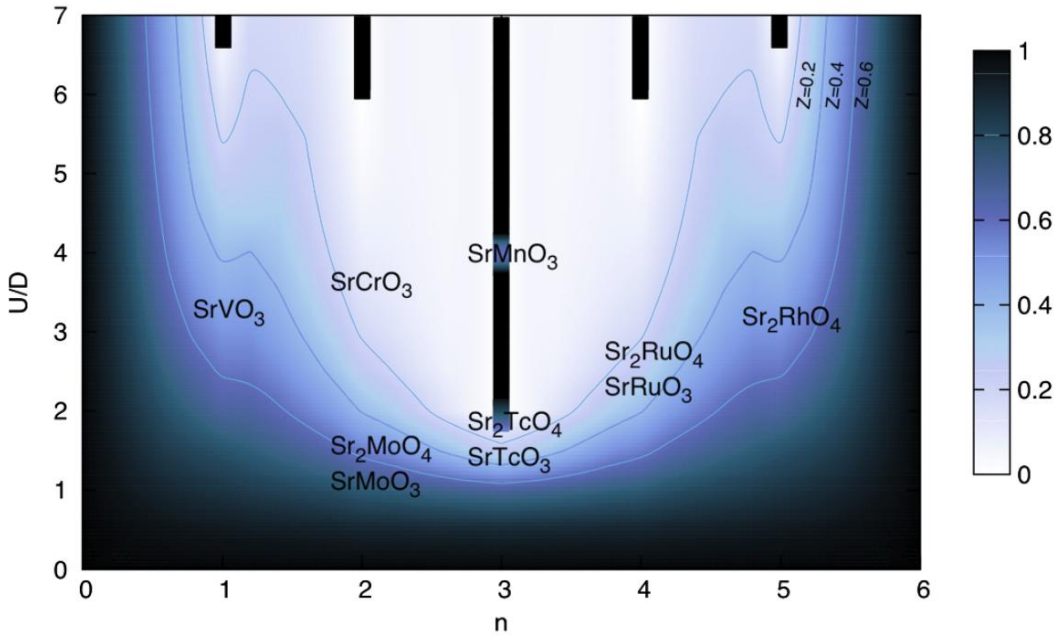

Figure 3.14: Color plot of the quasiparticle weight Z in a three orbitals model, for $J/U = 0.15$, as a function of filling and strength of the interaction U, normalized to the half-bandwidth D (taken from Ref. [76]), solved within DMFT approach. The thick black bars represents the Mott insulating phases for any integer filling. The metallic regime is presented with darker color, whereas the lighter regions correspond to bad metals. One can observe around the case with 2 electrons (or 2 holes) the system displays bad-metallic behavior in a wide range of the interaction strength.

A very similar picture can be drawn for larger number of orbitals. Indeed the arguments we gave for the appearance of the Janus physics for 2 electrons (holes) in three orbitals can be generalized to N orbitals populated by an integer number of electrons different from N. In fact, in Ref. [76] it is shown that the Janus effect gets more pronounced increasing the number of orbitals $N \geq 3$, and it is the strongest when $N \pm 1$ electrons populate N orbitals.

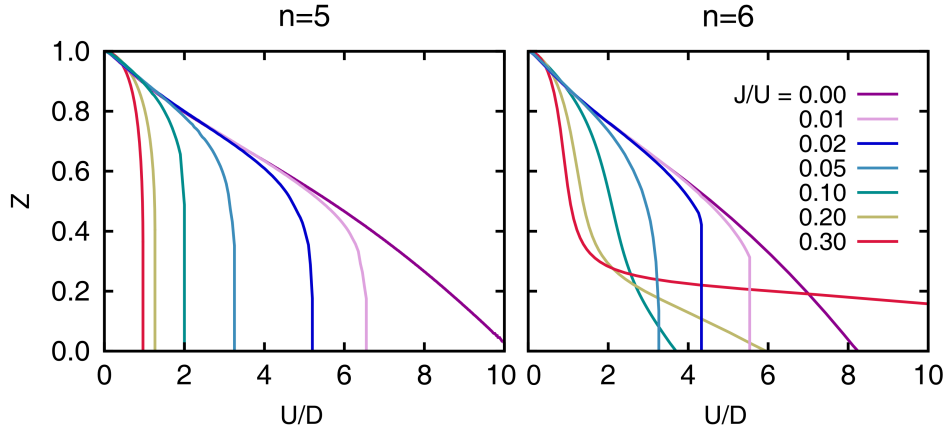

Figure 3.15: Quasiparticle weight Z as a function of Coulomb interaction U in a five-orbital degenerate Hubbard-Kanamori model, for different integer filling $n = 5, 6$. The presence of Hund's coupling J has different effect on these two cases, particularly $n = 6$, with the emergence of the Janus effect.

In Fig. 3.15 we present the results for the five-orbital case obtained within the Gutzwiller approach. The overall shape of the curves that define the quasiparticle weight is very similar to the ones presented in Fig. 3.10, and –as expected– the Janus effect is even stronger here [17, 76, 84, 85].

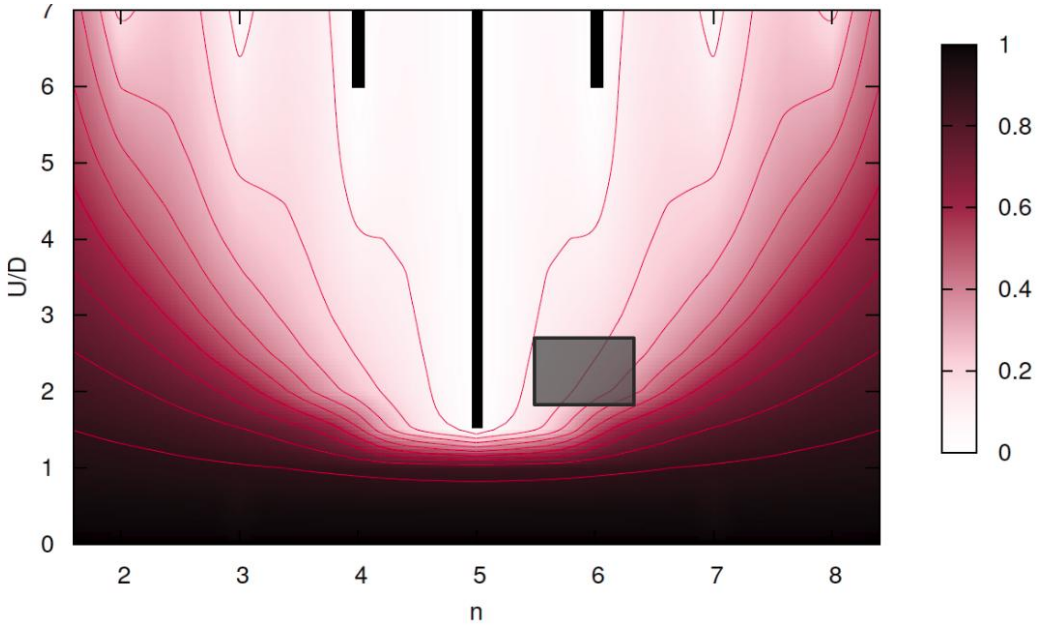

Figure 3.16: Color plot of the quasiparticle weight Z in a five orbitals model, for $J/U = 0.2$, as a function of filling and strength of the interaction U, normalized to the half-bandwidth D (taken from Ref. [17]), solved within Slave-spin mean-field approach. The thick black bars represents the Mott insulating phases for any integer filling. The metallic regime is presented with darker color, whereas the lighter regions correspond to bad metals. One can observe around the case with 4 electrons (or 4 holes) the system displays bad-metallic behavior in a wide range of the interaction strength. The shaded square shows the realistic range for the FeSC, (typical filling ranging from 5.5 to 6.2).

Fig. 3.16, taken from Ref. [17], reports the complete phase diagram for a five-orbital degenerate Hubbard model (with half-bandwidth D), showing the quasiparticle weight Z for different doping and interaction strength, at fixed value $J/U = 0.2$. The calculations are performed using Slave-spin mean-field approach. The region of parameters relevant for the iron-based superconductors is highlighted in a rectangular box. The plot suggests that the best way to understand the correlation effects in this regime is not to refer it to the Mott insulator at $n = 6$, but rather to describe them as arising from the doping of the half-filled Mott insulator, thereby establishing a new connection between iron-based superconductors and cuprates [14].

We notice that neglecting the spin-flip and pair-hopping terms does not have a crucial effect on the phase diagram, whose shape emerges as a general property of Hund's correlated systems.

3.4.3 Charge correlations in Hund's metals and orbital decoupling

In this section we explore in more depth the properties of the Hund's correlated metal that we have described in the previous sections. We will follow Ref. [20] where an extensive analysis of the charge-charge correlations has been carried out.

The analysis of the quasiparticle weight highlights a special role of the $n = 5$ region in determining the degree of correlations and its dependence on density as long as J/U is sufficiently large. In a single-band model the approach to the Mott transition can be mapped either via Z or

by the behavior of the charge fluctuations

$$C_{n_T} = \left\langle \hat{n}_T^2 \right\rangle - \langle \hat{n}_T \rangle^2 = \left\langle (\delta \hat{n}_T)^2 \right\rangle , \tag{3.20}$$

where $\hat{n}_T = \sum_{a=1,\ldots,N} \hat{n}_a$, $\hat{n}_a = \hat{n}_{a\uparrow} + \hat{n}_{a\downarrow}$, $\delta \hat{n}_T = \hat{n}_T - \langle \hat{n}_T \rangle$, and $\langle \hat{n}_T \rangle = n$. This quantity is indeed the most direct indication of Mott localization, which is nothing but the correlation-induced freezing of charge fluctuations.

From Fig. 3.17 one can trace the behavior of Z and C_{n_T} for fixed U as a function of J/U, for two electrons in three orbitals and six electrons in five orbitals. Clearly, this figure shows that the two quantities stop to behave similarly in multi-orbital models with sizable Hund's coupling. In particular we can clearly see that when the inclusion of J reduces Z as we discussed before, the charge-charge correlations increase, undoubtedly showing that the increase of correlations in the Hund's metal does not coincide with Mott localization.

We have observed that in the bad metallic regime (Fig. 3.17) we can drive the system towards the more correlated states and still have high charge fluctuations. However, so far we have shown the behavior of the total charge fluctuations.

Much more insight can be gained by observing that the total charge fluctuation consists not only of the intra-orbital charge fluctuations, defined as $C_n^{intra} = \left\langle \hat{n}_a^2 \right\rangle - \langle \hat{n}_a \rangle^2 = \left\langle (\delta \hat{n}_a)^2 \right\rangle$, where $\delta \hat{n}_a = \hat{n}_a - \langle \hat{n}_a \rangle$, and $\langle \hat{n}_a \rangle = n/N$, but also of the inter-orbital one, $C_n^{inter} = \langle \hat{n}_a \hat{n}_b \rangle - \langle \hat{n}_a \rangle \langle \hat{n}_b \rangle = \langle \delta \hat{n}_a \delta \hat{n}_b \rangle$ and $a \neq b$, which arises from the interaction between electrons in different orbitals. Considering N degenerate orbitals, we can write the following relation

$$C_{n_T} = N \left(C_n^{intra} + (N-1)\, C_n^{inter} \right) , \tag{3.21}$$

where C_n^{intra}, by definition positive or zero, is largest in the non-interacting limit. On the other hand, C_n^{inter} is negative for repulsive interactions and it vanishes in the absence of interactions as the charge in different orbitals is not correlated.

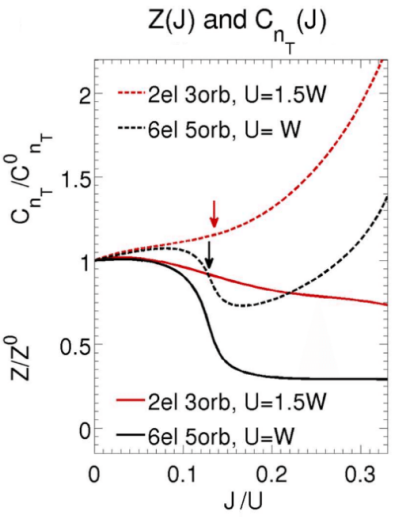

Figure 3.17: Quasiparticle weight Z and charge fluctuations C_{n_T} (renormalized) as a function of Hund's coupling J for fixed U value. The results are present for three- and five-orbital model, using the Slave-spin approach. The enhancement of C_{n_T} concomitant with the suppression of Z is evident. This behavior differs from the one associated to Mott correlated states [20].

The first thing to be observed from Fig. 3.18 is that C_n^{intra} (right panel), after the strong suppression, has a constant value both in the Mott phase (black) and Hund's metal (blue), defined by Z (left panel). On another hand, the entrance into the Hund's metal has a very strong effect on C_n^{inter}, that exhibits a modulation in J. Taking into account Eq. (3.21), having C_n^{intra} constant, brings to conclusion that the suppression of the inter-orbital part of charge fluctuations is responsible for the enhancement of the total charge fluctuations with J (due to the different sign of intra- and inter-part). Except at half-filling, C_n^{intra} and C_n^{inter} do not vanish in the Mott insulator but their contributions cancel each other leading to zero C_{n_T}.

The most convenient way to understand the previously described situation is to study the hopping processes in the system with N orbitals and $n \neq N$ electrons. For that purpose let us consider the hopping between two atoms with all present spins parallel one to each other such to satisfy the Hund's rules. If we allow for the hopping processes, an electron can happen to end up in an empty orbital with the spin parallel (a) or antiparallel (b) to the spins of all the other

present spins in the hosting atom, with the energy cost $E_{\uparrow\uparrow} = U - 3J$ or $E^{\uparrow\downarrow}_{inter} = U + (n-3)J$, respectively, or eventually an occupied orbital, forming the double occupied configuration (c) paying the energy $E^{\uparrow\downarrow}_{intra} = U + (n-1)J$ [2]. Fig. 3.19 shows these possible processed if $n = 2$ in three-orbital systems, say for simplicity, but the same hold for the particle-hole symmetric case, thus when $n > N$.

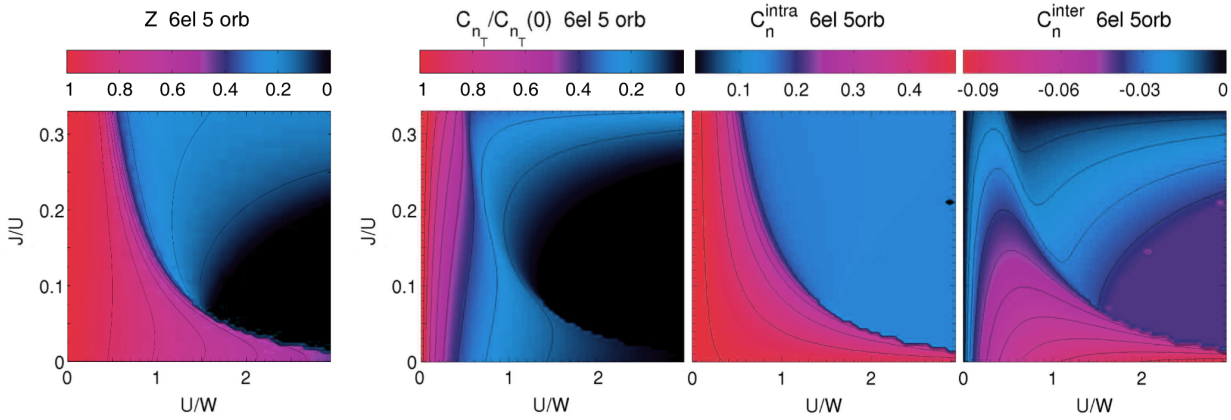

Figure 3.18: Left panel: Quasiparticle weight Z as a function of intra-orbital interaction U and Hund's coupling J for 6 electrons in five orbitals, the filling typical for undoped iron-based superconductors (U and J are in units of the bare bandwidth W and U). Right panel: Total, intra-orbital C_n^{intra} and inter-orbital C_n^{inter} charge fluctuations (renormalized) as a function of U and J for the same model [20]. See text for detailed explanation.

At half-filling, $n = N$, all the orbitals are occupied, hence the Pauli exclusion principle forbids the processes (a) and (b). On another hand, the (c) process controls the critical $U_c(J)$ for the Mott transition, and, as we have stressed so far, it is strongly decreased by the Hund's coupling J. Yet, for any other commensurate filling one finds that, increasing J, the process (a) becomes the most preferable one, whereas the U_c is pushed to the larger values [77].

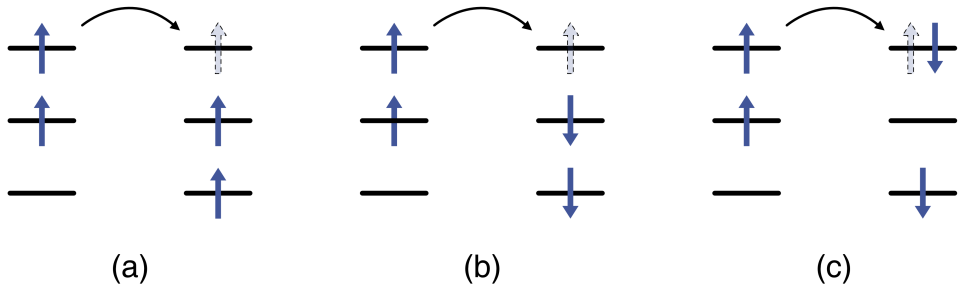

Figure 3.19: Hopping processes between two atoms with three orbitals and two electrons, in the presence of Hund's coupling. All present spins are parallel one to each other such to satisfy the Hund's rules. If we allow for the hopping processes, an electron can happen to end up in an empty orbital with the spin parallel (a) or antiparallel (b) to the spins of all the other present spins in the hosting atom, or eventually an occupied orbital, forming the double occupied configuration (c).

If we take a look at Fig. 3.18, we can see that the Mott insulating phase (characterized with $Z = 0$), where the doubly occupied configurations are completely suppressed, coincides with the region where C_n^{intra} is constant. Yet, this quantity remains constant also at the entrance of the Hund's metal, signalizing that the process (c) is excluded.

[2] For simplicity, only density-density interactions are included while calculating the interaction energy cost.

Process (b) is n-dependent such that it is suppressed by J for $n > 3$ and promoted for $n < 3$. For this reason one can notice a qualitative discrepancy in Fig. 3.17 between three-orbital systems with 2 electrons, and five-orbital with 6 electrons. Namely, in the former case the suppression of Z and the enhancement of C_{n_T} with J are smoother and favors the enhancement of C_{n_T}, whereas in the later case these quantities are a bit modified in some intermediate J-regime. Nevertheless, at large J limit for any $n \neq N$ filling, all the processes but (a) are completely blocked, giving rise to the spin polarized state in the Hund's metal.

Moreover, increasing the value of J the effective interaction between electrons, $U - 3J$, is decreasing, and finally vanishes when $J/U = 1/3$, together with the inter-orbital charge fluctuations. Particularly, this value is a characteristic of this model and we will come back to its physical meaning in the Chapter 5.

These arguments provide us with another characterization of a property which has been underlined in several previous studies of Hund's correlated models, namely a substantial reduction of the orbital correlations when we enter in the Hund's metal region[14, 24, 71, 77] which is also supported by the simple intuition that the spin is maximized by spreading the electrons in different orbitals and any attempt to change this orbital distribution will unavoidably lead to a decrease of the total spin, which is clearly against the effect of the Hund's coupling.

As a consequence, the orbitals in a Hund's correlated metal are effectively decoupled, a property which leads in turn to an increased tendency towards a differentiation of the correlation strength among the electrons in the various orbitals, as long as any small effect breaks the full orbital rotation invariance. It has been shown that such differentiation is connected to the presence of the half-filled Mott insulator even on filling ranges quite far from half.

Additionally, let us stress that the above argument was analytically confirmed in Ref. [71], performing the perturbative expansion on the two-orbital half-filled model (as being the most simple model to deal with, where one can assume the existence of the Hund's rule coupling). Indeed, it was shown that, in the large J limit, the critical interaction strength U_c at which the Mott transition occurs for each of the two orbitals decouple, owing to the presence of Hund's coupling J.

So far we have considered the fully degenerate Hubbard models, in order to understand the effect of Hund's coupling in the most general sense. Such system may be considered as an open playground for different investigations. Having each orbital independent gives possibility to perform independent tuning of the correlation strength in each orbital. Hence only by introducing a small difference in the model one may expect a wide range of new phenomena, leading to the coexistence of weakly and strongly correlated electrons in these materials. Therefore, in real materials we can discover that even small differences in the choice of parameters can give rise to the different physics in the correlated regime. Such scenario was supported by a wide range of experiments, as we will see in the following.

3.4.4 Orbital selectivity

We have seen that real materials, such as transition-metal oxides, can be described by multi-orbital models, where several orbitals are involved. This gives rise to quite rich and more complex physics that is still lacking of complete and clear description. It is, therefore, important to understand how different effects affect the Mott transition once we lift the orbital degeneracy (by introducing the crystal-field splitting, different bandwidths etc.). Eventually, one can find the extreme case of selective differentiation in correlations, where electrons in subset of orbitals are localized, while the rest of the system remain itinerant. This multi-stage quenching of the charge degrees of freedom has been named the orbital-selective Mott transition (OSMT) [86]. A variety of different mechanism have been shown to give rise to OSMT, but in virtually all cases

it turns out that the Hund's coupling favors this physics by promoting the orbital decoupling we have just described.

Different bandwidth

The simplest case of multi-orbital Hubbard model with different bandwidths, that captures all the relevant physics of such system, is the two-orbital Hubbard model with different hopping for the two orbitals, which has been analyzed in many studies [72, 82, 86–95] using different techniques. It was shown that, at half-filling, depending on the choice of the interactions present in the system, one can have the two-stage localization, coined as "orbital-selective Mott transition" (OSMT) [86], and consequently, an intermediate orbital-selective Mott phase (OSMP) where the wide-band electrons are metallic and the narrow-band ones are Mott localized. Furthermore, the stability of this intermediate phase strongly depends on how the Hund's rule coupling is taken into account. The results of previous studies can be summarized in Fig. 3.20 in form of two

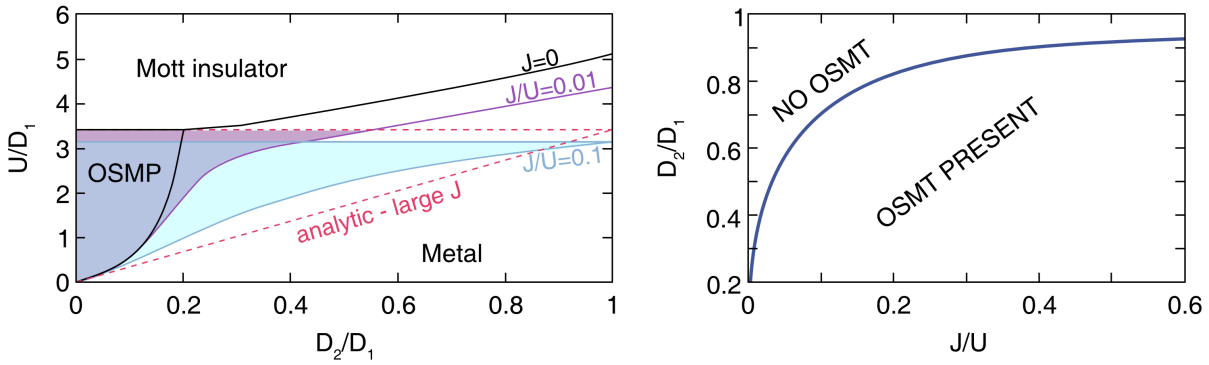

Figure 3.20: Left panel: Phase diagram of the two-orbital Hubbard model with different bandwidths, in dependence of bandwidth ratio (D_2/D_1) and interaction strength (U/D_1), for several values of Hund's coupling J/U and for $J = 0$ (adapted from [72] and obtained with Slave-spin mean-field treatment). The analytic result showing how in the large J limit the orbitals get decoupled is obtained in [71]. Right panel: the critical ratio $(D_2/D_1)_c$ below which an OSMT is observed as a function of J/U (results are taken from [95], and obtained within the Gutzwiller approach, coinciding with the predictions of Ref. [72]).

phase diagrams, depending on the interaction strength U, Hund's coupling J and bandwidth ratio D_2/D_1 (where $D_1 \neq D_2$ are the two different half-bandwidths of a semi-circular densities of states). An OSMP is observed in between a metal at low interaction strength U and a Mott insulator at high U (left). It is evident that the Hund's coupling favors the OSMP, due to the large extension of this region already for small J. These results were confirmed in detailed analytical investigation (also present in the plot) within Gutzwiller approach [95] and Slave-spin technique [71].

In the following we will present some sample calculations for three-band models which are more related to the content of the other chapters of this thesis. We start from some new calculations we performed in a three-orbital system with different bandwidths, with purely Coulomb interaction $U = U'$ and $D_1 = D_2 \neq D_3$, shown in Fig. 3.21. Also in this case we find an OSMT when the ratio D_3/D_1 is sufficiently small (the critical value is around 0.1) and a phase diagram which is very similar to the one of the two-orbital model (right panel). We show two sets of data for Z_1 and Z_3, one before and the other after the OSMT (left panel).

We underline that in this model, just like in the two-orbital version [71, 72, 95], a critical and relatively small values of the bandwidth ratio is necessary for the OSMT because the inter-orbital interaction allow for orbital fluctuations which would lead to a single Mott transition [71] as

shown in the left panel of the figure. These results were confirmed by DMFT calculations. However, they give clear evidence that the localized band is not a conventional Mott insulator but has spectral weight down to arbitrarily low energies [72, 95]. This subtle aspect is not captured by the Gutzwiller approximation and related mean-field theories.

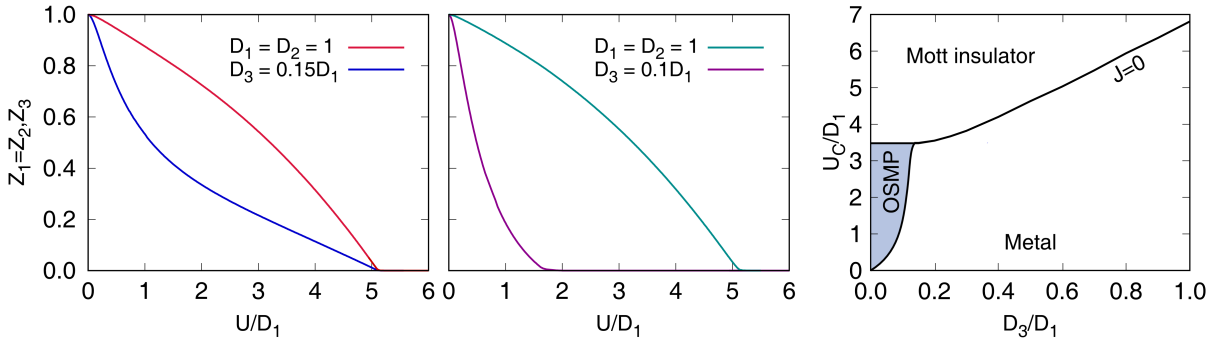

Figure 3.21: Left panel: Quasiparticle weight Z of the three-orbital Hubbard model with different bandwidths, for the wide bands $D_1 = D_2$ and for the narrow band D_3, obtained with the Gutzwiller wave-function for different ratios of the bandwidth D_3/D_1 and $J = 0$. Right panel: Phase diagram for the same model, done using the same method, in dependence of bandwidth ratio (D_3/D_1) and interaction strength (U/D_1). One can note the accordance with the results of Fig. 3.20 that presents the two-orbital case.

On another side, once Hund's coupling included, one finds that the OSMT is strongly favored already for small values of J, as depicted in Fig. 3.20. Indeed, the same was found in Ref. [77] for the three-orbital system with three different bandwidths, as shown in Fig. 3.22. A three-step Mott localization is found in the Slave-spin mean-field (left panel) and confirmed in the more accurate DMFT (right panel). Moreover, the plot for the later case shows the orbital correlations for this particular case. One can notice a strong suppression of the orbital fluctuations between localized and itinerant bands, leading to a decoupled behavior.

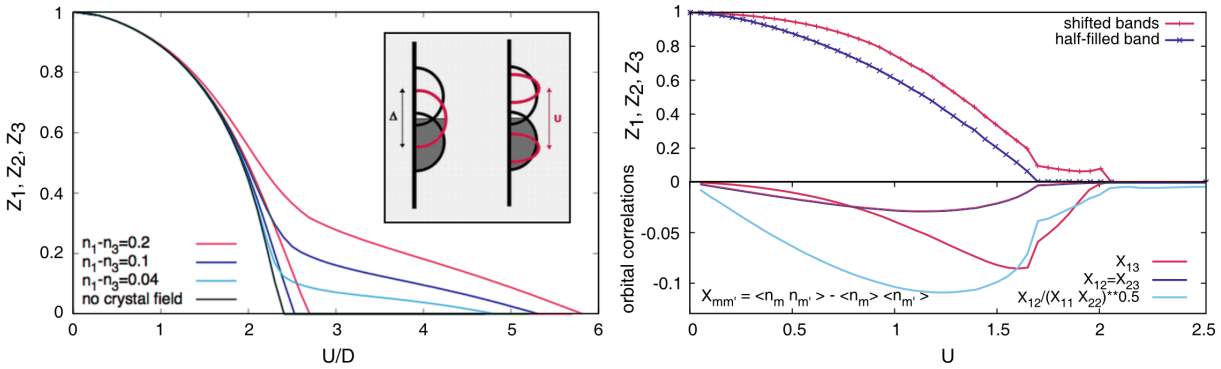

Figure 3.22: Left panel: Slave-boson results for for the quasiparticle weight Z of a three-orbital Hubbard model with bandwidths $W = 4, 2, 1$, for fixed Hund's coupling $J/U = 0.25$ and half-filling in each orbital. One can notice an almost completely decoupled behavior due to the presence of J. Right panel: The same model as the one assumed in the left panel, though results are obtained using DMFT method; the quasiparticle residue for each band (upper panel), and the orbital correlations (lower panel), which are suppressed between the localizing band and the itinerant ones, while they remain sizable between the two itinerant bands. Taken from Ref. [77].

Crystal-field

Different studies [24, 25, 70, 77, 86, 87, 96–98] have shown that an OSMT scenario can take place also when the symmetry between the orbitals is lifted by a crystal-field splitting rather than a difference between the bandwidths W. In such systems it is sufficient that the Hund's coupling J reaches a value above some critical J_c needed to trigger the OSMT. However, after many different attempts to describe the mechanism that would lead to an OSMT of such system [24, 25, 86, 96], it was only recently that such role was ascribed to the Hund's rule induced decoupling [20, 77].

In order to understand better this idea, let us consider a three-orbital model with equal bandwidths, populated with 4 electrons. Let us now assume the existence of a crystal-field splitting such that one orbital has a higher energy Δ with respect to the other. The phase diagram for this particular case was obtained using the Slave-spin mean-field approach and adjusting the crystal-field such to have the number of electrons per each band fixed [24], and it is reported in Fig. 3.23 (left).

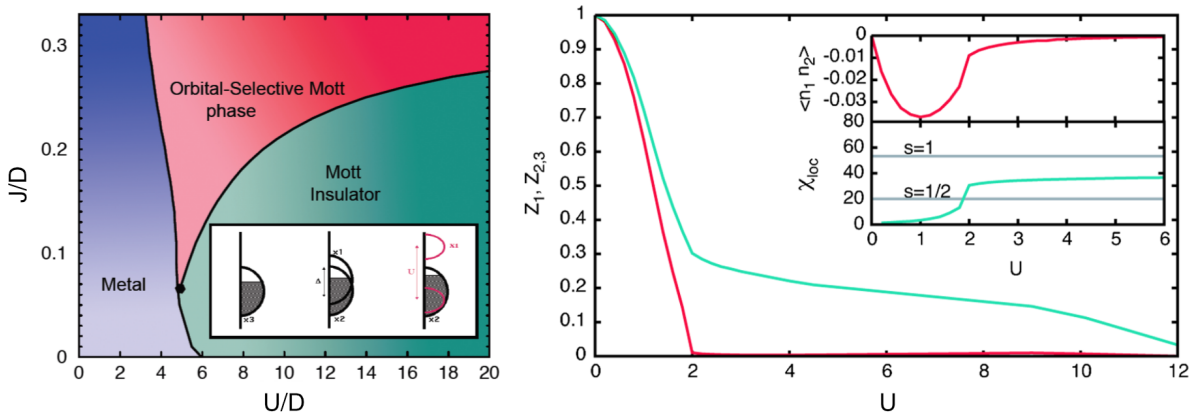

Figure 3.23: Orbital-selective Mott physics in presence of the Hund's coupling J: Left panel shows the phase diagram of a three-orbital Hubbard model populated by 4 electrons, in dependence of correlation strength U/D and Hund's coupling strength J/U. As shown in the inset, the crystal-field lifts the three-fold degeneracy such that the upper band becomes half-filled, whereas the lower two bands remain degenerate, populated with 3 electrons. An orbital-selective Mott phase, in which the half-filled band has a gap, is driven by J. Right panel presents the quasiparticle residue as a function of U/D, for fixed Hund's coupling $J/U = 0.25$ and populations for three bands, namely $n = (1, 1.5, 1.5)$. The results are obtained within DMFT approach. Inset: inter-orbital correlations (top panel) and local spin susceptibility (bottom panel). Reproduced from [24].

This setting will tune the orbital population. Namely, for $\Delta = 0$ all the orbitals will have a population $n_m = 4/3$ (where $m = 1, 2, 3$ is the orbital index). Increasing the splitting the higher band will become less and less populated, until it becomes exactly half-filled, whereas the lower two degenerate bands are filled with 3 electrons in total. If the Coulomb repulsion is large enough to cause the localization of this upper half-filled band, but yet smaller than the critical value for the remaining three electrons in the lower two bands, upper band opens a Mott gap and becomes selectively localized, while the other two remain metallic, leading to an OSMT. It is worth to underline that in this case the OSMT occurs despite the electrons have the same bandwidth and it is driven by a change in the occupation of the orbitals.

This phase is found for a finite Hund's coupling $J > J_c$, for quite large range of U and J values, with the tendency to widen as J is increased [24, 77]. On another hand, for $J < J_c$ a direct transition from a metal to a Mott insulator is found, as shown in Fig. 3.23 (left). Here the crucial mechanism is reaching the commensurate filling in the upper band, which is favored by the orbital decoupling mechanism we just discussed.

This description of this type of OSMT reminds the one done in the previously studied cases of systems with unequal bandwidth. However, unlike in case with different bandwidths, here the Hund's rule coupling J is the minimal requirement to induce OSMT and stabilize OSMP. Though the Mott insulator transition occurs when the Coulomb interaction strength reaches some critical value, as evident from Fig. 3.23, the OSMP is totally absent if $J = 0$ [98]. Therefore, as shown [77], the main effect causing the OSMT in these system of equal bands should be traced within the suppression of the orbital correlations induced by J, rather than the hopping processes of the kinetic content of such system. This picture is able to explain why simultaneously the Mott gap of the lower two bands occupied by a single hole diminishes with J, giving rise to the extended region of OSMP in the phase diagram.

The predictions of these Slave-spin calculations are confirmed by the more accurate DMFT, as shown in Fig. 3.23 (right). The quasiparticle weight of the upper orbital vanishes first, while the same quantity for the lower orbitals remains finite for the large extent of Coulomb coupling, even if it has a clear change in behavior when the upper orbital becomes localized. In the inset one can observe the behavior of the inter-orbital charge fluctuations compared with the spin susceptibility. For small interaction strength, the enhancement of correlations is the consequence of the predominant role of U. Nevertheless, once the effect of J starts being important, the electrons tend to localize more and to form local high-spin states (as shown by the plot of the magnetic response in the bottom panel). The inter-orbital charge correlations begin to decrease, slowly approaching zero-value, signaling the effective decoupling of the bands. At this point the upper band localizes, exploiting the orbital decoupling to completely separate its destiny from the others.

The interplay between the crystal-field splitting and the Hund's rule coupling terms induces the redistribution of electrons among the different orbitals (and correspondingly in each band, if there is no hybridization), giving rise to different individual band filling [71, 77]. This leads to a rich variety of phase diagrams [98]. However, we will not go through some deeper investigation of an OSMP itself, since it is out of the scope of this work. The main point was to stress the role of Hund's coupling in such systems, which brings a large range of further investigations and different phenomena. We suggest further reading in Ref. [70, 72, 77, 97, 98], where more involved effects of different parameters' interplay are discussed. Specifically, Ref. [70] gives a comparison with realistic transition-metal oxides that can be described with partially lifted t_{2g} shell, making these predictions more reliable.

Up to now we did a brief review of the simple examples of non-degenerate systems, where crystal-field splittings or bandwidth differences characterize the unequal orbitals. We have seen that in such systems the Hund's coupling indeed acts as a band-decoupler, giving rise to the individual behavior of each orbital, depending on the structure and filling. On another side, the inter-orbital hopping or local hybridization acts against Hund's rule coupling. In principle, this is also true for the crystal-field splitting (since the both effects favor a singlet ground state, unlike Hund's rule that tends to maximize the spin locally). However as long as the effect of Hund's coupling remains predominant, the presence of hybridization can be treated as a perturbation which competes with the orbital-selective physics. Moreover, the OSMP of such system is typically turned into a phase with coexistence of strongly and weakly correlated electrons in the same conduction bands. Recent investigations [14] showed that such scenario can be the basis of the correlation properties in the normal state of iron-based superconductors.

4

The Gutzwiller variational method

As we have discussed in the Introduction, the solution of many-body fermionic systems with strong correlations has been so far elusive even for the simple single-band Hubbard model, except fot the limiting cases of one and infinite dimensions. This led to the development of a variety of different theoretical techniques ranging from fully numerical approaches to more analytical approaches.

One of the simplest, yet effective, approaches is based on the variational wave-function and the connected approximation introduced in the early 60's by Martin C. Gutzwiller [99–101] to describe magnetic metals, and particularly itinerant ferromagnetism in the framework of a Hubbard model. The main idea of this method was to include electronic correlations on an otherwise uncorrelated wave-function $|\Psi_0\rangle$ by defining the independent local projectors $\mathcal{P}_i$ that act on the local Hilbert space at site i. The role of $\mathcal{P}_i$ was to project out, partially or completely, the configurations in $|\Psi_0\rangle$ that contain double occupancy (in the case of the single-band Hubbard model), in order to reduce the energy cost on each site. This was accomplished by introducing the Gutzwiller variational wave-function of the form

$$|\Psi_G\rangle = \mathcal{P}_G\,|\Psi_0\rangle = \prod_i \mathcal{P}_i\,|\Psi_0\rangle\ . \tag{4.1}$$

where the Gurzwiller projector $\mathcal{P}_G$ is given as a product of local projectors $\mathcal{P}_i$. In the original formulation by Gutzwiller, the projector was parameterized as $\mathcal{P}_i = g_i^{D_i}$, where D_i is the local double occupation operator on site i. The idea is to use the standard variational principle and minimize the energy as a function of the parameters g_i. Despite the simplifiation, the expectation value of the Hamiltonian can not be computed analytically in two and three dimensions, and one has to either resort to a numerical evaluation or to a futher approximation. The latter direction has been taken by Gutzwiller and it will be pursued also in the present thesis.

Of course, the limited variational freedom and the further approximation limit the use of the approach. In particular, genuine Mott insulators without spatial symmetry breaking can not be obtained by Gutzwiller wave-function in the case of singe-band Hubbard model. The approximation proposed by Gutzwiller [101] failed in predicting a ferromagnetic ground state in one dimension, but Gutzwiller realized that its accuracy improved in two and three dimensions [101]. Nevertheless, it was two decades later that the work of Metzner and Vollhardt [102, 103] showed that Gutzwiller approximation was actually variationally exact in the limit of the infinite dimen-

sionality. Even if the method is not able to describe a Mott insulator, it provides a reasonable and effective description of the disappearance of the metallic solution, usually referred to as Brinkman-Rice transition.

The success of Gutzwiller approximation in describing the strongly correlated single-band model gave rise to the generalization of this approach to more realistic complex systems. Bunemann, Gebhard and collaborators developed an approach particularly suitable for the case of multi-orbital models [104, 105]. This approach was later on extended by Fabrizio and Lanatá [106–108]. They introduced a parametrization that simplifies further numerical calculations, bringing into connection Gutzwiller approximation with the Rotationally-invariant slave-boson approach (RISB) [83], previously introduced by Lecherman and coworkers.

4.1 The Gutzwiller approximation for multi-orbital systems

Let us consider the following tight-binding multi-orbital Hubbard Hamiltonian:

$$\mathcal{H} = -\sum_{\langle i,j\rangle}\sum_{\alpha,\beta=1}^{2M}\left(t_{ij}^{\alpha\beta}c_{i\alpha}^{\dagger}c_{j\beta} + h.c.\right) + \sum_{i}\mathcal{U}_i\,, \tag{4.2}$$

where operator $c_{i\alpha}^{\dagger}$ creates and $c_{j\beta}$ annihilates an electron at site i and j, respectively, and indices α and β denote single particle states and stand both for different orbital (assuming M orbitals) and spin ($\uparrow$ and $\downarrow$) degrees of freedom. The first term, that we will label as $\mathcal{H}_0$, accounts for the kinetic energy where $t_{ij}^{\alpha\beta}$ represents the hopping amplitude between the two nearest neighbors sites i and j, whereas the second term is associated to a purely local many-body interaction $\mathcal{U}_i$.

Having more than one orbital on each site i gives rise to several different electronic configurations in the local Hilbert space, that are denoted as $|\Gamma, i\rangle$ and of the form

$$|\Gamma, i\rangle = \left(\prod_{\alpha\in\Gamma} c_{i\alpha}^{\dagger}\right)^{n_\alpha}|0\rangle_i\ , \tag{4.3}$$

where $|0\rangle_i$ is the local vacuum state of a given site i and $n_\alpha = 0, 1$ ($\alpha = 1, ..., 2M$) are occupation numbers that define the Fock states $|\Gamma, i\rangle$. Knowing this, one can now define the projection operator $\mathcal{P}_i$ in the most general way as

$$\mathcal{P}_i = \sum_{\Gamma\Gamma'}\lambda_{i\Gamma\Gamma'}\,|\Gamma, i\rangle\langle\Gamma', i|\ . \tag{4.4}$$

Here $\lambda_{i\Gamma\Gamma'}$ represents the variational parameters that modify the weights of the on-site electronic configurations $|\Gamma, i\rangle$ with respect to their values in the uncorrelated wave-function $|\Psi_0\rangle$. Particularly, the role of the operator $\mathcal{P}_i$ in the single-band Hubbard model is to decrease the weight of doubly occupied configurations, in order to minimize the Coulomb repulsion $\mathcal{U}_i$. In a multi-orbital Hubbard model, the effect of the Coulomb interaction is to reduce the weight of configurations with a local occupation different from the average value. If other interactions, such as the Hund's exchange coupling, or single-particle effects like a crystal-field splitting are included, less obvious contraints are imposed on the local configurations, leading to a richer physical picture.

Therefore our goal is to try to calculate the variational parameters $\lambda_{i\Gamma\Gamma'}$ by acting with the projector $\mathcal{P}_i$ on the variational function $|\Psi_0\rangle$, as it follows from Eq. (4.1). Given that for the method we are dealing with is convenient to choose $|\Psi_0\rangle$ as a single-particle wave-function such that the Wick's theorem [109] holds (for reasons that will be more clear later). Since we are

not discussing superconducting solutions or spin-orbit coupling, we use a single-particle Slater determinant.

Eventually, both $\mathcal{P}_i$ and $|\Psi_0\rangle$ have to be determined in the variational way [110] by minimizing the average value of the Hamiltonian (4.2) such that

$$E = \frac{\langle \Psi_G | \mathcal{H} | \Psi_G \rangle}{\langle \Psi_G | \Psi_G \rangle} , \tag{4.5}$$

where $E > E_0$ since the variational principle gives us an upper bound to the ground state energy E_0. Obviously, the ground state found this way gives us the best approximation to the true ground state of our Hamiltonian $\mathcal{H}$.

The exact analytical evaluation of the average values over the variational wave-function $|\Psi_G\rangle$ is possible only in the limit of infinite dimensionality or (equivalently) coordination number $z \to \infty$, where the variational calculation reduces to calculate expectation values on the Slater determinant uncorrelated wave-function $|\Psi_0\rangle$. This is analytically feasible since Wick's theorem applies, and it is shown in the Appendix B how one can manipulate and simplify all the expressions that come in the following, in order to get manageable formulas. We recall that the same approximation has been proposed by Gutzwiller as a sort of spatial mean-field approximation. As a matter of fact, the limit of infinite coordination enforces a spatial mean-field.

The analytical treatment is possible as long as these two constraints are satisfied [105]:

$$\langle \Psi_0 | \mathcal{P}_i^\dagger \mathcal{P}_i | \Psi_0 \rangle = 1 , \tag{4.6a}$$

$$\langle \Psi_0 | \mathcal{P}_i^\dagger \mathcal{P}_i C_i | \Psi_0 \rangle = \langle \Psi_0 | C_i | \Psi_0 \rangle , \tag{4.6b}$$

where C_i is the local single particle density matrix operator at site i, with the elements $c_{i\alpha}^\dagger c_{i\beta}$ $(\forall \alpha, \beta)$[1]. In the expression (4.6) the equality (a) is always satisfied, without reducing the variational freedom, since $\mathcal{P}_i$ is defined up to a normalization factor, whereas the equation (b) limits it. Nevertheless, the advantage of the expression (b) lies in the fact that the density matrix of the non-interacting system $\langle \Psi_0 | C_i | \Psi_0 \rangle$ is trivially known, which simplifies the further calculations. However, one should not be induced by the expression (b) to believe that the correlated and uncorrelated local density matrices have to coincide. In fact, in general one finds $\langle \Psi_G | C_i | \Psi_G \rangle \neq \langle \Psi_0 | C_i | \Psi_0 \rangle$. Regardless, as long as the Gutzwiller correlator $\mathcal{P}_i$ commutes with the local density-matrix C_i [105, 111], the total number of electrons calculated on the variational wave-function $|\Psi_G\rangle$ and $|\Psi_0\rangle$ is the same (and it is a conserved quantity).

These expressions are exact only when $z \to \infty$ and the calculation of the expectation values on the Gutzwiller wave-function is simplified. However, we can enforce the same constraints and exploit the same simplifications also in finite dimensions, where they imply an approximation with respect to the exact variational calculation. This way one encounters the so-called Gutzwiller approximation.

4.1.1 The expectation values in infinite lattice coordination

As stressed before, the Gutzwiller approach is variationally exact only in the limit of infinite coordination lattice, provided that the constraints (4.6) are satisfied. This originates from the fact that all expectation values turn out to be purely local in this limit.

[1] In the most general case, the single particle density matrix C_i contains also the off-diagonal terms, $c_{i\alpha}^\dagger c_{i\beta}^\dagger$ and $c_{i\alpha} c_{i\beta}$. Since they contribute to the superconductivity problem, which is not of our interest, we will not take them into account.

Recalling Eq. (4.1) and imposing the two conditions, we can calculate all the average values of interest for our problem in the spirit of the Gutzwiller approximation.

Local operator

Let us assume a general local many-body operator O_i acting on a site i. The expectation value can be reduced in infinite lattice coordination (see Appendix B), giving

$$\langle \Psi_G | O_i | \Psi_G \rangle = \langle \Psi_0 | \mathcal{P}_i^\dagger O_i \mathcal{P}_i | \Psi_0 \rangle \ . \tag{4.7}$$

If we now recall expression (4.2), we can rewrite the interacting part of the Hamiltonian as

$$\langle \Psi_G | \mathcal{U}_i | \Psi_G \rangle = \langle \Psi_0 | \mathcal{P}_i^\dagger \mathcal{U}_i \mathcal{P}_i | \Psi_0 \rangle \ . \tag{4.8}$$

Non-local operator

In addition it also follows that

$$\langle \Psi_G | O_{ij} | \Psi_G \rangle = \langle \Psi_0 | \mathcal{P}_i^\dagger \mathcal{P}_j^\dagger O_{ij} \mathcal{P}_i \mathcal{P}_j | \Psi_0 \rangle \ . \tag{4.9}$$

This expression is valid only for the non-local one-particle operator.

Now, if we return back to Hamiltonian (4.2), we find that the expectation value of a quadratic off-site operator $c_{i\alpha}^\dagger c_{j\beta}$ has the following form:

$$\langle \Psi_G | c_{i\alpha}^\dagger c_{j\beta} | \Psi_G \rangle = \langle \Psi_0 | \mathcal{P}_i^\dagger \mathcal{P}_j^\dagger c_{i\alpha}^\dagger c_{j\beta} \mathcal{P}_i \mathcal{P}_j | \Psi_0 \rangle \ . \tag{4.10}$$

where we have taken advantage of the constraints (4.6) for local quantities. We can rewrite Eq. (4.10) as

$$\langle \Psi_0 | \left(\mathcal{P}_i^\dagger c_{i\alpha}^\dagger \mathcal{P}_i \right) \left(\mathcal{P}_j^\dagger c_{j\beta} \mathcal{P}_j \right) | \Psi_0 \rangle \ . \tag{4.11}$$

given that a local projector $\mathcal{P}_i$ commutes with all the other projectors and operators that act on the sites different than i.

A simple way to proceed is to define the parameter $R_{i\beta\gamma}$ from the equality

$$\langle \Psi_0 | c_{i\alpha}^\dagger \mathcal{P}_i^\dagger c_{i\beta} \mathcal{P}_i | \Psi_0 \rangle = \sum_\gamma \langle \Psi_0 | c_{i\alpha}^\dagger c_{i\gamma} | \Psi_0 \rangle R_{i\beta\gamma} \ , \tag{4.12}$$

which is itself a function of both $|\Psi_0\rangle$ and $\mathcal{P}_i$. After some computational manipulation (see Appendix B), we arrive to the expression

$$\langle \Psi_G | c_{i\alpha}^\dagger c_{j\beta} | \Psi_G \rangle = \sum_{\gamma\delta} R_{i\gamma\alpha}^\dagger R_{j\beta\delta} \langle \Psi_0 | c_{i\gamma}^\dagger c_{j\delta} | \Psi_0 \rangle \ . \tag{4.13}$$

Calculating the expectation values of off-site quadratic operators, putting in relation eqs. (4.11), (4.12) and (4.13), one finds that creation and annihilation operator are effectively renormalized:

$$c_{i\alpha}^\dagger \to P_i^\dagger c_{i\alpha}^\dagger P_i = \sum_\gamma R_{i\alpha\gamma}^* c_{i\gamma}^\dagger \ , \qquad c_{j\beta} \to P_j^\dagger c_{j\beta} P_j = \sum_\delta R_{j\beta\delta} c_{j\delta} \ , \tag{4.14}$$

namely a particle with given quantum numbers turns into a linear combination of effective particles (quasiparticles) with all the possible quantum numbers and amplitudes given by the matrix elements of the matrix R_i. The non-diagonal character of the mapping between physical fermions and quasiparticles is a very important feature which generalizes over the original

Gutzwiller of Slave-boson formulation. In the context of Slave-boson this is a key aspect of the RISB method.

If we now write down (4.13) together with the hopping amplitude $t_{ij}^{\alpha\beta}$, we get the average value of the non-interacting part of the Hamiltonian (4.2) that we shall denoted as E_*:

$$E_* = \langle\Psi_G|\mathcal{H}_0|\Psi_G\rangle = \sum_{ij}\sum_{\alpha\beta} t_{ij}^{\alpha\beta}\,\langle\Psi_G|c_{i\alpha}^\dagger c_{j\beta}|\Psi_G\rangle = \sum_{ij}\sum_{\gamma\delta} t_{*ij}^{\gamma\delta}\,\langle\Psi_0|c_{i\gamma}^\dagger c_{j\delta}|\Psi_0\rangle = \langle\Psi_0|\mathcal{H}_*|\Psi_0\rangle\ , \tag{4.15}$$

where R_i renormalizes the hopping amplitude

$$t_{*ij}^{\gamma\delta} = \sum_{\alpha\beta} R_{i\gamma\alpha}^\dagger t_{ij}^{\alpha\beta} R_{j\beta\delta}\ . \tag{4.16}$$

This way we can define a new one-body effective Hamiltonian $\mathcal{H}_*$ with the renormalized hopping amplitudes $t_{*ij}^{\gamma\delta}$

$$\mathcal{H}_* = \sum_{ij} t_{*ij}^{\gamma\delta} c_{i\gamma}^\dagger c_{j\delta} \tag{4.17}$$

Once we diagonalize $\mathcal{H}_*$ in momentum space, we get the set of eigenfunctions that describe the metallic states. These renormalized single-particle states can be connected to the concept of Landau quasiparticles, where $\mathcal{H}_*$ can be interpreted as the non-interacting Hamiltonian of the quasiparticle, and the overall renormalization factor described by Eq. (4.16) can be associated with the quasiparticle weight Z, i.e., the weight of coherent low-energy excitation in the interacting many-body spectrum. Due to the local character of the approximation, which would correspond to a momentum-independent self-energy one has $Z = m_0/m^*$, where m_0 is the bare band mass, and m^* is the interaction-induced effective mass, which measures the reduction of the mobility of the quasiparticle excitations due to the strong interactions. The increase m^*/m_0 describes how a good metal turns into a bad one, and a divergent effective mass (or vanishing Z) signals Mott localization. As a matter of fact, following the behavior of Z will be the signature of Mott localization in all our analysis with the Gutzwiller approximation.

4.1.2 Variational problem

Finally, we can write down the expression for the expectation value of the generic tight-bonding multi-orbital Hubbard model (4.2):

$$E\left[\mathcal{P}_i, \Psi_0\right] = \langle\Psi_G|\mathcal{H}|\Psi_G\rangle = \langle\Psi_0|\mathcal{H}_*|\Psi_0\rangle + \sum_i \langle\Psi_0|\mathcal{P}_i^\dagger \mathcal{U}_i \mathcal{P}_i\,|\Psi_0\rangle\ . \tag{4.18}$$

The variational problem consists of variationally determining both $|\Psi_0\rangle$ and $\mathcal{P}_i$ by minimizing the average energy (4.18), under condition that $\langle\Psi_G|\Psi_G\rangle = 1$ is normalized. The Slater determinant that minimizes the energy E is the ground state of the non-interacting Hamiltonian $\mathcal{H}_*$, as it follows from Eq. (4.15).

While solving this problem, one encounters two main drawbacks: (I) $|\Psi_0\rangle$ and $\mathcal{P}_i$ are connected by the constraints (4.6) hence they are not independent variables; (II) in case of multi-orbital models one should be careful since the number of variational parameters scales exponentially with the number of orbitals. In order to further simplify this problem, let us introduce a new parametrization [106–108], which, apart of giving solution for (I) and significantly reducing the number of variational parameters in (II), it also includes the possibility to treat multi-orbital systems with arbitrary on-site interactions and hybridizations.

4.2 Reformulation of the Gutzwiller approach

In the previous section we have introduced the main concepts behind the Gutzwiller formalism. We not introduce some recent extensions. It turns out that this approach is equivalent to the Rotationally-invariant slave-bosons (RISB), which have been introduced in Ref. [83]. In order to simplify our problem, we introduce two slight modifications to our formulation, which actually resembles the RIBS formalism.

Let us start from the definition of the projector $\mathcal{P}_i$ in Eq. (4.4). Here $|\Gamma, i\rangle$ and $\langle\Gamma', i|$ are standard many-body Fock states where we populate states of fixed spin and orbital indices. We will refere henceforth to this basis as the "original basis".

Now we can also introduce the uncorrelated local probability distribution $\hat{P}_i^0$ with elements [106]

$$P^0_{i\Gamma\Gamma'} \equiv \langle\Psi_0|\,|\Gamma', i\rangle\,\langle\Gamma, i|\,|\Psi_0\rangle = \delta_{\Gamma\Gamma'} P^0_{i\Gamma}\,. \tag{4.19}$$

We can define a matrix $\hat{\lambda}_i$ (the hat will be used to denote matrices in the following) with linear dimension equal to the size of the local Hilbert space whose elements are the variational parameters $\lambda_{i\Gamma\Gamma'}$ and introduce a new definition [106, 107]

$$\hat{\phi}_i = \hat{\lambda}_i \sqrt{\hat{P}_i^0}\,, \tag{4.20}$$

Since $\hat{P}_i^0$ are positive quantities according to Eq. (4.20) the square root is always defined. The choice of this trivial redefinition will become clear in the following.

Consequently, with the above definition we can conveniently recast the two conditions (4.6) into the following form

$$\mathrm{Tr}\left(\hat{\phi}_i^\dagger \hat{\phi}_i\right) = 1\,, \tag{4.21}$$

$$\mathrm{Tr}\left(\hat{\phi}_i^\dagger \hat{\phi}_i \hat{c}_{i\alpha}^\dagger \hat{c}_{i\beta}\right) = \langle\Psi_0|c_{i\alpha}^\dagger c_{j\beta}|\Psi_0\rangle\,. \tag{4.22}$$

In Eq. (4.22) also the fermionic operators are represented as matrices acting on the local Hilbert space

$$c_{i\alpha} \rightarrow (c_{i\alpha})_{\Gamma\Gamma'} = \langle\Gamma, i|\, c_{i\alpha}\,|\Gamma', i\rangle\,. \tag{4.23}$$

As before, the expectation values of all the operators within the Gutzwiller formalism can be evaluated in infinite coordination lattice, imposing these two conditions. Hence the expectation value of any local observable O_i is given by [105, 106]

$$\langle\Psi_G|O_i|\Psi_G\rangle = \mathrm{Tr}\left(\hat{\phi}_i^\dagger \hat{O}_i \hat{\phi}_i\right)\,. \tag{4.24}$$

We can now express Eq. (4.8) in terms of this matrix formulation, and the local term becomes:

$$\langle\Psi_G|\mathcal{U}_i|\Psi_G\rangle = \langle\Psi_0|\mathcal{P}_i^\dagger \mathcal{U}_i \mathcal{P}_i|\Psi_0\rangle = \mathrm{Tr}\left(\hat{\phi}_i^\dagger \hat{U}_i \hat{\phi}_i\right)\,. \tag{4.25}$$

The elements of the matrix $\hat{U}_i$ read as

$$\left(\hat{U}_i\right)_{\Gamma\Gamma'} = \langle\Gamma, i|\,\hat{U}_i\,|\Gamma', i\rangle \tag{4.26}$$

having $|\Gamma, i\rangle$ and $|\Gamma', i\rangle$ as a local Fock states.

Recalling Eq. (4.12) one straightforwardly obtains the wave-function renormalization $\hat{R}_i$ inverting the equation

$$\langle\Psi_0|c^\dagger_{i\alpha}\mathcal{P}^\dagger_i c_{i\beta}\mathcal{P}_i|\Psi_0\rangle = \mathrm{Tr}\left(\sqrt{\hat{P}^0_i}\hat{c}^\dagger_{i\alpha}\frac{1}{\sqrt{\hat{P}^0_i}}\hat{\phi}^\dagger_i\hat{c}_{i\beta}\hat{\phi}_i\right) = \sum_\gamma \mathrm{Tr}\left(\hat{\phi}^\dagger_i\hat{\phi}_i\hat{c}^\dagger_{i\alpha}\hat{c}_{i\gamma}\right)R_{i\beta\gamma} = \sum_\gamma \langle\Psi_0|c^\dagger_{i\alpha}c_{i\gamma}|\Psi_0\rangle R_{i\beta\gamma} \tag{4.27}$$

$R_{i\beta\gamma}$ being a matrix element of a matrix $\hat{R}_i$.

At this point we can notice that within this redefinition of the Gutzwiller problem the interaction energy contribution (4.25) (and in general all the local expectation values) depends only on the parameters $\phi_{i\Gamma\Gamma'}$ that define the matrix $\hat{\phi}_i$, whereas the Slater determinant $|\Psi_0\rangle$ still enters in the expectation value of the hopping term by means of (4.27). Hence also in the matrix formulation the renormalization factor in Eq. (4.27) still retains its complicated form. It will be shown that this can be improved passing to a new representation simply by performing a transformation of the basis in the local Fock state.

4.2.1 Mixed state representation

In order to obtain a more efficient numerical implementation of the Gutzwiller approximation for multi-orbital problems with general interactions and single-particle terms, it is convenient to introduce a new representation. Therefore, let us introduce a new basis $|n,i\rangle$, defined by $f_{i\alpha}$ operators and related with the original ones $c_{i\alpha}$ by unitary transformation $\hat{W}_i$ such that

$$\mathcal{W}^\dagger_i c_{i\alpha}\mathcal{W}_i = f_{i\alpha} = \sum_\beta W_{i\alpha\beta}c_{i\beta} \tag{4.28}$$

where the unitary operator $\mathcal{W}$ maps $c_{i\alpha}$ onto a new basis set $f_{i\alpha}$ of single-particle operators. Let us choose $\mathcal{W}$ such that it diagonalizes the local density matrix operator $C_{i\alpha}$ in the Slater determinant

$$\langle\Psi_0|f^\dagger_{i\alpha}f_{i\beta}|\Psi_0\rangle = \delta_{\alpha\beta}n^0_{i\alpha} \tag{4.29}$$

having $0 \leq n^0_{i\alpha} \leq 1$ as its eigenvalues. Hereafter, we will refer to this new basis as the *natural basis*. As we shall see the introduction of this basis leads to a very useful simplification of the formalism.

If we now redefine the Slater determinant $|\Psi_0\rangle$ and the projector $\mathcal{P}_i$ in terms of previously introduced transformation $\mathcal{W}$ and assuming $\mathcal{W}^\dagger\mathcal{W} = 1$, we get:

$$|\Psi_0\rangle \rightarrow \prod_i \mathcal{W}_i|\Psi_0\rangle\ , \qquad \mathcal{P}_i \rightarrow \mathcal{P}_i\mathcal{W}^\dagger_i\ . \tag{4.30}$$

Returning back to Eq. (4.1) one immediately sees that the transformation leaves the Gutzwiller wave-function $|\Psi_G\rangle$ invariant. It is worth to stress that, being the transformation unitary, the transformed $|\Psi_0\rangle$ remains a Slater determinant.

The crucial step is to use a mixed-basis parameterization for the projector $\mathcal{P}_i$, namely

$$\mathcal{P}_i = \sum_{\Gamma n}\lambda_{i\Gamma n}|\Gamma,i\rangle\langle n,i| \tag{4.31}$$

where the Fock states $|\Gamma,i\rangle$ remain defined in the original $c_{i\alpha}$-basis, while the $\langle n,i|$ are defined in the natural basis of $f_{i\alpha}$ operators. Here one should notice that the new matrix $\hat{\lambda}_i$ is defined in the mixed original-natural basis. A generic state $|n,i\rangle$ can be written as

$$|n,i\rangle = \left(\prod_{\beta\in n} f^{\dagger}_{i\beta}\right)^{n_\beta} |0\rangle_i \tag{4.32}$$

where $n_{i\beta} = 0, 1$ is the occupation number of the natural states β with $\beta = 1, ..., 2M$.

Let us briefly stress that is quite common, for the practical reasons, to use the convention that the order of the configurations $|\Gamma, i\rangle$ and $|n, i\rangle$ is the same. That means that

$$\left(c^{\dagger}_{\alpha}\right)_{ij} = \left(f^{\dagger}_{\alpha}\right)_{ij} , \ \forall\alpha, i, j , \tag{4.33}$$

knowing that the operators $c^{\dagger}_{\alpha}$ and $f^{\dagger}_{\alpha}$ act on their own Fock space.

We can now introduce the uncorrelated density distribution in the natural basis

$$P^0_{inm} \equiv \langle\Psi_0| \, |m,i\rangle \langle n,i| \, |\Psi_0\rangle = \delta_{nm} P^0_{in} . \tag{4.34}$$

The matrix $\hat{P}^0_i$ has diagonal form in this basis, and the matrix elements P^0_{in} are easily computed as

$$P^0_{in} = \prod_{\beta=1}^{2M} \left(n^0_{i\beta}\right)^{n_{i\beta}} \left(1 - n^0_{i\beta}\right)^{1-n_{i\beta}} , \tag{4.35}$$

where the factor $n^0_{i\beta}$ appears when a given orbital in the configuration $|n, i\rangle$ is occupied, and the $1 - n^0_{i\beta}$ factor is present for empty orbitals. Seemingly, recalling Eq. (4.20), the expression of the local projector (4.31) becomes

$$\mathcal{P}_i = \sum_{\Gamma n} \frac{\phi_{i\Gamma n}}{\sqrt{P^0_{i,n}}} |\Gamma, i\rangle \langle n, i| . \tag{4.36}$$

where $\phi_{i\Gamma n}$ are the the variational parameters of mixed-basis representation that define a local variational matrix $\hat{\phi}_i$.

Essentially, within the mixed-state representation the first condition (4.21) remains unchanged, since, as stressed before, it does not depend on the transformation. On the other hand, the condition (4.22), together with (4.29), changes into

$$\mathrm{Tr}\left(\hat{\phi}^{\dagger}_i \hat{\phi}_i \hat{f}^{\dagger}_{i\alpha} \hat{f}_{i\beta}\right) = \delta_{\alpha\beta} n^0_{i\alpha} , \tag{4.37}$$

while the matrix representation of the operator $f_{i\alpha}$ in its own local Fock space is

$$f_{i\alpha} \rightarrow (f_{i\alpha})_{nm} = \langle n| \, f_{i\alpha} \, |m\rangle . \tag{4.38}$$

Finally, the renormalization factor can be expressed from

$$\begin{aligned} \langle\Psi_0|f^{\dagger}_{i\beta}\mathcal{P}^{\dagger}_i c_{i\alpha}\mathcal{P}_i|\Psi_0\rangle \equiv \sum_{\gamma} \langle\Psi_0|f^{\dagger}_{i\beta}f_{i\gamma}|\Psi_0\rangle R^{\mathcal{W}}_{i\alpha\gamma} = \sum_{\delta} W^{\dagger}_{i\delta\beta} \langle\Psi_0|c^{\dagger}_{i\delta}\mathcal{P}^{\dagger}_i c_{i\alpha}\mathcal{P}_i|\Psi_0\rangle = \\ = \sum_{\rho\delta} W^{\dagger}_{i\delta\beta} R_{i\alpha\rho} \langle\Psi_0|c^{\dagger}_{i\delta}c_{i\rho}|\Psi_0\rangle = \sum_{\gamma\rho} W^{\dagger}_{i\rho\gamma} R_{i\alpha\rho} \langle\Psi_0|f^{\dagger}_{i\beta}f_{i\gamma}|\Psi_0\rangle = R^{\mathcal{W}}_{i\alpha\beta} n_\beta \end{aligned} \tag{4.39}$$

where we have used the condition (4.37) and the inverse transformation of Eq. (4.28).

Under the transformation $\hat{W}$ the renormalization factor transforms into

$$R_{i\alpha} \rightarrow R^{\mathcal{W}}_{i\alpha} = \sum_{\beta} R_{i\beta} W^{\dagger}_{\beta\alpha} \,, \tag{4.40}$$

giving

$$P^{\dagger}_{i} c^{\dagger}_{i\alpha} P_{i} \rightarrow \sum_{\gamma} R^{\mathcal{W}*}_{i\alpha\gamma} f^{\dagger}_{i\gamma} \,, \qquad P^{\dagger}_{j} c_{j\beta} P_{j} \rightarrow \sum_{\delta} R^{\mathcal{W}}_{j\beta\delta} f_{j\delta} \,. \tag{4.41}$$

After some analytical manipulation (see Appendix A) one can show that the renormalization factors obtain the simple form

$$R^{\mathcal{W}}_{\alpha\beta} = \frac{\mathrm{Tr}\left(\hat{f}^{\dagger}_{i\beta} \hat{\phi}^{\dagger}_{i} \hat{c}_{i\alpha} \hat{\phi}_{i}\right)}{\sqrt{n^{0}_{\beta}\left(1 - n^{0}_{\beta}\right)}} \,, \qquad R^{\dagger\mathcal{W}}_{\beta\alpha} = \frac{\mathrm{Tr}\left(\hat{\phi}^{\dagger}_{i} \hat{c}^{\dagger}_{i\alpha} \hat{\phi}_{i} \hat{f}_{i\beta}\right)}{\sqrt{n^{0}_{\beta}\left(1 - n^{0}_{\beta}\right)}} \,. \tag{4.42}$$

This simplification of the renormalization factor which controls the reduction of metallic behavior is one of the main results of the use of the mixed representation for the matrix of variational parameters. Another consequence is that now also the renormalization factor becomes dependent only on $\hat{\phi}_i$ like the local operators.

It is important to stress that the introduction of the mixed representation simplifies the formalism at little cost. Indeed our derivation shows that the implementation of the approach does not require the explicit knowledge of the transformation connecting the original and the natural basis [107].

Rather naturally, for models in which the density matrix is already diagonal (as in models with purely density-density interactions) we have that the natural and orbital basis coincide, hence the previously introduced reformulation of the Gutzwiller problem becomes redundant.

4.3 Variational energy of the multi-orbital model

In this section we detail the implementation of the approach for a generic multi-orbital model using the mixed-basis formulation for the variational problem that we have just outlined. For simplicity we adopt the notation $\hat{R}^{\mathcal{W}}_{i} \rightarrow \hat{R}_{i}$.

Using the above results one can write the expectation value of the Hamiltonian (4.2) within the Gutzwiller approximation is of the following form, including Lagrange multipliers which enforce the condition (4.37). This leads to the expression

$$E = E_{*} + \sum_{i} \mathrm{Tr}\left(\hat{\phi}^{\dagger}_{i} \hat{H}_{i} \hat{\phi}_{i}\right) \,. \tag{4.43}$$

The variational energy (4.43) has to be minimized with respect to the variational parameters, $\hat{\phi}_i$ and $|\Psi_0\rangle$, ensuring that condition (4.37) is satisfied. In order to include this constraint, we introduce the Lagrange multipliers $\mu_{i\alpha\beta}$:

$$E = \sum_{i} \mathrm{Tr}\left(\hat{\phi}^{\dagger}_{i} \hat{U}_{i} \hat{\phi}_{i}\right) + \sum_{ij} \sum_{\alpha\beta\gamma\delta} \langle \Psi_0 | f^{\dagger}_{i\gamma} f_{j\delta} | \Psi_0 \rangle \, R^{\dagger}_{i\gamma\alpha} t^{\alpha\beta}_{ij} R_{j\beta\delta} - \sum_{i} \mu_{i\alpha\beta} \left(\langle \Psi_0 | f^{\dagger}_{i\alpha} f_{i\beta} | \Psi_0 \rangle - \mathrm{Tr}\left(\hat{\phi}^{\dagger}_{i} \hat{\phi}_{i} \hat{f}^{\dagger}_{i\alpha} \hat{f}_{i\beta}\right)\right) \tag{4.44}$$

We have already stressed that $|\Psi_0\rangle$ must be the one that minimizes the average value of non-interacting Hamiltonian $\langle \Psi_G | \mathcal{H}_0 | \Psi_G \rangle$.

Moreover, if we require to have the single-particle density-matrix with the eigenvalue $n^0_{i\alpha}$, as in (4.37), we realize that $|\Psi_0\rangle$ that satisfies such condition is the ground state of the following variational Hamiltonian:

$$\sum_{ij}\sum_{\alpha\beta\gamma\delta} f^\dagger_{i\alpha} R^\dagger_{\alpha\beta} t^{\beta\gamma}_{ij} R_{\gamma\delta} f_{i\delta} - \sum_{\alpha\beta} \mu_{i\alpha\beta} f^\dagger_{i\alpha} f_{i\beta} \,. \tag{4.45}$$

The first term in Eq. (4.45) we can denote as $\mathcal{H}_*$. Here the Lagrange multipliers $\mu_{i\alpha}$ maximize the ground state energy. Imposing the value of the parameter $\mu_{i\alpha}$, E_* from (4.43) is obtained as

$$\langle\Psi_0|\mathcal{H}_* - \mu|\Psi_0\rangle = \langle\Psi_G|\mathcal{H}_0|\Psi_G\rangle \equiv E_* \tag{4.46}$$

Once this task is done, one needs to minimize the variational energy per site, and with respect to all the variational parameters:

$$\frac{\partial E}{\partial \phi^\dagger} = \hat{U}\phi + \frac{\partial E_*}{\partial \phi^\dagger} + \sum_{\alpha\beta} \mu_{\alpha\beta}\phi f^\dagger_\alpha f_\beta - \Lambda\phi = 0 \tag{4.47a}$$

$$\frac{\partial E}{\partial \Lambda} = \mathrm{Tr}\left(\hat{\phi}^\dagger_i \hat{\phi}_i\right) - 1 = 0 \tag{4.47b}$$

$$\frac{\partial E}{\partial \mu_{\alpha\beta}} = \mathrm{Tr}\left(\hat{\phi}^\dagger_i \hat{\phi}_i \hat{f}^\dagger_{i\alpha} \hat{f}_{i\beta}\right) - \delta_{\alpha\beta} n^0_{i\alpha} = 0 \tag{4.47c}$$

where we have dropped out the lattice site index i, since in case of paramagnetic wave-function the translational symmetry in not broken, so the variational parameters do not depend on site. The last term in (4.47) corresponds to imposing one more constraint, on the normalization condition (4.21). Let us also stress that the elements of the matrix $\hat{U}$ correspond to the original basis representation, whereas $\hat{\phi}$ has rows written in the original and columns in the natural basis.

This way, with Eq. (4.47), we are given a set of non-linear equation. The number of these equations depends on the number of the variational parameters $(\hat{\phi}, \mu, \Lambda)$, and his problem can be solved iteratively using different numerical tools.

4.3.1 An explicit example: The single band Hubbard model

So far we have seen that the ground state energy of an interacting model can be mapped via Guzwiller approximation to an effective model, with renormalized hoppings that account for the presence of the interactions of the system. Now we will show an example of how this approximation can be applied to the simple half-filled single-orbital paramagnetic Hubbard model (2.5) - in such definition this model is particle-hole symmetric and spin-rotationally invariant.

The local Fock states for the single-orbital Hubbard model are defined with

$$|0\rangle, |\uparrow\rangle, |\downarrow\rangle, |\uparrow\downarrow\rangle \,. \tag{4.48}$$

Since the local density matrix is already diagonal in this representation, the original and natural basis coincide. Therefore, any local operator is represented in a form of 4×4 matrix, such as the $\hat{\phi}$ matrix, that can be written as

$$\hat{\phi}_{i\Gamma\Gamma'} = \hat{\phi}_{i\Gamma}\delta_{\Gamma\Gamma'} = \begin{pmatrix} \phi_{i0} & 0 & 0 & 0 \\ 0 & \phi_{i\uparrow} & 0 & 0 \\ 0 & 0 & \phi_{i\downarrow} & 0 \\ 0 & 0 & 0 & \phi_{i\uparrow\downarrow} \end{pmatrix}. \tag{4.49}$$

On another hand, the Gutwiller constraints Eq. 4.6 get the form

$$\begin{aligned} |\phi_0|^2 + 2|\phi_1|^2 + |\phi_2|^2 &= 1 \\ 2|\phi_1|^2 + 2|\phi_2|^2 &= 2n\,. \end{aligned} \tag{4.50}$$

Requiring the paramagnetic solution implies $\phi_{i\uparrow} = \phi_{i\downarrow} = \phi_{i1}$, where we changed the notation due to simplicity. On another side, the particle-hole symmetry at half-filling gives $\phi_{i0} = \phi_{i\uparrow\downarrow} = \phi_{i0}$. Now it comes apparent that Eq. (4.50) coincide in such conditions, since at half-filling in single-orbital model we have that $n = 1/2$, giving one unique constraint. Namely

$$2\left(|\phi_0|^2 + |\phi_1|^2\right) = 1\,. \tag{4.51}$$

Further, all the variational parameters are site-independent in the homogeneous situation, as well as the hoping renormalization factor that reads

$$R = \frac{\phi_0^*\phi_1 + \phi_1^*\phi_0}{\sqrt{n(1-n)}} = 2\left[\phi_0^*\phi_1 + \phi_1^*\phi_0\right]. \tag{4.52}$$

Since the Hamiltonian is real we can also assume wave-functions to be real, hence the same can be assigned to ϕ parameters.

Utilizing the condition (4.51) we can get rid of one parameter, say ϕ_1, and, knowing that the interaction term (4.8) obtains the form

$$\mathcal{H}_i = U\begin{pmatrix} 0 & 0 & 0 & 0 \\ 0 & 0 & 0 & 0 \\ 0 & 0 & 0 & 0 \\ 0 & 0 & 0 & 1 \end{pmatrix}, \tag{4.53}$$

we write the variational energy as a function of the single variational parameter ϕ_0:

$$E = \min_{|\Psi\rangle,\phi_0^2}\left[-R^2(\phi_0)t\sum_{\langle i,j\rangle,\sigma}\langle\Psi_0|c_{i\sigma}^\dagger c_{j\sigma}|\Psi_0\rangle + U\sum_i \phi_0^2\right]. \tag{4.54}$$

As before, the $|\Psi_0\rangle$ represents the non-interacting Fermi sea. Formula (4.54), with its elegant formulation, gives the energy in dependence on purely single variational parameter ϕ_0^2 which we will substitute as $\phi_0^2 = D$, to coincide with the original Gutzwiller's formulation of the single-band model. Further, if we define the average kinetic energy $\bar{\epsilon}$ as

$$\bar{\epsilon} = \frac{t}{N_s}\sum_{\langle i,j\rangle,\sigma}\langle\psi_0|c_{i\sigma}^\dagger c_{j\sigma}|\psi_0\rangle + H.c. \tag{4.55}$$

N_s being the number of sites, Eq. (4.54) gets the form

$$E(D) = -N_s\, 8D(1-2D)\bar{\epsilon} + UDN_s\,, \tag{4.56}$$

where we found that

$$R^2 = 8(1-2D)D\,. \tag{4.57}$$

Minimizing $E(D)$ from Eq. (4.56) with respect to the variational parameter D, one obtains

$$\begin{cases} D(U) = \frac{1}{4}\left(1 - \frac{U}{U_c}\right) & U < U_c\,, \\ D(U) = 0 & U \geq 8\bar{\epsilon}\,. \end{cases} \tag{4.58}$$

Here $U_c \equiv 8\bar{\epsilon}$ is defined as a critical value of the interaction at the Mott transition when $U = U_c$. The number of doubly occupied sites, measured by the double occupation probability D, is expected to be zero in this limit.

On another hand, plugging (4.58) into the expression (4.57) and (4.56), the kinetic energy renormalization becomes

$$Z = 1 - \frac{U^2}{U_c^2}\,, \tag{4.59}$$

whereas the expression for the total energy of the single-orbital Hubbard model reads

$$E = -N_s\bar{\epsilon}\left(1 - \frac{U}{U_c}\right)^2\,. \tag{4.60}$$

Apparently, the energy (4.60) increases with U and becomes identically zero at $U = U_c$. Since the energy dies out with a quadratic dependence on U, this would suggest that at U_c the transition will be of the second order.

These results are obtained within the Gutzwiller approximation and they describe a metal-insulator transition. For $U < U_c$ departing from the Fermi liquid with a renormalized kinetic energy, the quasiparticle weight Z, that, as we have stressed, can be associated to the renormalization factor R, monotonically decrease with increase of the interaction strength U. The vanishing Z at U_c is the consequence of the suppression of double occupied configurations that prevents the hopping processes between two different sites, forcing these quantities to be zero at the insulating side. Together with the reduction of the double occupation probability one encounters the enhancement of the spin fluctuations, leading to the formation of the local magnetic moment at the Mott transition. Indeed, it was found that at this point the spin susceptibility diverges. Apparently, one can conclude that the correlations in such systems have a non-trivial effect on the emerging physics phenomena. However, the Mott insulator at $U > U_c$ has zero energy and is completely featureless within the Gutzwiller approximation.

Lastly, let us stress that the expression (4.60) gives the same result as the one obtained by Brinkman and Rice [42], and it holds for $n = 1/2$. Apparently, when $n \neq 1/2$, the results is rather different. Due to its dependency on the filling of the system, the Brinkman-Rice transition immediately disappears in this, non-half-filing case.

4.4 Final remark

Summing up all previously said, let us give some conclusion about the applicability and reliability of the method we have introduced in this chapter.

As stressed before, the paramagnetic Gutzwiller wave-function brings improvements in describing the strongly correlated systems since it suppresses (partially projects out) the double occupations driven by the Coulomb repulsion between the electrons. Yet, it fails in describing in correct way the Mott transition in the non-infinite lattice coordination. The main reason for this is its incapability to account properly for spacial correlations, which, in fact, are not so crucial

in the limit of infinite coordination number since the effect of all the neighboring sites on an arbitrary one can be seen as an average mean-field. Nevertheless, the question remains whether this wave-function is the best choice for the ground state or not.

In order to improve the Gutzwiller wave-function by providing these intersite correlations, one can use density-density Jastrow factor as in Ref. [112]

$$|\Psi_G\rangle \rightarrow exp\left[-\sum_{ij} v_{ij} n_i n_j\right] |\Psi_G\rangle \tag{4.61}$$

where v_{ij} are variational parameters whereas n_i is the occupation number at site i. Though more accurate with respect to original GW wave-function, Gutzwiller-Jastrow wave-function can only be implemented numerically, using Variational Monte Carlo, which suffers from the finite-size of the system [113].

Nevertheless, the development of Dynamical mean-field theory (DMFT) [44, 114], which is indeed exact in the limit of infinite coordination, gave us the possibility to test the quality of Gutzwiller wave-function, giving the physical meaning of the Gutzwiller approximation. In fact, comparing these two methods it was shown that for single-orbital Hubbard model, in infinite dimensions, the Gutzwiller wave-function does properly describes the behaviour of the quasiparticle [44], at least qualitatively. Besides, knowing that the local correlations play the crucial role in the metallic phase, it is justified to assume that changes in the quasiparticle properties while approaching the transition do not depend very much on dimensionality d, in case when $d > 1$.

The Gutzwiller approximation scheme turns out to be reliable whenever the Gutzwiller wave-function is able to faithfully describe the ground state [103]. Therefore, despite it fails to describe the Mott insulator, relatively simple Gutzwiller approach is convenient choice when one takes the metallic regime under the consideration, as will be our case.

The formulation of the Gutzwiller variational problem described within this chapter, that leads itself to efficient numerical implementation, will be suitable for investigating the multi-orbital models in the rest of this thesis.

5

Hund's metals: A tale of two insulators

In the previous chapter we have reviewed some of the recent literature which has contributed to develop the concept of 'Hund's metal', a strongly correlated metal which is however far from Mott localization, in the sense that increasing the Coulomb interaction U does not lead to further correlation and localization. As we discussed above, this physics has been widely studied and characterized in a number of studies highlighting different remarkable properties of the Hund's metal or happening at the crossover between a standard metal and the novel regime.

On the other hand, much less activity has been focused on understanding the physical mechanism for which a metal can survive to a very strong value of the Hubbard U and the Hund's coupling J. This is also particularly surprising because both U and J are expected to reduce the effective kinetic energy of the electrons by imposing different constraints on the electronic motion: The first term limits charge fluctuations, while the second freezes spin fluctuations. In this chapter we focus exactly on this question and we actually connect the existence of the Hund's metal with a balance between the effects of the two interactions.

More precisely, we will show that the correlation-resistant metal emerges from the competition between two distinct insulating states, namely a high-spin Mott and a charge disproportionated insulator, favored respectively by the Coulomb interaction or the exchange coupling, and characterized by a different ionic valence. This competition results in an asymptotic mixed-valence metallic state in the region where the interaction parameters are balanced. In particular, we show that along a given line of the U-J phase diagram, the two insulators are degenerate and the metal survives even for divergent interactions as long as the hopping is finite.

Before entering our analysis, that can be found also in Ref. [115], we summarize some important basic properties of our model which will be useful in the subsequent analysis.

5.1 Model and atomic multiplets

In this study we will consider the three-orbital lattice Hamiltonian composed of a single particle term describing the kinetic energy and a local interaction part of the general form

$$\hat{H} = \hat{H}^{kin} + \sum_i \hat{H}_i^{int} \,. \tag{5.1}$$

The simplest version of (5.1) includes only nearest-neighbor intra-orbital hopping t_m, such that

$$\hat{H}^{kin} = -\sum_{\langle ij\rangle m\sigma} t_m d^{\dagger}_{im\sigma} d_{jm\sigma} \tag{5.2}$$

where $d^{\dagger}_{im\sigma}(d_{im\sigma})$ is creation (annihilation) operator. Here $\sigma = \uparrow, \downarrow$ are the spin components and the sum runs over $m = 1, 2, 3$ degenerate orbitals, so that we can further use the notation $t_m = t$. This way $\hat{H}^{kin}$ contains only diagonal elements in orbital space and gives identical eigenvalues for all three orbitals, meaning that $\hat{H}^{kin}$ remains invariant under orbital rotations. The details of the hopping term will not be relevant for our discussion, at least as long as there is no local hybridization between the different orbitals.

For the discussion of this chapter it is particularly useful to remind the form of the Kanamori Hamiltonian (3.13), which is written in an explicitly symmetric form in terms of the total density, spin and angular momentum operators on each lattice site

$$\hat{H}^{int} = (U - 3J)\frac{(\hat{n} - 3)^2}{2} - J\left(2\,\mathbf{S}^2 + \frac{1}{2}\mathbf{L}^2\right), \tag{5.3}$$

keeping in mind that $\hat{n} = \sum_{m\sigma} d^{\dagger}_{m\sigma} d_{m\sigma}$ represents the local[1] electron number operator, m labeling the t_{2g} orbitals, whereas $\mathbf{S}$ and $\mathbf{L}$ are spin and angular momentum operators, respectively. In the expression above we have properly redefined the chemical potential in order to make this expression explicitly particle-hole symmetric around half-filling $n = 3$. Further, it is convenient to denote the on-site repulsion between electrons in the first term as $U^* = (U - 3J)$, which will be useful in the following.

In the atomic limit the Hamiltonian is easily diagonalized in the basis of the atomic multiplets $|\Gamma\rangle = |n, \ell, s\rangle$ that are simultaneously the eigenstates of the density operator $\hat{n}$ and of the orbital and spin angular momentum operators $\mathbf{L}^2$ and $\mathbf{S}^2$, as well as their z-components L_z and S_z. The eigenvalues are trivially

$$E_\Gamma = E(n, \ell, s) = (U - 3J)\,\frac{(n - 3)^2}{2} - J\left(2s(s + 1) + \frac{1}{2}\ell(\ell + 1)\right), \tag{5.4}$$

where the degeneracy associated to each eigenvalue is associated with the possible values of the S_z and L_z operators and it is simply given by

$$g_\Gamma = g(n, \ell, s) = (2\ell + 1)(2s + 1)\,. \tag{5.5}$$

The atomic eigenstates $|\Gamma\rangle$, classified according to the quantum numbers n, ℓ, s, together with the corresponding eigenvalues and degeneracy defined with Eq. (5.4) and (5.5), respectively, are listed in Table 5.1. The particle-hole symmetry of the Hamiltonian (5.3) becomes apparent from the eigenvalues E_Γ presented in the table.

In this chapter we solve the model defined by Eqs. (5.1), (5.2) and (5.3) using both the Gutzwiller approximation (GW) (see Chapter 4) and the Rotationally-invariant slave-boson (RISB) formalism [83]. In both these approaches, as well as in Dynamical mean-field theory, the kinetic energy term only enters through the non-interacting density of states. Here, for simplicity, we consider a flat density of states of width W which we will use as our reference energy unit. Indeed we could easily use a tight-binding dispersion and even a more realistic and material-oriented density of states. However, the choice of a simplified density of states stems

[1] From now on we will drop the site-label i due to simplicity.

from the attempt to identify those physical effects that are purely driven by interactions and not related to a specific lattice structure.

In that spirit, the GW/RISB formalism is particularly suited to study, in a quasi-analytical fashion, multi-orbital systems characterized by local interactions that cannot be cast in the form of density-density terms, such as Hund's rule coupling in the Kanamori Hamiltonian (3.10). The rotational invariance of the formalism guarantees that all interacting terms are treated on an equal footing. The method represents, therefore, an ideal tool for investigating the interplay between Coulomb and exchange couplings, and the physics that emerges from their competition.

No.	$\|\Gamma\rangle = \|n,\ell,s\rangle$	n_Γ	ℓ_Γ	s_Γ	g_Γ	E_Γ	$\phi_{\|\Gamma\rangle}$
1	$\|0,0,0\rangle$	0	0	0	$\boxed{1}$	$\frac{9}{2}(U-3J)$	$\phi_{\|0,0,0\rangle}$
2	$\left\|1,1,\frac{1}{2}\right\rangle$	1	1	$\frac{1}{2}$	$\boxed{6}$	$2(U-3J)-\frac{5}{2}J$	$\phi_{\left\|1,1,\frac{1}{2}\right\rangle}$
3	$\|2,0,0\rangle$	2	0	0	1	$\frac{1}{2}(U-3J)$	$\phi_{\|2,0,0\rangle}$
4	$\|2,1,1\rangle$	2	1	1	$\boxed{9}$	$\frac{1}{2}(U-3J)-5J$	$\phi_{\|2,1,1\rangle}$
5	$\|2,2,0\rangle$	2	2	0	5	$\frac{1}{2}(U-3J)-3J$	$\phi_{\|2,2,0\rangle}$
6	$\left\|3,0,\frac{3}{2}\right\rangle$	3	0	$\frac{3}{2}$	$\boxed{4}$	$-\frac{15}{2}J$	$\phi_{\left\|3,0,\frac{3}{2}\right\rangle}$
7	$\left\|3,1,\frac{1}{2}\right\rangle$	3	1	$\frac{1}{2}$	6	$-\frac{5}{2}J$	$\phi_{\left\|3,1,\frac{1}{2}\right\rangle}$
8	$\left\|3,2,\frac{1}{2}\right\rangle$	3	2	$\frac{1}{2}$	10	$-\frac{9}{2}J$	$\phi_{\left\|3,2,\frac{1}{2}\right\rangle}$
9	$\|4,0,0\rangle$	4	0	0	1	$\frac{1}{2}(U-3J)$	$\phi_{\|4,0,0\rangle}$
10	$\|4,1,1\rangle$	4	1	1	$\boxed{9}$	$\frac{1}{2}(U-3J)-5J$	$\phi_{\|4,1,1\rangle}$
11	$\|4,2,0\rangle$	4	2	0	5	$\frac{1}{2}(U-3J)-3J$	$\phi_{\|4,2,0\rangle}$
12	$\left\|5,1,\frac{1}{2}\right\rangle$	5	1	$\frac{1}{2}$	$\boxed{6}$	$2(U-3J)-\frac{5}{2}J$	$\phi_{\left\|5,1,\frac{1}{2}\right\rangle}$
13	$\|6,0,0\rangle$	6	0	0	$\boxed{1}$	$\frac{9}{2}(U-3J)$	$\phi_{\|6,0,0\rangle}$

Table 5.1: Eigenstates $|\Gamma\rangle$ and eigenvalues E_Γ of the t_{2g} rotationally-invariant Hamiltonian (5.3) in the atomic limit, assuming particle-hole symmetry (included in the Hamiltonian). The boxed numbers denote the ground-state degeneracies for $J > 0$. Number of electrons n, spin s and orbital number ℓ are given for the corresponding eigenstates. The last column shows the slave-boson amplitudes for the description of the eigenstates in the RISB formalism, equivalnt to rotationally-invariant Gutzwiller.

Within the RISB approach we associate an amplitude $\phi_{|\Gamma\rangle}$ to every multiplet $|\Gamma\rangle$, which corresponds directly to the projectors defined in the Gutzwiller method. Indeed, we have pointed out in Sec. 4.2 that the two approaches turned out to be equivalent, what, indeed, we have shown by our present results, obtained by both approaches, which showed a perfect match. In the following we will keep on calling the projectors as 'slave-boson amplitudes', always refering to both approaches.

Once we implement all the symmetries we are left with the thirteen slave-boson amplitudes corresponding to the multiplets listed in the Table 5.1 out of 64 states defining the local Hilbert space.

5.2 Mott transition at $\bar{n} = 3$ and $\bar{n} = 2$

We start by discussing the Mott transition in our model for two characteristic average densities $\bar{n} = 2$ and $\bar{n} = 3$. In Fig. 5.1 we display the quasiparticle weight Z for different J/U ratios, at two different average densities, $\bar{n} = 2$ and $\bar{n} = 3$. We obviously reproduce the results discussed in Chapter 3. At half-filling case the increase of J/U tends to enhance the correlations in the system, decreasing the value of critical interaction strength U_c, while the transition always remains of first order for any finite J. On the other hand, in the $\bar{n} = 2$ case we find the two-stage behavior, and eventually the Janus-faced role of Hund's rule coupling for sizable J/U ratio, pushing forward the U_c for the metal-insulator Mott transition. For $J/U = 1/3$ the critical U actually diverges and the system remains always metallic. The transition is of first order only for $J/U < 0.1$, well before the Janus regime sets in. In the third panel we compare, for the two densities, the spinodal line where the metallic solution disappears with the point where the energy of the metal becomes higher than that of the insulator and the actual Mott transition occurs. The difference is significant only for relatively small J/U also for $\bar{n} = 3$, and it reduces for very large J/U, where the coexistence region actually shrinks.

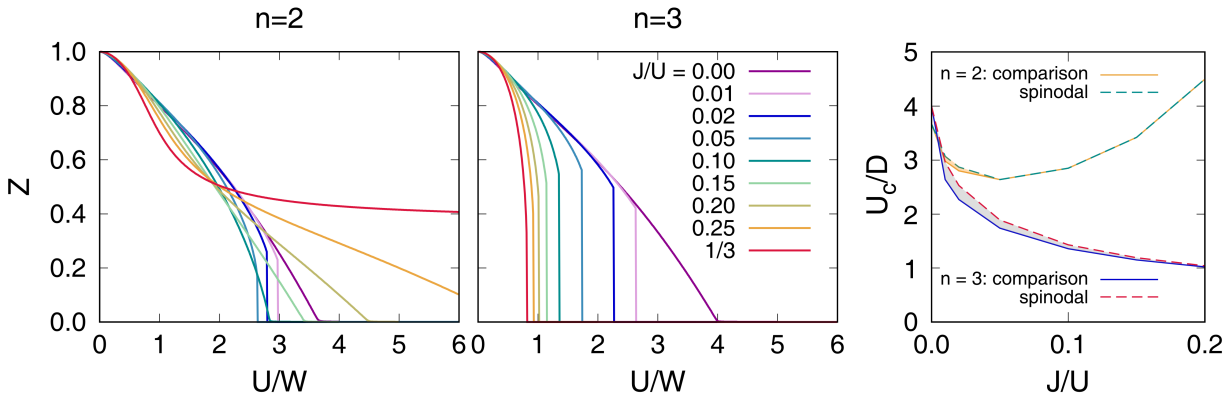

Figure 5.1: Quasiparticle weight Z as a function of U, for different J/U ratios, at commensurate filling $\bar{n} = 2$ (equivalent to $\bar{n} = 4$) and $\bar{n} = 3$. In the third panel we plot the U_c extracted from the plots of the other panels compared with the spinodal line of the metallic solution in the two cases.

In Fig. 5.2 we follow the population of each multiplet as a function of U, for the two cases $\bar{n} = 2$ and $\bar{n} = 3$, keeping J/U fixed to few different values ranging from the pure Hubbard model to the value $J/U = 1/3$ where the charge-charge repulsion vanishes ($J/U = 0.0, 0.02, 0.2, 1/3$). These plots can be seen as the generalization to a multi-orbital case of the decrease of double occupations as a function of U in the single-band Hubbard model. The generalization also reveals the two different effects of the Hubbard U and of the Hund's coupling J.

For $U = 0$ the independent electrons picture suggests that all slave-boson amplitudes, each associated to a corresponding multiplet state, are equal, hence all multiplets are populated according to their degeneracy. For $J = 0$, as U becomes larger, the Coulomb energy of a local configuration depends only on the total charge per site, as suggested by Eq. (5.3). Therefore, the system tends to favor just those multiplets from the particle number sector that corresponds to the value of total charge, namely those with $\bar{n} = 2$ (Fig. 5.2 - left) and $\bar{n} = 3$ (Fig. 5.2 - right) for our two cases (see Table 5.1). The amplitudes of all the multiplets with $n \neq \bar{n}$ vanish at the Mott transition.

When we include also a finite Hund's coupling J, a further filtering takes place, and high-spin configurations are favored at the expenses of those with lower spin. For relatively small values

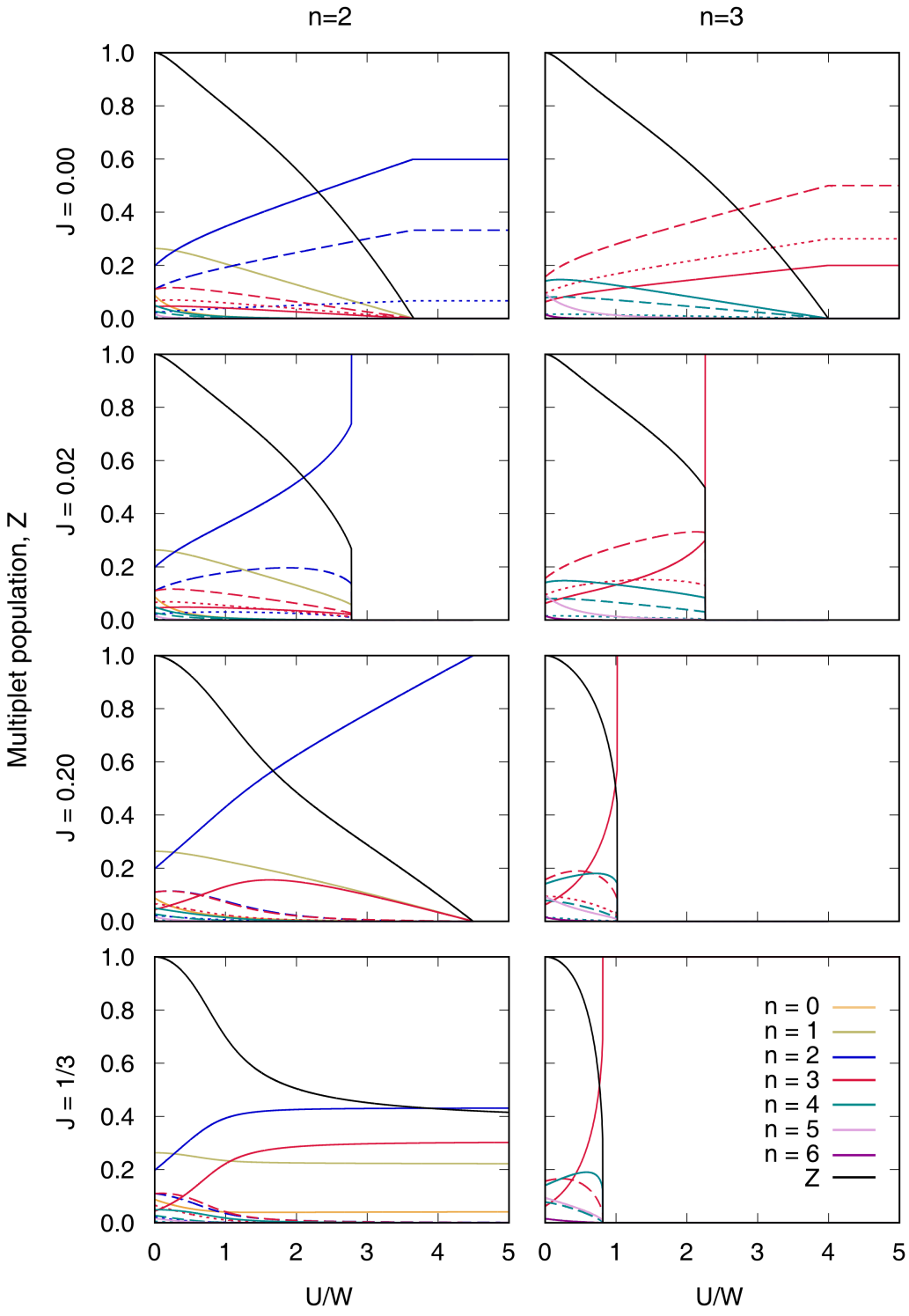

Figure 5.2: Multiplet population (obtained by inequivalent slave-boson amplitudes $\phi_{|\Gamma\rangle}$ (see Table 5.1), for different J/U ratios, at commensurate filling $\bar{n} = 2$ (equivalent to $\bar{n} = 4$) and $\bar{n} = 3$. Full lines represent the multiplets with the maximum spin, whereas the dashed ones represent the remaining multiplets belonging to the same number sector as the former one. The scale of the U axis is the same for all plots in order to stress the effect of the Hund's coupling on the critical value of the interaction.

of J, the effect of the latter is a small correction to the hierarchy between multiplets dictated by the Hubbard interactions, but the competition becomes indeed more subtle when J grows.

In the half-filling $\bar{n} = 3$ case, an increasing J appears to facilitate the Mott transition by filtering (among the states with $\bar{n} = 3$) only the high-spin state, as it is apparent comparing the four right panels in Fig. 5.2. The very fast reduction of the populations of most multiplets reduces the possibility of charge fluctuations and of hopping processes. Therefore the quasiparticle weight Z measuring the effective kinetic energy falls very rapidly. When J is sufficiently large, all the electrons are very rapidly frozen into the quadruplet $|3, 0, 3/2\rangle$, while all other multiplet populations are equal to zero, as shown in Fig. 5.2. This effect gets more pronounced the more we increase the value of J/U ratio, forcing the system to localize for much smaller values of U. In this case U and J cooperate in driving a very rapid and abrupt Mott localization, as we have already shown in the plots of the quasiparticle weight Z.

The situation for $\bar{n} = 2$ is indeed very different. However, for small values of U and J the picture resembles the one from $\bar{n} = 3$ case. Both U and J reduce the populations of the various multiplets and Z falls correspondingly. Instead, increasing further U, for the small values of J/U one finds that the most dominant multiplet is the one with the maximum spins configuration, ie. $|2, 1, 1\rangle$, forming a high-spin Mott insulator for $U > U_c$. Nevertheless, when J/U reaches a certain range of values ($J/U = 0.2$ in our example), one enters a regime in which the high-spin states with occupation different from the average value $\bar{n} = 2$ survive for a relatively large range of interactions, as shown in Fig. 5.2 (left). When this happens, the decrease of Z slows down and we enter in the Hund's metal, which is characterized by local valence fluctuations. Therefore the Hund's coupling is competing with the Hubbard U. For $J/U = 1/3$ we see that all the four different high-spin multiplets belonging to the four different particle number sectors, $n = 0, 1, 2, 3$, survive for arbitrary values of U. As a result, Z remains finite and constant in the same region, and the Mott insulator is never reached. A much more subtle interplay between the two interaction is leading to the Hund's metal.

We complement this information by reporting, in Fig. 5.3, the charge correlation functions defined in Sec. 3.4.3. As we did in the previous discussion, we contrast the behavior of the total charge correlation per orbitals (C_{tot}), with the intra-orbital (C_{intra}) and inter-orbital (C_{inter}) charge-correlation function, satisfying Eq. (3.21). As stressed before, the intra-orbital and inter-orbital contributions have, by definition, the opposite sign.

Just like the multiplets, the results for $J = 0$ do not reveal particular differences between the different densities $\bar{n} = 2$ and $\bar{n} = 3$. In both cases the total charge correlations vanish at the Mott transition, $C_{tot} = 0$. This is realized by a cancellation between the positive intra-orbital correlation and the negative inter-orbital ones. In particular the former are basically constant as a function of U, while the latter increase from zero to a value that cancels out the intra-orbital contribution (see Appendix C).

When we introduce the Hund's coupling at half-filling (right panel in Fig. 5.3), we modify this scenario as the vanishing of C_{tot} happens abruptly and it is the result of C_{intra} and C_{inter}, which both decrease in absolute value before canceling out at the Mott transition. The main effect of J is thus to reduce C_{intra}, helping the Mott localization adding a further constraint to electronic motion, in agreement with the previous analysis of the multiplet population. In some sense, the cooperative effect of U and J leads to a kind of super-localization of Mott-Hund character.

For $\bar{n} = 2$ (left panel in Fig. 5.3), after a weak-J regime where the picture is not different from the one at half-filling, with a slight reduction of the absolute values of both C_{intra} and C_{inter}, we enter in the Hund's dominated region. Here C_{inter} is modulated owing to the fact that the electrons in different orbitals interact with a coupling $U - 3J$, which is reduced as J increases and it vanishes for $J/U = 1/3$, as shown in the left bottom panel. On the other hand the intra-orbital correlations C_{intra} tend to flatten as a function of U as J/U is increased, since

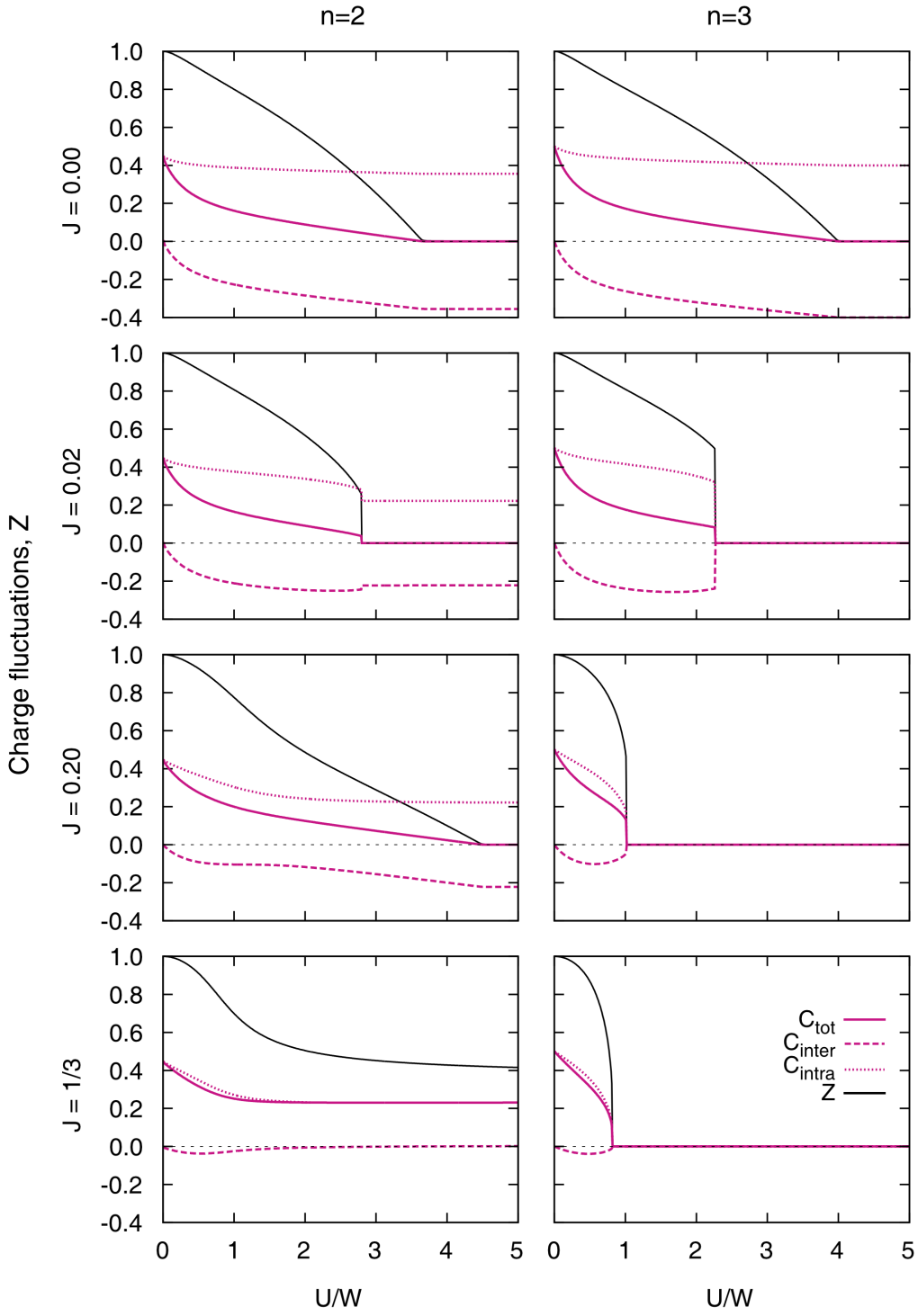

Figure 5.3: Charge correlation (total, inter-orbital and intra-orbital), for different J/U ratios, at commensurate filling $\bar{n} = 2$ (equivalent to $\bar{n} = 4$) and $\bar{n} = 3$. The scale of the U axis is the same for all plots in order to stress the effect of the Hund's coupling on the critical value of the interaction.

the intra-orbital correlations are essentially related to the double occupancy which, as shown by Fig. 5.2, is already quenched when the crossover from the standard metal to the Hund's metal takes place. The vanishing of inter-orbital correlations is a signature of the orbital decoupling, which becomes more and more complete as $J/U = 1/3$ is approached.

5.3 Extended phase diagram in the U-J plane

The symmetric form of the interaction of the Kanamori model, expressed with Eq. (5.3), shows clearly that the condition $U = 3J$ has a special role in the properties of the model. For this value of the interaction the charge-charge repulsion vanishes, leaving to the second term the role of the only interaction. Moreover, on the same line, namely $J/U = 1/3$, one finds from Eq. (3.10) that the coefficient of the equal-spin inter-orbital Coulomb repulsion vanishes, which leads to the orbital decoupling. One can also notice that for $U - 3J$ the atomic estimate of the Mott gap vanishes. All these phenomena underlay or accompany the onset of a metallic state which survives even when U and J become exceedingly larger than W.

Needless to say, this suggests that the line $U - 3J = 0$ is a very special boundary in the phase diagram of the model, and indeed most studies assumed that this boundary could not be crossed assuming that all Coulomb term must be positive, hence $U^* > 0$. However, the presence of strong electron-phonon interactions and Jahn-Teller (JT) distortions may substantially renormalize both U and the exchange coupling J, yielding an effective J whose value may lie outside the aforementioned limit, with the negative values of Coulomb coupling $U^* < 0$. We shall, therefore, treat this term as a generalized effective coupling, exploring the whole paramagnetic phase diagram of Eq. (5.3) as a function of U and J, treated as independent interaction parameters [116]. Besides its potential direct interest for system with sizable electron-phonon coupling, we believe that, at the very least, a theoretical analysis beyond this line, $J/U = 1/3$, will help to shed light on the Hund's induced correlation effects. In the final part of this chapter we will also consider the case in which $J < 0$, a situation which can again be induced by a strong electron-phonon coupling. This comparison will help us to strengthen our conclusions by showing the existence of a different yet, comparable correlation-resilient metal also in this negative-J regime.

We start, however, our presentation from the case $J > 0$ which is the main object of the present thesis of the overwhelming majority of manuscripts discussing the Hund's metal.

In the phase diagram of Fig. 5.4 we show, for independent values of U/W and J/W, the quasiparticle spectral weight Z in the paramagnetic state for a commensurate filling $\bar{n} = 2$. As before, Z measures the degree of metallicity of the system, with values close to 1 (yellow) correspond to a non-interacting metal, while $Z = 0$ (dark blue) describes localized electrons of a correlated insulator.

5.3.1 Two insulators

The main feature of our extended diagram is the presence of a wide metallic region appearing as a ribbon centered around the $J/U = 1/3$ (light blue) line, which corresponds to $U^* = 0$, surrounded by two insulating regions. Both these insulators are characterized by a vanishing quasiparticle spectral weight $Z = 0$ (dark blue), hence they are not band insulators, but some kind of correlation-induced states.

The insulator in the $J/U < 1/3$ (positive-U^*) region is the standard high-spin Mott insulator. Having 2 electrons per three orbitals, in average, means that in the Mott state each lattice site will be occupied by exactly two electrons, populating the lowest energy multiplet[2] with maximum spin configuration $|2, 1, 1\rangle$ (state 4 in Table 5.1), as shown in the left box of Fig. 5.5. Since U^* is positive and large, the charge fluctuations are frozen, as shown in Fig. 5.3. The effect of the positive J is to arrange the two electrons in a high-spin configuration.

The other insulating region for $J > U/3$ (with the exception of a peculiar region at $J/U > 3/4$, which we shall discuss later on) is a less standard state in which only two multiplets are populated,

[2] In the paramagnetic phase all components of a given multiplet, with $\ell_z = -\ell, \ldots, \ell$ and $s_z = -s, \ldots, s$, are equally populated.

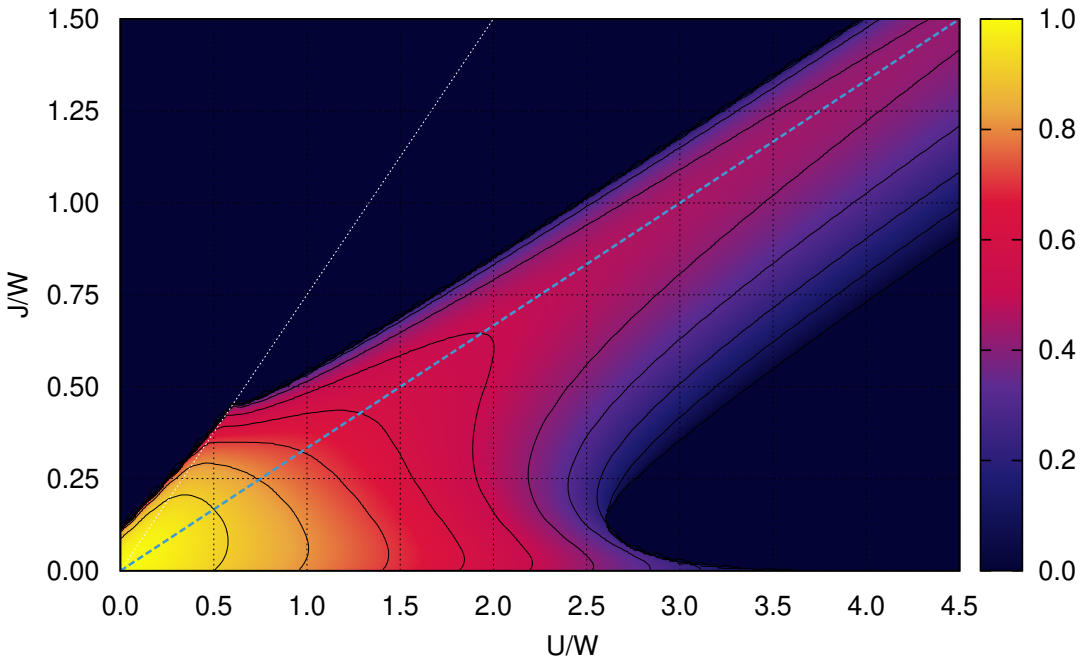

Figure 5.4: Paramagnetic phase diagram of the Hund system at commensurate filling $\bar{n} = 2$. Here, the dark region on the right is a Mott insulator, whereas in the upper left part there are two insulating states: A Hund insulator, in the region between the dashed and dotted lines, and an extreme negative charge-transfer insulator above the dotted line. The dashed ($J/U = 1/3$) and dotted ($J/U = 3/4$) lines indicate the degeneracy between the parent insulating states. The inset shows the same phase diagram (with identical scales for U, J, and Z) for a commensurate filling $\bar{n} = 3$. In this case, the Mott and Hund insulators coincide.

namely the high-spin multiplet with three electrons $|3, 0, 3/2\rangle$ (state 6 in Table 5.1) with a probability $p_3 = 2/3$, and the empty site $|0, 0, 0\rangle$ (state 1 in Table 5.1) with a probability $p_0 = 1/3$. We can picture this as a state where in every group of three sites we have two sites populated by three electrons in the high-spin state and one empty site, as depicted in the right box of Fig. 5.5. It is easy to picture this state as the result of a compromise between an attractive local interaction $U^* < 0$ which wants to concentrate charge on every site and a large Hund's coupling which maximizes the local spin. This favors configurations with three electrons on a site in high-spin state at as much sites as possible (depending of the average number of electrons present in the system). Obviously, for a system with 2 electrons per site this would mean that this non-homogeneous insulator will consist of 2 sites occupied by exactly three electrons each and one site empty, leading to a charge disproportionation.

We can refer to this state as a Hund insulator[3]. This means that the energy gain one obtains by realizing this spin 3/2 configuration overcomes the imbalance in charge created this way. Like in the Mott insulating state, also here charge fluctuations are suppressed; however, it is not the Coulomb repulsion that gaps them, but rather the energy gain associated with maximizing the local spin.

In the following we want to connect the existence of these two insulators with the correlation-resilient metal which intrudes between them. It is particularly interesting that the metal appears

[3]Within a single-site mean-field, like GW/RISB, but also DMFT in the paramagnetic state, this state is insulating and the empty sites are randomly distributed. Indeed, one can build an effective model in the large J regime which features both antiferromagnetic spin and nearest-neighbor repulsive terms of order t^2/J and a three-electron hopping term of the order t^3/J^2. The derivation and solution of this model are beyond the aim of the present manuscript, and our conclusions remain valid also in the case the insulator becomes a bad metal.

between the two insulators even when U and J are both very large with respect to W.

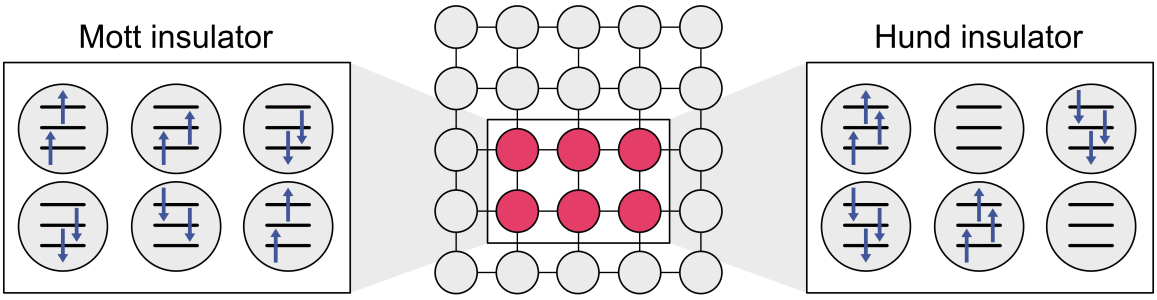

Figure 5.5: Schematic plot of the realization of the two distinct insulating states: a high-spin Mott and a charge disproportionation insulator, favored either by the Coulomb interaction or the exchange coupling, respectively. While in the Mott insulator all sites are populated by the lowest energy multiplet with maximum spin configuration $|2,1,1\rangle$, in the non-homogeneous Hund insulator the system tends to populate as much as sites as possible with the high-spin state $|3,0,3/2\rangle$ (with probability $p_3 = 2/3$), on expense of leaving some site empty (with probability $p_0 = 1/3$).

Owing also to the fact that both insulators have atomic nature, we start our analysis from the atomic limit with the aim of understanding how a metallic solution can appear in this limit.

In the atomic limit we can build the energy of the Mott insulator and of the Hund insulator simply by using the eigenvalues E_Γ listed in Table 5.1. The Mott insulator has energy $E_M = \frac{1}{2}(U - 3J) - 5J$, while the one corresponding to the Hund insulator reads $E_H = -5J$. Therefore the Mott insulator is stable for $0 < J/U < 1/3$ and the Hund insulator is the lowest energy state for $1/3 < J/U < 3/4$. At the extreme value $J/U = 3/4$ the Hund insulator becomes energetically unfavorable with respect to a fully disproportionated state with six electrons on one site every two empty sites.

The Hund and Mott insulating states are degenerate exactly along the line $J/U = 1/3$. Noteworthy, along the same line another inhomogeneous insulator is degenerate with the Mott and Hund insulators discussed above. This insulating state consists of sites with either one or three electrons (populating the maximal spin multiplet, $|1,1,1/2\rangle$ and $|3,0,3/2\rangle$, respectively, corresponding to states 2 and 6 in Table 5.1), with equal amplitudes. This state is never stable in the atomic limit except for the special line $U^* = 0$, where it contributes to the increase of the degeneracy of the ground state and, as we shall see, to the stabilization of the Hund's metal.

We notice that this maximal degeneracy can be tracked down to the specific form of the Kanamori Hamiltonian, in particular to the factor 4 between the coefficients of the $\mathbf{S}^2$ and $\mathbf{L}^2$ terms in Eq. (5.3) which favors the spin over the orbital angular momentum. It is worth mentioning that this relation between the coefficients is obviously not a necessary condition for the rotational invariance of the Hamiltonian and any linear combination of $\mathbf{L}^2$ and $\mathbf{S}^2$ would have satisfied the same condition. A different ratio between the two terms would result in a simpler twofold degeneracy between the Mott and Hund insulators, which appears than as a fundamental fact which simply follows from symmetry properties and not by arbitrary choices in the definition of the Hamiltonian.

Another peculiar consequence of the factor 4, strictly connected with the maximal degeneracy mentioned above, is the fact that the degeneracy line $J/U = 1/3$ corresponds also to the vanishing of the $(\hat{n} - 3)^2/2$ coefficient of $U^* = (U - 3J)$ in the Hamiltonian (5.3). In terms of the explicit Kanamori parametrization, this corresponds to the aforementioned inter-orbital decoupling. We believe there is nothing fundamental about the coincidence between the vanishing of U^* and the degeneracy of the insulators, apart from the aforementioned enlarged degeneracy. A

different ratio between the coefficients would result in a degeneracy line at some $U^* \neq 0$ and a clear separation between the two phenomena.

All above said is a consequence of the observation [77] that the $U = 3J$ line is the locus at which the atomic Mott gap $\Delta(\bar{n}) = E_0(\bar{n}+1) + E_0(\bar{n}-1) - 2E(\bar{n}) = U - 3J$ vanishes, where $E_0(\bar{n})$ is the atomic ground state for $\bar{n}$ electrons. The vanishing of the atomic Mott gap for $U = 3J$, and its small value for values of J/U close to this specific one, have already been noted in Ref. [77] as an argument for the resilience of the metallic region. However, the definition based on the inability of the system to open a Mott gap does not provides us with an explicit characterization of the Hund's metal which we discuss in the following section.

5.3.2 The Hund's metal as a bridge between the two insulators

We can now move to the inspection of the metallic solution ($Z > 0$) that separates the Mott and Hund insulating states. Although the metallic region is fully connected, in contrast to the insulating ones, we can, nevertheless, differentiate between two profoundly different regimes as a function of the interaction strength, which are nothing but the standard metal and the Hund's metal that we discussed in previous sections. The data of the first panel of Fig. 5.1 correspond to cuts along straight lines, defined with fixed J/U ratio. Namely, passing from the origin of the phase diagram of Fig. 5.4, they show that the evolution from the region of small U and J is nothing but the Hund's crossover we have widely discussed.

In the left bottom panel of Fig. 5.2 we have already shown the evolution of the multiplets as a function of U along the $U^* = 0$ line. In the region of small J and U (bottom left part of the phase diagram of Fig. 5.4), connected to the non-interacting solution ($Z = 1$) at $J = U = 0$, all the atomic multiplets are populated and a large number of hopping processes can be realized, leading to the maximum kinetic energy available in our model. Nevertheless, an increase of either U or J has the same net effect of reducing Z by disfavoring some multiplets, thereby reducing the phase space for hopping processes: an increase of U tends to reduce the population of multiplets with particle number different from the average filling (in this case, $\bar{n} = 2$), whereas an increase of J tends to reduce the population of multiplets with low spin. Both effects reduce the number of available hopping channels between sites, weakening the metallic properties measured by Z. For small values of the interaction parameters this reduction is smooth and relatively slow.

Then a rather sharp crossover occurs, where Z flattens. As we discussed above, the only populated multiplets are those with local occupation 0, 1, 2 and 3, and the largest spin configuration, namely $|0, 0, 0\rangle$, $|1, 1, 1/2\rangle$, $|2, 1, 1\rangle$, and $|3, 0, 3/2\rangle$. We now realize that these states are also those featured in the degenerate atomic insulators. The crucial observation is that the hopping Hamiltonian has finite matrix elements between these states even when U and J are very large. Therefore we can exploit the charge fluctuations between the different atomic insulators and obtain a metal with a significant kinetic energy. As a matter of fact, Z does not drop as a function of U because the populations of the different states remain constant. This is the physical reason for the resilience of the Hund's metal. We are able to satisfy the constraints due to J and U without killing the charge fluctuations.

The link between the Hund's metal and the insulators is clarified by Fig. 5.6, where we show the populations of the atomic multiplets along a cut at fixed $U/W = 3.5$, which connects both the insulating regions, Mott and Hund one, respectively, by increasing J/W value. One can observe that in the vicinity of the Mott transition the metallic state is formed by transferring a fraction of the population of $|2, 1, 1\rangle$ multiplet to the $|1, 1, 1/2\rangle$ and $|3, 0, 3/2\rangle$ multiplets, in equal amount. Hence, close to the Mott transition the insulators that give rise to the mixed valence state are only the Mott insulator and the additional degenerate insulator characterized

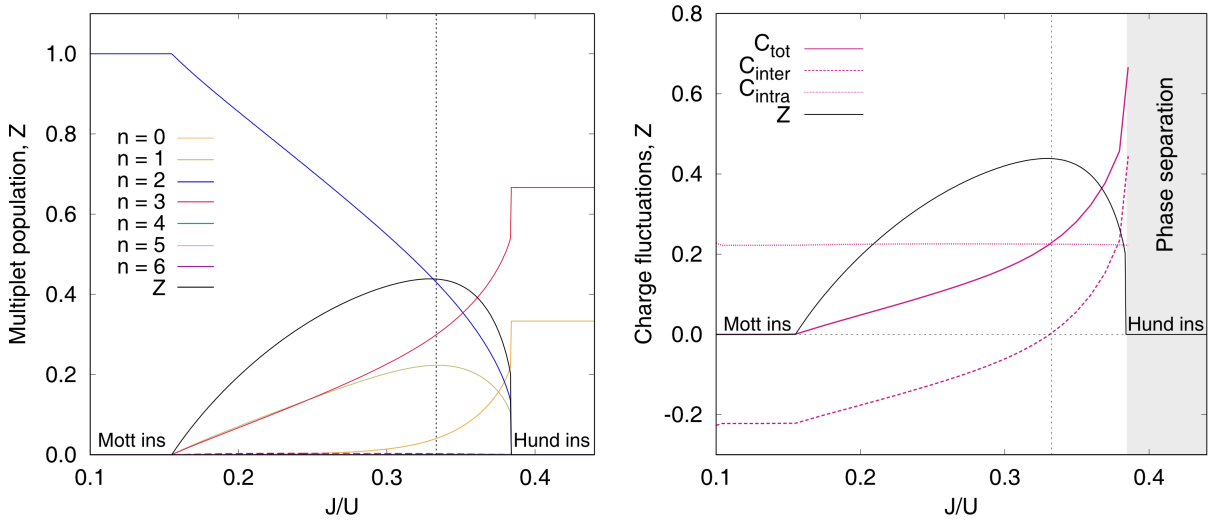

Figure 5.6: Left panel: Population of the various multiplets as a function of J/U at fixed $U/W = 3.5$ and $\bar{n} = 2$. Right panel: Charge-charge correlations (total, inter-orbital, and intra-orbital) for the same parameters as in the left panel. This particular cut is chosen in order to demonstrate the connection between two distinct insulators, Mott and Hund across the Janus phase. For this purpose, we present in both plots the quasiparticle weight (depicting the Janus tail) as a reference.

by one and three electrons per site (with $p_1 = p_3 = 1/2$). However, by going deeper into the Hund's metal region, the Hund insulator comes also into play, signaled by the rising of the $n = 0$ population already for $J/U < 1/3$, i.e., before the degeneracy line is reached. Eventually, at the line of degeneracy the $n = 1$ population reaches its maximum and starts to decrease, whereas the $|0, 0, 0\rangle$ and $|3, 0, 3/2\rangle$ populations continue to rise, thereby suggesting that the Hund insulator is now dominating the mixed-valence state. Therefore, the Hund's metal appears as a kind of a bridge between the different atomic insulators, and its mixed valence character results from the disproportionated character of two of the three insulators. As we mentioned above, the degeneracy between the Mott and Hund insulator is expected to be realized also in other models which respect spin and orbital rotation invariance.

5.3.3 Charge fluctuations

In order to better understand the interplay between the degeneracy of the atomic states and the orbital decoupling, we now study the charge response of the system along the same line, $U/W = 3.5$, presented in Fig. 5.6 (right panel).

In the Mott insulator one finds that the total charge fluctuations are equal to zero, as expected in a state where the charge fluctuations are completely frozen. This is actually realized as a sum of positive and negative values of intra-orbital and inter-orbital contributions, respectively, as discussed above. In this region the intra-orbital fluctuations are constant. The reason for this is that we are already far in this region where the Coulomb repulsion U is very large, and forbids any type of processes leading to two electrons in the same orbital (since these processes are penalized by U). However, the inter-orbital fluctuations can still be active, since we have the possibility to distribute two electrons in three orbitals. In this way we can allow them to move, always avoiding having the two electrons in the same orbital.

Entering the correlated Hund's metal region, the negative inter-orbital correlations start to increase, and eventually become zero just at the value $J/U = 1/3$, which corresponds to the inter-orbital decoupling. As discussed before, the value of the interaction $U - 3J$ between the

electrons in different orbitals is basically zero, and then it changes sign across the line. At this point the inter-charge fluctuation changes sign and starts increasing very rapidly as long as we move towards the charge disproportionated Hund insulator. Consequently, the total charge fluctuations here grow all the way to the Hund insulating region. Once we enter the Hund insulating region, which is a non-homogeneous state, Eq. (3.21) can not be used. Nevertheless, at least locally, one can always find that the charge fluctuations will be equal to zero. To conclude, it is important to stress that, due to the freezing of the intra-orbital charge fluctuations, the inter-orbital processes are the one to enable this metallic region.

5.3.4 Region $J/U > 3/4$

For the sake of completeness, let us briefly explain the peculiarity of the $J/U > 3/4$ region. In this extreme case of negative charge gap, $U^* < -5/4U$, the insulating ground state is simply the state that maximizes the charge imbalance, so that each site has either the minimum ($n = 0$) or maximum ($n = 6$) number of electrons even if these states have zero spin. In order to fulfill the average filling $\bar{n} = 2$, the fractions of empty or fully occupied sites will be $p_0 = 2/3$ and $p_6 = 1/3$, respectively. Importantly, despite the fact that this insulator is degenerate with the Hund insulator at $J/U = 3/4$, no metallic state emerges along the degeneracy line at strong coupling. In other words, there is a direct first-order transition between the two insulators. The reason is that the two insulators cannot be connected by simple hopping processes between multiplets that are already present in the insulators, and in order to form a metallic state one would have to populate all the multiplets with intermediate particle number between zero and six, paying a high potential energy cost. This region, in any case, is most likely unphysical for any real material.

5.4 The case $\bar{n} = 3$. Mott and Hund insulators coincides

We have stressed repeatedly that the Hund's metal physics is not realized at half-filling, where a more standard Mott transition is realized, even if with some peculiarity that we discussed.

The link between the degeneracy of the atomic insulators and the realization of a Hund's metal can be better understood by looking at Figs. 5.7, where the phase diagram is shown for a commensurate filling $\bar{n} = 3$. The difference with $\bar{n} = 2$ is apparent. Here the insulating region is fully connected and the metallic behavior is limited to a relatively small region of small U and J. This is clearly generalizing to the region of $J/U > 1/3$ the results we have presented in Fig. 5.1.

The key observation to understand the lack of a Hund's metal state in the large U and J regime is that, for this density, there is no competition between Hund's coupling and Hubbard U. Indeed the state $|3, 0, 3/2\rangle$ satisfies simultaneously the Hubbard term, which selects states with 3 electrons, and the Hund's coupling since we obtain the highest possible spin. Therefore, the Mott and the Hund insulator simply coincide and they amount to a single multiplet with fixed population. Consequently, for large U and J there is no coexistence of multiplets with different population, hence the kinetic term has no matrix elements and the system remains insulating. As we have seen before, the effect of the interactions is simply to filter out the Hund/Mott insulating state out of the many multiplets, leading to a progressive (actually abrupt) decrease of Z.

Finally, in Fig. 5.8 we show the quasiparticle weight, multiplet population and charge correlations at fillings $2 \leq \bar{n} \leq 3$, connecting the two limiting cases we have considered so far, $\bar{n} = 2$ and $\bar{n} = 3$. We focused on the same point of the two phase diagrams, belonging to the degeneracy line, where $U/W = 3.5$ and $J/U = 1/3$. We see the progressive filtering of the $\bar{n} = 3$

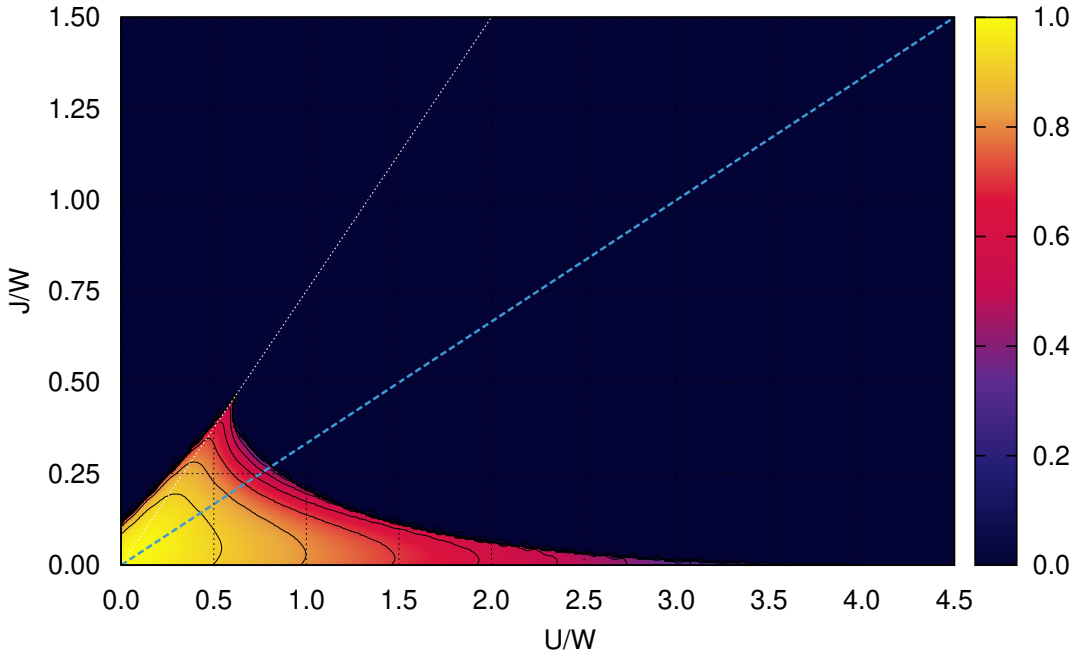

Figure 5.7: Paramagnetic phase diagram of the Hund system at commensurate filling $n = 4$. Here, the dark blue region on the right is a Mott insulator. The dashed ($J/U = 1/3$) and dotted ($J/U = 3/4$) lines indicate the degeneracy between the parent insulating states. Here the Mott and Hund insulators coincide.

Mott insulating multiplet out of the bunch of populated multiplets for $\bar{n} = 2$. As a matter of fact the system survives in a Hund's metal for every doping different from $\bar{n} = 3$, even if the valence fluctuations are reduced by approaching half-filling. The evolution of the charge correlation functions shows that the whole region of densities is characterized by vanishing inter-orbital correlations, confirming our previous statement that Hund's metal physics is realized everywhere but in the Mott insulator.

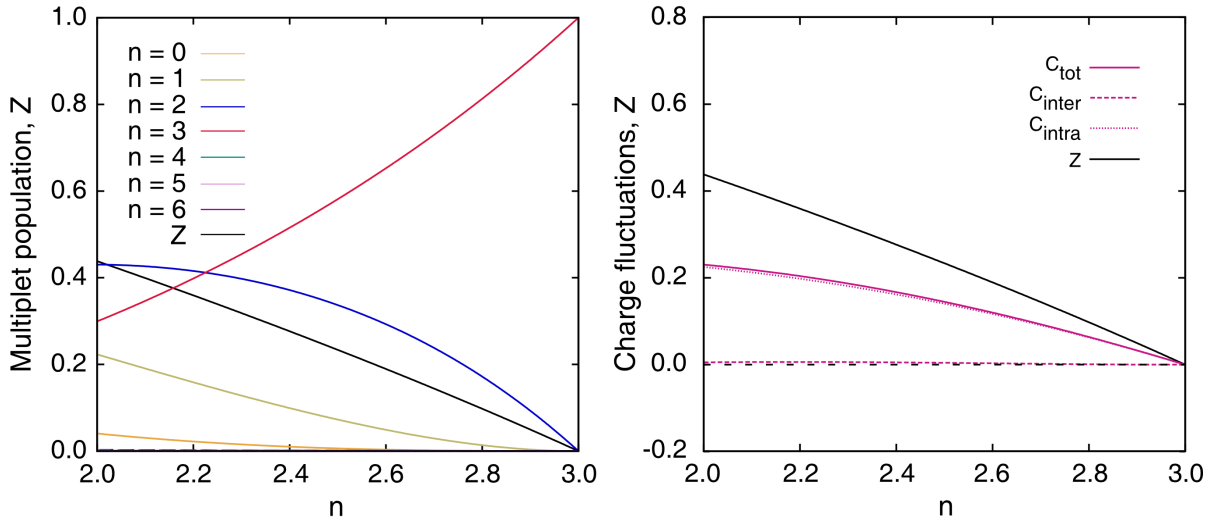

Figure 5.8: Multiplet populations (left), charge correlations (right) and quasiparticle weight (both) as a function of the average density connecting the Hund's metal and Mott insulator at $U/W = 3.5$ and $J/U = 1/3$.

5.5 Phase diagrams for negative J

In this chapter, as in the rest of the thesis, we have so far considered the 'physical' case of a positive Hund's coupling $J > 0$. The sign of the Hund's exchange descends indeed from the repulsive character of the Coulomb interaction which reflects in an exchange mechanism favoring high-spin (and high-orbital angular momentum) configurations. However, it can be interesting to extend our analysis also to the case of $J < 0$, a regime which can be useful to strengthen our conclusions, and that can also find a physical realization in some materials.

The physical mechanism to obtain an inversion the Hund's rules is the coupling with phonons. In particular, for a multi-orbital electron-phonon system, one has Holstein modes, which couple to the total charge and therefore reduce the value of U, and Jahn-Teller modes, which couple with internal degrees of freedom and lead to an attractive term in the spin and orbital channels. Formally, one can integrate out the phonon modes, which leads to an effective attractive electron-phonon interaction that depends on the frequency. If we assume, for formal simplicity, an antiadiabatic limit for the electron-phonon coupling, we can neglect the frequency dependence and the phonons give rise to terms which are exactly of the same form of the Coulomb interaction, but with opposite sign. This is the case of alkali-metal doped fullerides A_3C_{60} (where A = K, Rb, Cs), where it has been shown [117–121] that the attractive contribution due to phonons has the same functional form of the Hund's exchange, but it has a larger strength with respect to the repulsive Coulomb term (the J we used so far). Therefore, we have $J_{eff} = J - J_{phonons} < 0$. In the following we will use the standard symbol J for J_{eff} and we will consider $J < 0$, which means that the system now favors low-spin and low-orbital-angular momentum states. We notice that this model, with small values of J, has been shown to describe (actually predict) the phase diagram of Cs_3C_{60} under pressure and the whole dependence of the superconducting phase on the lattice spacing in these materials, which features a first-order transition between a Mott antiferromagnet and an s-wave superconductor. After DMFT calculations at model level have shown that this physics is a direct consequence of a large U and a finite negative J [118, 119], this scenario has been made quantitative by ab-initio modeling [120, 121]. More recently, DMFT calculations have shown that for larger values of J/U one finds a kind of Jahn-Teller metal which is the negative-J counterpart of the Hund's metal [122].

We now follow the same strategy we used for $J > 0$ case and explore the phase diagram of the model for the same densities $\bar{n} = 2$ and $\bar{n} = 3$. We start from the half-filling system, which is motivated by the physics or alkali-doped fullerides.

In the phase diagram in the right panel of Fig. 5.9 we show the quasiparticle spectral weight Z in the normal state (inhibiting the superconducting ordering, which is also realized using RISB [123]). It is evident that the phase diagram is different from the repulsive-J model at the same density, but it is reminiscent of the situation we found for $\bar{n} = 2$ in the previous model. In fact, in contrast to the Hund system, the case of negative J sees the competition between distinct insulating states, promoted by either U or J.

The insulator (dark region) on the right side of the plot is again a standard Mott insulator with three electrons localized on every site. In this case, the three electrons now populate the lowest-spin multiplet $|3, 1, 1/2\rangle$ (state 7 in Table 5.1). The insulator in the left-upper part of the diagram is instead a charge-disproportionated insulator favored by the negative Hund's coupling. In this case this is a simpler state formed by equal proportions of sites populated by two or four electrons in the low-spin configuration, namely the $|2, 0, 0\rangle$ and $|4, 0, 0\rangle$ multiplets (states 3 and 9 in Table 5.1). It is interesting to note that in this case the 'Jahn-Teller insulator' is a superposition of singlets with different occupations which can be seen as a precursor of the superconducting state. In this sense it is reminiscent of the pairing insulator found in the

attractive Hubbard model when superconductivity is inhibited [124, 125]. This suggests an interesting link between the mixed-valence metal and superconductivity.

We can, therefore, follow the same line of thought of the $J > 0$ case and discuss the stability of the two insulators. Also here the two insulators become indeed degenerate along a certain line with constant $|J|/U$ ratio, in this case $|J|/U = 1/2$, while the two insulators are stable above and below the line in the atomic limit.

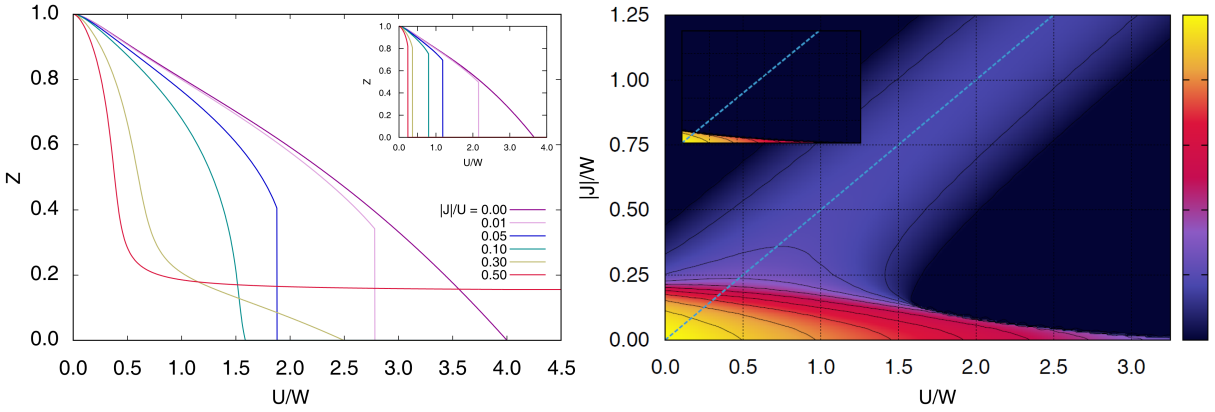

Figure 5.9: Left panel: Quasiparticle weight Z as a function of interaction strength U and different values of fixed $|J|/U$ for a JT system at $\bar{n} = 3$ (and $\bar{n} = 2$ in the inset). Right panel: The same quantity for a whole range of U and J. For $\bar{n} = 3$ and $|J|/U = 1/2$ (degeneracy between Mott and pairing insulators), Z remains asymptotically finite at arbitrarily large U. Corresponding cuts at fixed $|J|/U$ are shown in the left panels.

Let us now turn to the metallic state which, as the phase diagram shows, fully separates the Mott and pairing insulators. Also in this case the metal undergoes a clear crossover moving from the weakly correlated region at small U and J, where all the multiplets are populated and the quasiparticle weight decreases as a function of both U and $|J|$. On the other hand, the highly correlated region located along the degeneracy line represents a JT metal (in analogy with the Hund's metal), where the only populated multiplets are those already present in the insulating states on the left and right of the region, namely $|3, 1, 1/2\rangle$, $|2, 0, 0\rangle$ and $|4, 0, 0\rangle$. As in the Hund system, the emergent JT metal can be regarded as a mixed-valence state where, in the presence of a degeneracy between two insulating states, the systems gains additional kinetic energy by allowing hopping processes that connect the eigenstates of the two insulators. The maximum energy gain and maximum quasiparticle weight are reached exactly on the line of degeneracy, where the multiplet population reveals a state that is a symmetric mixture of the two insulators. The analogies between JT and Hund's metals are further strengthened by the similarity in the Janus effect, shown in the left panel of Fig. 5.9, where we plot cuts at fixed $|J|/U$. We also note that, as a result of the lower degree of degeneracy that characterizes the JT system, and the corresponding smaller number of hopping processes that take place in the JT metal, the asymptotic value of the quasiparticle weight is smaller, here, in comparison to the Hund system. It should be clear that this result strongly supports our interpretation which considers the degeneracy between strongly correlated insulators as the key condition for the existence of the correlation-resilient metal regardless of the precise model at hand.

A last confirmation of our picture is given by the phase diagram for $\bar{n} = 2$ (inset in right panel of Fig. 5.9). In this case, just like for $\bar{n} = 3$ and positive J, the pairing insulator and the Mott insulator coincide and they are simply given by the single state $|2, 0, 0\rangle$ (obviously the same would happen for $\bar{n} = 4$), which clearly satisfies both the Hubbard U, since charge fluctuations are frozen, and the negative Hund's coupling, since the state has $S = 0$ and $L = 0$. In this case

the Jahn-Teller-Mott insulator [117] invades a large area of the phase diagram and no Jahn-Teller metal is stabilized. The metallic solution survives only in the bottom left part of the phase diagram.

There is yet an important difference between the JT and Hund systems, namely the link between the degeneracy line between competing insulating states and the vanishing charge-transfer gap. While in both systems the degeneracy line is the place where the mixed valence JT or Hund's metals are stabilized, in the JT system the degeneracy line is not linked with a vanishing charge-transfer gap as in the Hund system. In fact, the charge-transfer gap remains positive for any value of $J < 0$. Consequently, in the JT system the metallic solution at half-filling and large $U \sim 2|J|$ remains stable upon doping, and the effects of the $|J|/U = 1/2$ ratio are characteristic only of the $\bar{n} = 3$ commensurate filling.

5.6 Conclusions

In this chapter we have extended the usual range of the parameter U and J associated to the Kanamori model, with the scope to study the origin of the Hund's metal. We have shown, exploring the full U-J phase diagram of the system with two electrons in three-orbitals, that the correlation-resilient metal emerges precisely in the region between the two distinct insulating states: a high-spin Mott insulator, favored by the Hubbard repulsion U, and a charge disproportionation insulator, or so-called Hund insulator, favored by the exchange coupling and characterized by the inhomogeneous spatial charge distribution.

The competition between the two insulators results in an asymptotic mixed-valence metallic state in the region where the interaction parameters are balanced. Indeed, we have shown that the Hund and Mott insulating states are degenerate exactly along the line $J/U = 1/3$, appearing at arbitrarily large interaction strength. Moreover, along the same line we find another inhomogeneous insulator, degenerate to the Mott and Hund insulator, which, indeed, contributed to the hopping processes needed for the realization and stabilization of Hund's metal. However, this state is never stable in the atomic limit.

In order to confirm this picture and make it more general, we compared this situation with the one of the global half-filling $\bar{n} = 3$, where we have seen that the Hund's metal can not be found. Even making the further comparison with a case with negative Hund's coupling, corresponding to the Jahn-Teller coupling with some local phononic modes, we found that the correlations-resilient metal emerges along the line where the disproportionated insulators are degenerate.

These results provide a characterization of the Hund's metal state and connect its presence with possible charge instabilities, which have indeed been observed in chromates, and have proposed to play a crucial role in iron-based superconductors.

6

Orbital dependent interactions

In this thesis we have accounted for some of the many interesting results which have been obtained in the last years for strongly correlated multi-orbital models. Most of the results have been obtained for very symmetric models in which both the electronic bands and the interactions do not depend on the individual orbitals and they are parameterized by two parameters, U and J, which can be takes in its full Kanamori form and in the Ising version. Already with these important simplifications these models reveal a rich physics [71, 78], which can flourish in a number of directions once we consider deviations from the symmetric case.

As we commented in Chapter 3, the effect of breaking the symmetry between the orbitals has been mainly taken into account in the single-particle properties, in particular considering different hoppings (bandwidths) for the various orbitals or a crystal-field splitting. We have briefly discussed how both these effects can lead to orbital differentiation and even orbital-selective Mott transitions. Both these orbital-selective phenomena are indeed strongly favored by the Hund's coupling, which decouples the orbitals, therefore favoring a different behavior among them. In this section we focus on a different way to induce orbital-selective phenomena, which is also motivated by the properties of real solids. Namely, we focus on the case where the interaction terms appearing in the Kanamori Hamiltonian are not independent on the chosen orbitals. This is in most cases the outcome of realistic estimates of the Coulomb integrals using, e.g., constrained-RPA [80], and it is certainly the case when we consider unit cells including different correlated atoms, which may be relevant for some interesting materials.

Already the symmetric problem depends on a number of parameters, namely J, U, the number of orbitals and the filling, and allowing for arbitrary values for the Coulomb and exchange integrals makes the parameter space hopelessly complicated. For this reason we will choose a few subset of parameters to reveal some main trends induced by non-symmetric interactions.

6.1 Non-uniform density-density interactions for $J = 0$

Symmetric interactions with $U' \neq U$

We start exploring the effect of non-uniform interactions on the Mott transition of multi-orbital Hubbard model. For that purpose, let us generalize the case we discussed in Sec. 3.2 of a multi-orbital Hubbard model in which we only have charge-charge interactions and let us take that the repulsion between electrons in different orbitals U' is smaller than the one for electrons in the same orbitals U. At this level we are not really invoking the breaking of rotational invariance between the orbitals, but this analysis can be used as a starting point. We start from results obtained in the absence of the Hund's coupling, $J = 0$, in order to examine how the orbital degeneracy effects a metal-insulator transition. Here we report the results for three-orbital model at the three independent integer electronic fillings. Since our goal is to study purely the role of the multi-orbital interactions on the Mott transition, we exclude the possibility of having the crystal-field splitting terms or any asymmetry regarding the width or shape of the bands, setting the inter-orbital hybridization to be equal to zero. For simplicity, we consider a flat density of states for each orbital, where W is the bandwidth of the non-interacting electron band, though our main conclusions should not depend on this choice.

Let us now try to investigate the behavior of the quasiparticle weight for the fillings different from $n = N$. We still assume that the inter-orbital Coulomb interaction can be expressed in terms of the intra-orbital one, equivalent in each orbital, with the dependence $U' = \alpha U$, where $\alpha \leq 1$. As we will see below, this particular case captures many important features observed in the more relevant ($J \neq 0$) case and allows a simple interpretation of the results. To write things explicitly, if the interaction is $\hat{H}_{int} = 1/2 \sum_{mn} U_{mn} \hat{n}_m \hat{n}_n$, here we are taking $U_{11} = U_{22} = U_{33} = U$ and $U_{12} = U_{23} = U_{13} = U'$.

In Fig. 6.1 we show the results for this model at filling $n \leq N$. The three plots show a striking similarity with those of Fig. 3.10 for the three-orbital Hubbard-Kanamori model with finite J, discussed in Sec. 3.3[1]. However, this should not come as a surprise recalling Eq. (3.10). Indeed, if we consider that the Kanamori Hamiltonian imposes $U' = U - 2J$, meaning that U' is constrained by the value of Hund's coupling J, we can see α as if it "carries" the portion of effect of J. In this sense one can write $U' = U - 2J = \alpha U \rightarrow 1 - \frac{2J}{U} = \alpha$. If we impose $\alpha = 1$ we get $J = 0$, both corresponding to the situation where $U' = U$. On another side, when $\alpha = 0$, we find that $U = 2J$, which is satisfied precisely when $U' = 0$ in Kanamori case. However, one should not conclude (wrongly) that the two models are the same. Namely, the Kanamori Hamiltonian (3.10) in the third term contains also the explicit contribution of J accounting for the interaction between aligned spins in two different orbitals (that, moreover, polarize the system), in which essentially all the Hund's physics is contained, whereas the condition $U' = U - 2J$ is a consequence of a chosen model. However, we can see the above mentioned similarities between two models as if the former one contains a portion of the effect of Hund's coupling in Kanamori model. This will become more clear in the following.

First, let us consider the situation with a single electron in three orbitals. This case is a quite trivial one, since having a single electron the system does not pay any energy cost due to the absence of other electrons. On another side, the reduction of α tends to decouple these three degenerate orbitals. Eventually, when $\alpha = 0$, meaning that the inter-orbital interaction is absent, one finds the situation where all the orbitals behaves as three independent single-orbitals with 1/3 electron in each of them. From this situation results the metallic behavior, that becomes more and more pronounced as the orbitals are more and more decoupled.

[1]Note that, however, the relative value of U is different since in the two cases we are assuming two different density of states: flat and semi-circular one, respectively.

On the other hand, the case $n = 2$ to some extent reminds the Janus effect described in Chapters 3 and 5, for the reason explained above. However, despite showing a well pronounced tail for large values of Coulomb repulsion, the strong decrease of Z for the small U found with Kanamori Hamiltonian is absent. This is due to the fact that once we include a complete J (or even its Ising component) we have a strong quenching of the hopping channels, since only processes which conserve the high-spin configurations are allowed. For this reason one finds a strong reduction of the effective kinetic energy and consequently of Z. On another side, in the model considered here we do not have any constraints on the choice of spin, in sense that an electron can hop to any position, as long as it satisfies the Pauli principle. Therefore, this model somehow features only half of the 'Janus' physics, namely the increase of the atomic gap, and a somehow intermediate scenario. Eventually, the tail remains metallic while decreasing α, having 2/3 of (uncorrelated) electron in (almost) decoupled three orbitals.

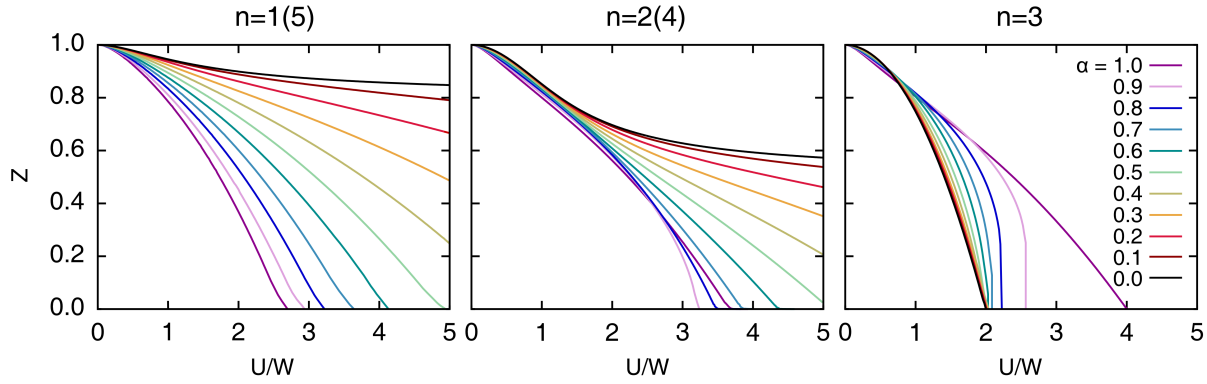

Figure 6.1: Quasiparticle weight Z as a function of interaction strength U_1/W (where W is the bandwidth of the flat density of states), for $n \leq N$ (and corresponding $n > N$ due to particle-hole symmetry). There is an evident resemblance with the behavior in Fig. 3.10 induced by Hund's coupling J (see in the text).

Finally, the half-filling case $n = 3$, anticipated in Chapter 3, was partially discussed in Ref. [74], by means of RIBS and DMFT approach. Here we confirm the ideas underlined within that study, or more precisely, that for $\alpha < 0.5$ the critical interaction U_c is independent of the value of U' and coincides with the one estimated for the single-orbital case. Also in this case orbital fluctuations are apparently completely quenched when α is below this threshold. Meanwhile, for larger α U_c is shifted towards higher values, owing to the enhancement of the charge fluctuations with increasing U' and correspondingly α. The maximum critical value of the interaction strength is obtained when $U' = U$, recovering the result for the fully rotationally-invariant model.

Let us make a short remark regarding this particular case, with $n = 3$ electrons. To be specific, let us compare it with the result from Fig. 3.10 for the same filling. The trend of decreasing α is similar to the one obtained by increasing J, as long as $\alpha > 0.5$. At this point, as already mentioned, a sudden decoupling between the orbitals takes place. In Kanamori one does not find this kind of rigid decoupling and the evolution as a function of J is more regular. As a first argument, we can attribute this to the several matrix elements connecting the different orbitals of the Kanamori model.

6.1.1 Asymmetric interactions

The previous section as well as a few previous studies have shown that once we reduce the symmetry of the interactions we immediately find deviations from the standard behavior of the Mott transition which partially recalls the effect of the Hund's coupling. In this section we

further reduce the symmetry of the interactions assuming a hierarchy between the different orbitals. More precisely, we decide that orbital 1 is more correlated than the other two orbitals, i.e., that their intra-orbital repulsion is not the same and in particular $U_{11} > U_{22} = U_{33}$. We may see this effect as arising from a different chemical nature of orbital 1 (as an extreme example, we can thing of copper oxides, assuming orbital 1 to be copper and orbitals 2 and 3 oxygen), or from some symmetry breaking induced by lattice deformations or other structural/chemical effects.

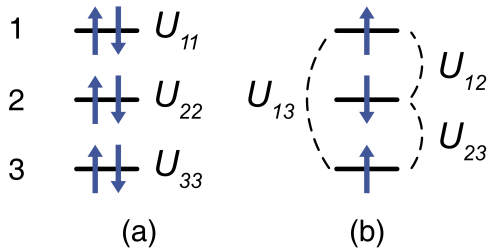

Figure 6.2: Asymmetric Coulomb interactions in multi-orbital systems: (a) intra-orbital, for each of the three bands, (b) inter-orbital, between two different bands

In order to describe this effect, we introduce the following parametrization:

$$\begin{aligned} U_{22} &= U_{33} = \beta U_{11} \\ U_{12} &= U_{13} = \alpha U_{11} \\ U_{23} &= \alpha\beta U_{11} = \beta U_{12} = \beta U_{13}\,, \end{aligned} \tag{6.1}$$

as graphically described in Fig. 6.2 We have defined, besides the α parameter introduced above, a new coefficient, β, which controls the ration between the Coulomb repulsion in orbitals 2 and 3 with respect to 1. α is again defined as the ratio between the off-diagonal interactions and the diagonal ones. Here we assume, somewhat arbitrarily, that also the off-diagonal interactions have a hierarchy, with the interaction between orbitals 2 and 3 smaller by the same factor β with respect to the repulsions involving also orbital 1 (U_{13} and U_{12}). For $\beta = 1$ we recover the model of the previous section. This choice is obviously motivated by the need for reduction of the number of parameters to allow for some characterization of the physics. We will avoid the limits where α and β are very small, where some pathological behavior can be realized.

We present our results along some lines with a fixed value of one parameter.

6.1.2 $\alpha = 1$

We start from the case where $\alpha = 1$ and where the only parameter introducing an asymmetry between the orbitals is β, meaning that $U_{11} = U_{12} = U_{13} = U_1$, and $U_{22} = U_{33} = U_{23} = \beta U_1$. The main effect of $\beta < 1$ is to make orbital 1 more correlated than the orbitals 2 and 3, at the same enhancing the repulsion between it and the other orbitals. The main expectation is that the decrease of β should induce a depopulation of orbital 1, an effect which, at least qualitatively, mirrors that one related to a crystal-field splitting, where orbital 1 has higher energy than the other two. In such situation the system will tent to prefer those configurations with the lower energy cost, namely the ones in the lower manifold (belonging to the orbitals 2 and 3). Obviously, this is expected to lead to a differentiation in the values of Z between the orbitals.

In Fig. 6.3 we plot Z_1 and $Z_2 = Z_3$ and the orbital occupations as a function of U_1, for three values of β and for the three densities $n = 2, 3, 4$ (notice that now $n = 2$ and $n = 4$ are not

equivalent because particle-hole symmetry is explicitly broken). We do not report results for $n = 1$, which is barely affected by the anisotropies and for $n = 5$ for reasons we describe below.

The main effect of β goes exactly in the direction we expected. For $\beta < 1$ increasing the absolute value of all the interactions leads to an increasing tendency to transfer charge from orbital 1 to orbitals 2 and 3. Therefore, in all the three cases we consider, we start from a homogeneous distribution between the three orbitals, but we rapidly induce a polarization where more and more charge is populating the two orbitals with smaller interaction. This leads to physically different scenarios according to the value of the total charge, namely n_1 and $n_2 = n_3$. In all cases we reach at some point a transition where orbital 1 is completely empty and the remaining electrons occupy the two-fold degenerate manifold, which then undergoes a Mott transition when U becomes large enough. The critical values of U_c reproduce that of a two-orbital model. For $n = 4$ we have instead a band insulator with $Z = 1$ occupied by four electrons. According to this picture, the case $n = 5$ leads to a situation with a half-filled band for orbital 1 and a completely full 2-3 manifold.

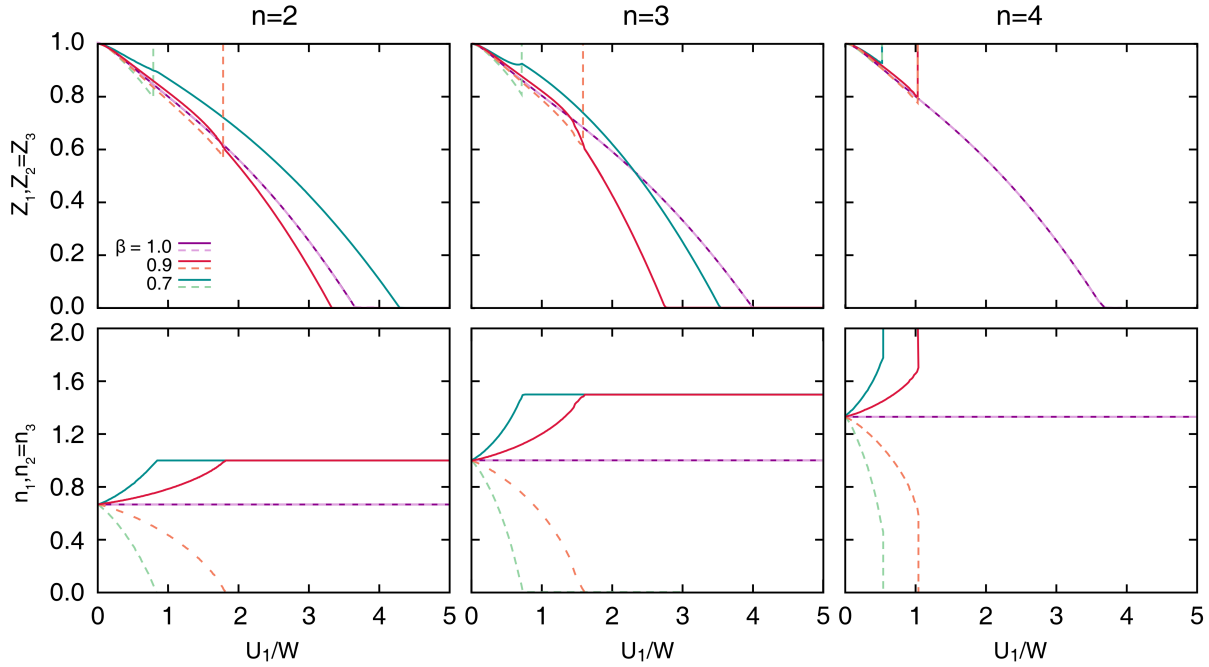

Figure 6.3: Quasiparticle weight Z_1 and $Z_2 = Z_3$ and orbital occupation n_1 and $n_2 = n_3$ in a three-orbital non-degenerate Hubbard model, for different integer filling $n = 2, 3, 4$. We set $\alpha = 1.0$ and $\beta = [0.7, 1.0]$.

Apparently, if we would have taken $\beta > 1$, making two orbitals more correlated, there would have been a sort of inversion between the results for $n = 2$ and $n = 4$ in Fig. 6.3.

6.1.3 $\alpha = 0.7$

Now we study the system as a function of β starting from a situation where $\alpha < 1$, which leads to a partial "decoupling" between the orbitals, as discussed above. In particular we consider $\alpha = 0.7$ (see Fig. 6.6). For this choice of α we are not yet in the regime where the model behaves as a collection of single-orbital models, but we are also quite far from the symmetric $\alpha = 1$ regime.

Once we allow the change of β that leads to a smaller energy cost of having an electron in the configurations related to the orbital 2 and 3, we fully lift degeneracy, setting the parameters from Eq. (6.1) to be all different. The results obtained for this model are presented in Fig. 6.4, where we

have presented the quasiparticle weights, Z_1 and $Z_2 = Z_3$, together with the occupation number for each band, n_1 and $n_2 = n_3$.

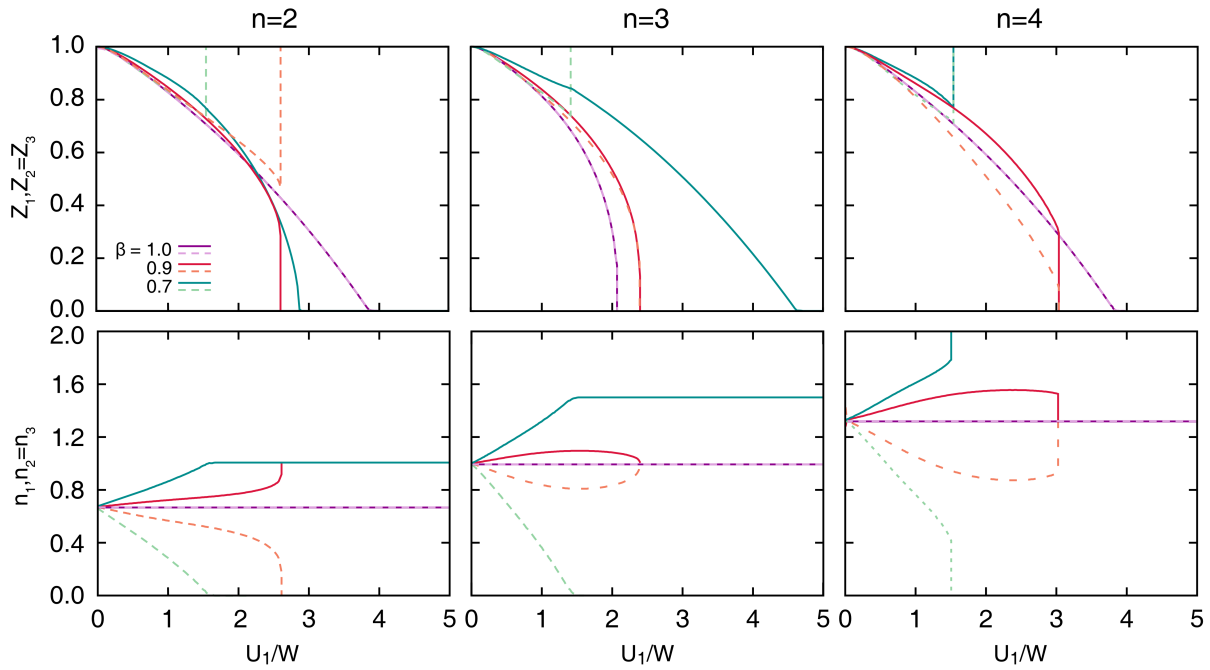

Figure 6.4: Quasiparticle weight Z_1 and $Z_2 = Z_3$ and orbital occupation n_1 and $n_2 = n_3$ in a three-orbital non-degenerate Hubbard model, for different integer filling $n = 2, 3, 4$. We set $\alpha = 0.7$ and $\beta = [0.7, 1.0]$.

Let us first, for simplicity, focus on the case $n = 3$. Clearly, situation $\alpha = 0.7, \beta = 1$ is the one observed in Fig. 6.1 with a rather fast Mott transition favored by the decoupling of the orbitals, as discussed above. If we slightly imbalance orbital 1 with respect to the others by taking $\beta = 0.9$, we can see that the Z-s are increased as well as the critical U_c for the Mott transition, inducing only very small differentiations between Z_1 and $Z_2 = Z_3$ and for the occupations, where n_1 becomes smaller than $n_2 = n_3$. When the initial differentiation is small, as in this case, the two orbitals do not decouple and, increasing the interactions counteract the initial bifurcation between the occupations. Indeed, by increasing U one obtains a single Mott transition where the Z-s of the three orbitals vanish simultaneously and we recover an even population of the three orbitals. When we further reduce β, we recover instead results similar to $\alpha = 1$, where the system polarizes at a critical U_c, meaning that the orbital 1 becomes empty and the remaining two orbitals host the three electrons with a Mott transition taking place by further increasing the interaction.

For $n = 4$ we have a similar trend with respect to $n = 3$. For moderate imbalance $\beta = 0.9$ we find an initial polarization of the orbital populations followed by a correlation-induced reduction of the same quantity. This leads also in this case to a single Mott transition which, however, appears to be of first-order, signaling that the competition between the effects of α and β is here stronger.

For $n = 2$ we find instead a scenario which is closer to the case of $\alpha = 1$ and to the results obtained for smaller β for the other two densities. Here already for the small value $\beta = 0.9$ we find that the polarization between the orbitals increases as a function of the interaction and leads to complete orbital polarization at a value of U which is reduced by decreasing β, that makes the system less symmetric. In this case it seems that the lower occupation of the orbitals with smaller repulsion allows for a more effective decoupling between them and orbital 1 with respect to the other densities.

6.1.4 $\beta = 0.8$

Finally, let us examine the behavior of the system at fixed β, such to split the intra-band Coulomb interactions that belong to two different manifolds, comparing results for different α-s which span from the fully symmetric regime $\alpha = 1$ to the completely decoupled limit $\alpha = 0$.

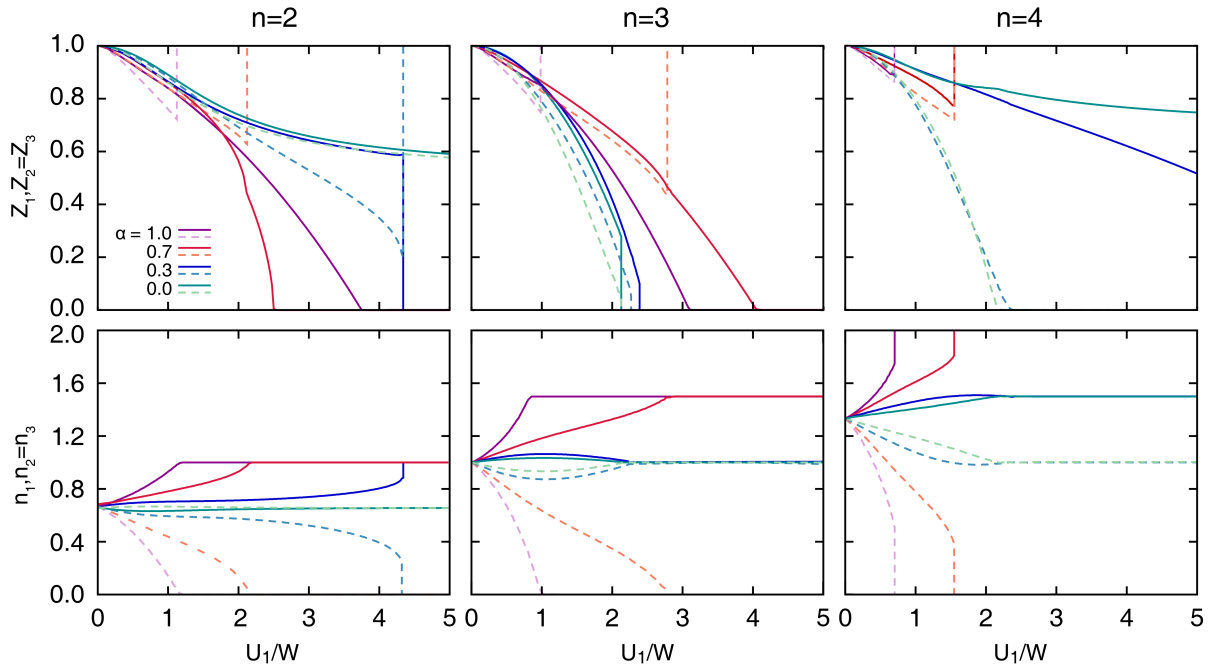

Figure 6.5: Quasiparticle weight Z_1 and $Z_2 = Z_3$ and orbital occupation n_1 and $n_2 = n_3$ in a three-orbital non-degenerate Hubbard model, for different integer filling $n = 2, 3, 4$. We set $\alpha = [0.0, 1.0]$ and $\beta = 0.8$.

The results for $n = 2$ confirm that this density is particularly susceptible to full orbital polarization which in turn leads to a completely empty orbital 1. At least for the chosen value of β we find indeed a complete polarization at some U, whose value grows when we reduce α. Just as in all the previous cases, after the polarization of orbital 1, we observe a more or less standard Mott localization in the remaining manifold of orbitals 2 and 3.

In the half-filling case, presented in Fig. 6.5, we see that the value of α triggers a clear change of behavior between the polarized limit and the case where we have a collective Mott transition, which is realized for small values of α.

Finally, $n = 4$ case shows a very interesting behavior. Namely, while decreasing α, the system "transits" from band insulator-metal regime, to an OSMT. This means that, instead of choosing between having one band empty and other two full, and all equivalently populated bands, the system prefers to split them such to have two independent Mott transitions. This is possible since the splitting between the manifolds is already sufficiently large and, moreover, the manifolds are almost decoupled ($\alpha \sim 0.3$) or fully decoupled ($\alpha \sim 0$). If we recall what we have previously anticipated, namely that decreasing α to some extend corresponds to an increase of J, we can observe some similarities in behavior between this situation and the one described in Sec. 3.4.4, for crystal-field split orbitals in the presence of the Hund's coupling.

Already these few snapshots assuming a very limited parametrization show the richness of the physics induced by orbital-dependent interactions, suggesting that these effects should be seriously taken into account in studies of real materials. We notice a strong dependence on small changes of parameters and on the charge density, which is characteristic of correlated materials.

6.1.5 Summary diagram

We can summarize the results of our model in a sort of phase diagram in the space of α and β. We consider the case of $n = 3$ which emerges as the most generic among the densities we have considered. Along the line $\beta = 1$ we have a "standard" metal-Mott insulator transition where the electrons are equally distributed among the orbitals, no matter the value of α (which affects only the critical interaction strength U_c). When we increase α, we introduce a competition with a phase where the orbitals are decoupled by α and polarized by β. Therefore we have a sort of critical α, growing with β above which we obtain the full polarization with an empty orbital 1 and a Mott transition limited to the 2-3 manifold. We can see this simple diagram as the skeleton of more realistic and complete descriptions of this physics. As we have seen above, the main competition between a single collective Mott transition and a polarized systems can also be enriched by other phases like an OSMT in the case of four electrons.

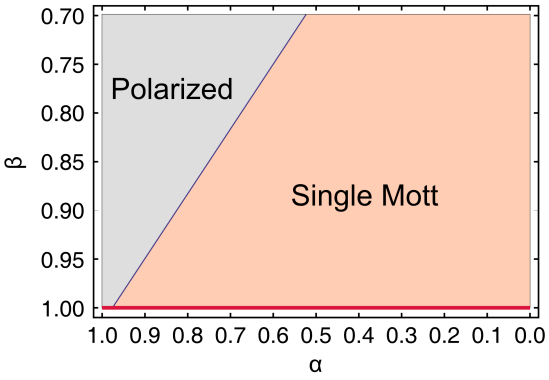

Figure 6.6: A sketch of two distinct regimes, polarized (blue) and singe Mott (red) emerging from the competition between two different parameters, α and β, defined in Eq. 6.1 or more precisely, between anisotropic Coulomb interactions. The red line for $\beta = 1$ shows the situation of symmetric interactions with $U \neq U'$.

6.2 Effect of the Hund's coupling

We finally briefly discuss the effect of a full Hund's coupling on the above physics. We introduce an orbital independent coupling

$$J = J_{12} = J_{13} = J_{23} = \gamma U_1 \,, \tag{6.2}$$

which we study as a small perturbation to the system.

A small value of J does not affect the physics along the line $\alpha = 1$, since the effective level splitting induced by the change of β is strong enough. Indeed, the Hund's coupling, which attempts to spread the electrons in different orbitals, is known to compete directly with the crystal-field splitting [78] and it is therefore expected to compete also with the similar effect induced by β. However, our orbital-dependent interactions are not completely equivalent to a crystal-field splitting. In particular, there is still an interaction between the orbitals which is expected to favor a metallic behavior in orbitals 2 and 3. Due to this dependence, the effective separation between the manifolds becomes even stronger than for a single-particle splitting, hence J has a harder time to affect the physics of such system.

Now, let us assume the case $\alpha = 0.7, \beta = 0.9$, where we still have that $U_{11} \sim U_{22} = U_{33}$ and a mild decoupling effect, so that the effect of J can be observed. In fact, Fig. 6.7 shows the effect of Hund's coupling on the quasiparticle weight and orbital occupation for global half-filling. One can notice the tendency of J to lower the critical U_c and to favour the first-order character of the transition regardless the initial behavior in the absence of J, precisely as in full symmetric case described in Chapter 3. Moreover, it is shown that Ising and Kanamori treatment of this interaction do not reveal any difference in the estimation of U_c. However, a slight discrepancy

is noted in the slope of the quasiparticle weight (and correspondingly oscillation in occupation number from the referent one) for the moderate values of U.

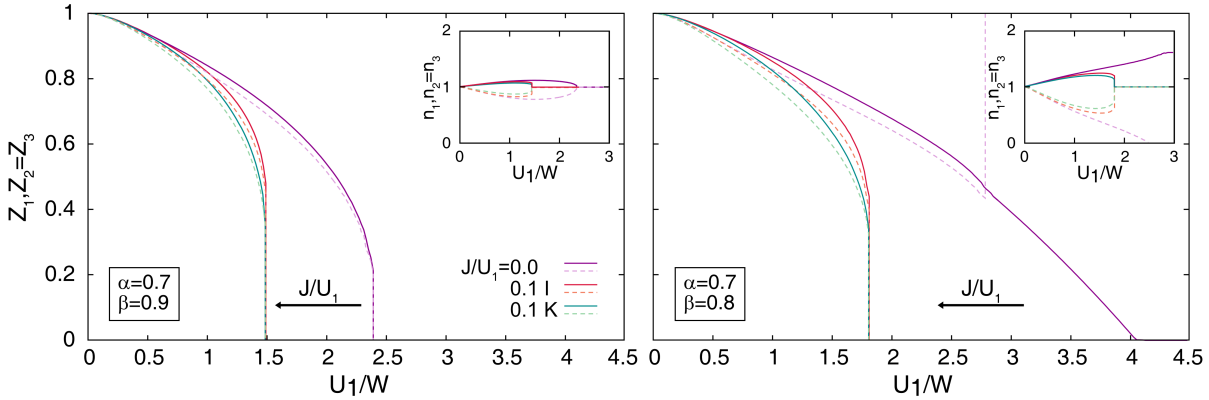

Figure 6.7: Quasiparticle weight Z_1 and $Z_2 = Z_3$, and orbital occupation n_1 and $n_2 = n_3$ presented in the inset, in a three-orbital non-degenerate half-filled Hubbard model, for $J \neq 0$. We have chosen two different points ($\alpha = 0.7, \beta = 0.9$ and $\alpha = 0.7, \beta = 0.8$), one of them close to the line splitting the two regimes in Fig. 6.6: one can observe the tendency of Hund's coupling J to drive the system towards the Mott insulating phase. No huge difference between Ising and Kanamori treatment is observed.

We finally examine the behavior close to the line separating the two regimes in Fig. 6.6. As we have seen so far, two regimes correspond to different physical behavior, with stronger effect of the energy splitting between the manifolds due to the imbalance between U-s on one side (blue region), and decoupled nature of the orbitals on another side (red regime). These two regimes compete along the above-mentioned line in Fig. 6.6. We take the point $\alpha = 0.7, \beta = 0.8$ in Fig. 6.7, where we observe a clear and strong tendency of J to push the system towards the stabilization of the Mott phase at the expenses of the region where the system polarizes into a two-orbital model. The qualitative effect is the most natural, since the Hund's coupling wants to spread the electrons between the orbitals and it does not like the full polarization, but the size and the rapidity of the effects are remarkable, confirming the huge sensitivity of this physics on details of the interaction terms.

6.3 Conclusions

We have investigated the effect of anisotropic Coulomb interaction in three-orbital Hubbard model, by means of Gutzwiller approximation. The results reveal a strong sensitivity to even small deviations from fully symmetric interactions. Already for values of our effective parameters α and β we find rapid deviations from the known results. An anisotropy of interactions between different orbitals acts to some extent as a crystal-field splitting, favoring an orbital polarization. In generic cases, the solutions are dominated by the competition between the tendency to have a single Mott transition with equal occupation of the various orbitals and the polarized regime favored by the anisotropy. We map out this competition in the space of α and β and we present also interesting dependencies on the filling. In particular, in the case where one orbital has a larger Coulomb repulsion than the others and when $n = 4$, we find an orbital-selective Mott transition reminiscent of that found in Ref. [24].

Finally, we have checked to which extent the Hund coupling affects the interplay among the intra- and inter-orbital Coulomb interaction and the metal-insulator transition. Moreover, we have observed that there are no huge differences between the Ising and Kanamori treatment, that

suggests us that in more realistic calculations, where the interactions are indeed non-uniform, the choice between the two does not induce any change nor novelty in a physical systems.

Already this very basic and simplified analysis assuming a very limited parametrization show the richness of the physics induced by orbital-dependent interactions, suggesting that these effects should be seriously taken into account in studies of real materials. We notice a strong dependence on small changes of parameters and on the charge density, which is characteristic of correlated materials.

7

Compressibility enhancement in multicomponent Hubbard models

In the previous sections we have reviewed some properties and emergent effects associated with the presence of a sizable Hund's exchange interaction in strongly correlated models [71, 76–78] and we presented a novel analysis which demonstrates the mixed-valence nature of the Hund's metal and its relationship with charge disproportionation instabilities. Following Ref. [11, 12, 14] we have stressed that the proximity of the half-filling Mott insulator (where the number of electrons per site n equals the number of orbitals N) has an essential effect on the nearby Hund's metal phase [71], which extends in a large regions of dopings, in particular when the filling is $n = N \pm 1$. This observation has several important consequences which are particularly relevant in the understanding of iron-based superconductors. Among this we focus on the recent observation that the charge compressibility can be enhanced and diverge at the Hund's metal crossover [21], which can be directly connected with mixed-valence behavior and charge ordering.

A divergent compressibility signals indeed a thermodynamic instability towards a macroscopic phase separation where the system is no longer stable in a homogeneous state. A similar state can be turned into a charge-ordered phase if longer-range Coulomb interactions are included, and it can also act as the source of a booster of a superconducting instability.

In Ref. [21] the Slave-spin mean-field has been used to compute the compressibility of the Kanamori model with only density-density interactions (or the so-called "Ising" type of Kanamori model) for different number of orbitals. These calculations have shown that the phase separation instabilities appear quite generally together with the Hund's metal phenomenology, but that they strongly depend on the number of orbitals. This suggests that the results can depend on other "details", such as the presence of the spin-flip and pair-hopping terms. In this chapter we extend this analysis to the more general case of a full Kanamori interaction and discuss in details the dependence on the number of orbitals and on the value of the Hund's coupling using the rotationally-invariant Gutzwiller approximation.

7.1 Compressibility in strongly correlated models

The electronic compressibility κ_{el}, which measures the response of the electronic system to an attempt to change its volume via an external pressure can be computed as

$$\kappa_{el} = \frac{1}{n^2}\frac{\mathrm{d}n}{\mathrm{d}\mu}\,, \tag{7.1}$$

where n is the total charge density and μ is the chemical potential of a system. This expression clearly shows that, besides the $1/n^2$ factor, the compressibility is proportional to the charge susceptibility $\chi_c = \partial n/\partial\mu$, being μ the conjugated variable to the density. Therefore, this quantity measures also the thermodynamic stability of the system with respect to an attempt to change the number of particles by moving the chemical potential. For this reason, this is a particularly useful and sensitive probe of the response of strongly correlated electron systems. In the following we will use, as it is customary done, κ_{el} for the charge susceptibility.

The Mott insulator is indeed an incompressible phase, characterized by a vanishing compressibility. This is a simple consequence of the fact that, in the Mott insulating phase, changing the change of chemical potential within the Mott gap will not induce any change to the number of particles. In the general case, the compressibility in the metallic state is finite and it tends to decrease approaching the Mott transition[1].

However, there are situations in which the approach to the Mott insulator displays a divergent charge response despite the incompressible nature of the insulating region. In particular, it has been widely debated whether phase separation occurs in two-dimensional strongly correlated models for the copper-oxygen planes of the high-temperature superconductors, namely the Hubbard model and the t-J model [126]. We do not want to enter the details of the debate, which go beyond the scope of this work, but we remind the basic ideas and the significance of this phenomena.

According to several studies, the charge compressibility diverges approaching the half-filled Mott insulator (which is typically antiferromagnetic), leading to a macroscopic phase separation between the half-filled magnet and a metallic phase with larger doping. We have, therefore, a spatial coexistence between two phases with different charge density. We underline that the divergence of the compressibility has been found only in two and one dimensions, and it is not expected to occur in three dimensions. It is certainly not found in Dynamical mean-field theory and in slave-particle approaches, which always find a finite compressibility in the metal all the way towards half-filling. A divergent compressibility can be however triggered, also at DMFT level, by additional interactions, such as the electron-phonon coupling [127]. This means that the divergence of compressibility that we discuss in this section is inherently associated with the multi-orbital character of our models and in particular to the physics of the Hund's coupling that we discussed in the previous chapters.

As we mentioned above, the divergence of the compressibility is not merely signaling an instability of the metallic state, but it opens the way to the realization of several phases. In particular, the phase-separated state can be seen as the ancestor of the charge-ordering instabilities which have been more recently identified in the cuprates. The idea is that, when longer-range Coulomb interactions are included, the thermodynamic phase separation is strongly frustrated because the concentration of charge-rich regions becomes energetically unfavorable. The system can therefore find a compromise between the two tendencies, leading to incommensurate charge-ordering patterns, whose precise nature and ordering vector depend on the doping and

[1] A crossover to standard band insulator can also result in zero compressibility at the metal to band insulator transition. However, the way how the system approaches the transition point is different, as discussed in Ref. [37].

on the details of the system. We refer to Ref. [128] for a recent review of this scenario in light of the evolving experimental scenario in high-temperature superconductors.

Moreover, we can connect the divergent compressibility to a wider class of instabilities. Within the Landau Fermi liquid theory one can obtain the following expression for the compressibility:

$$\kappa_{el} = \frac{D^*(\epsilon_F)}{1 + F_0^s}, \tag{7.2}$$

where $D^*(\epsilon_F)$ is the interacting density of states at Fermi level, associated to the quasiparticle, namely $D^*(\epsilon_F) = D(\epsilon_F)/Z$, Z is the quasiparticle weight and $D(\epsilon_F)$ is the bare density of states. On another hand, F_0^s is the isotropic, spin-symmetric Landau parameter which contains the information about the residual interaction between quasiparticles.

If the values of Z are positive and regular (as we found for all the multi-orbital models studied in this thesis), the only way in which a divergence of the compressibility can arise is through a vanishing denominator. This can happen only if $F_0^s \simeq -1$, which corresponds to an attractive interaction between the quasiparticles in the particle-hole channel, at $q = 0$, $\omega \to 0$. An attraction in the particle-hole channel can also be reflected in the particle-particle channel and give rise to an attractive scattering amplitude in the Cooper channel, hence to superconductivity. This has been originally proposed as an argument which connects the tendency towards phase separation with the very origin of the superconducting instability, and it has been realized in different microscopic models.

There is, however, an other scenario, in which superconductivity does not arise solely from the charge instability, but it can be associated with a low-energy instability driven, for example, by bosons. Also in this case, an enhancement or a divergence of the compressibility can help the superconducting phase by boosting the effective vertex. One can indeed show that $F_0^s \simeq -1$ leads to an enhancement of the vertex in various channels, which can increase an already existent instability. We will not elaborate further about the actual realization of this scenario both in models and in actual materials, but a similar idea can connect the common idea that pairing in the iron-based superconductors arises from spin fluctuations with the strong correlation physics that we described in this thesis.

7.2 Compressibility enhancement in Hund's metals: "Ising" Hamiltonian

In this section we review the results of Ref. [21] which represent the starting point of the present analysis. As we mentioned above, these results have been obtained within the Slave-spin mean-field approach. We do not discuss the details of this method, that can be seen as a derivation of the Slave-boson method, in which the auxiliary particles (which supplement the pseudofermion) are spin 1/2, one in correspondence of each fermionic species. Similarly to the Slave-boson, one rewrites the model in the extended Hilbert space and then introduces a mean-field approximation by decoupling the fermions from the spins. The practical advantage of the Slave-spin representation is the very low computational cost, while the main price to pay is the inability to treat interaction terms which are not in the density-density form. For more details we refer to Ref. [71]. In the context of this thesis, we can view the Slave-spin approach as a slightly less accurate approximation with the same philosophy of our Gutzwiller/RISB method.

Fig. 7.1 presents the chemical potential μ in a function of the total charge density n, for three different models: degenerate two-orbital (left panel), three-orbital (central panel) and five-orbital

(right panel) Hubbard model with semi-circular density of states of half-bandwidth D. The charge compressibility is given by the inverse of the slope of these curves.

We show results for a large number of values of the Coulomb interaction U and fixed ration between the Ising-type Hund's coupling J and U, ie. $J/U = 0.25$. This value is indeed quite large, substantially more than realistic estimates even for materials which are characterized by a large Hund's coupling as the iron-based superconductors, where one can estimate $J/U \simeq 0.15$. However, this choice has been shown to lead to a good agreement (even quantitative) with experiments in iron-based superconductors without any tuning when changing doping/nature of the compound. In some sense we can view this overestimate of J as a trick to compensate for the neglect of the spin-flip and pair-hopping terms. We define the chemical potential so that $\mu = 0$ corresponds to half-filling, which makes the model particle-hole symmetric. For this reason we only plot values of the density larger than half-filling, which are obviously representative also of the region of negative doping of the Mott insulator.

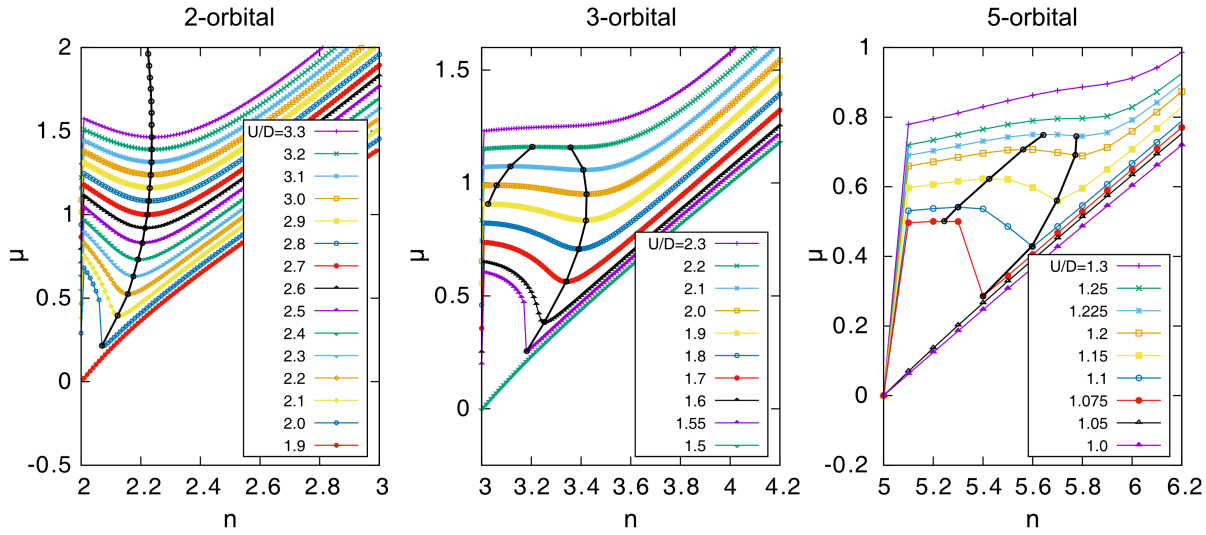

Figure 7.1: Degenerate two-orbital (left panel), three-orbital (central panel) and five-orbital (right panel) Hubbard model with semi-circular density of states of half-bandwidth D, and Ising-type Hund's coupling $J/U = 0.25$: μ vs. n curves for different values of U. The curves for $U > U_c$ show a negative slope inside a spinodal line departing from the Mott transition that is marked with black connected circles. In the 3- and five-orbital case most of the μ vs. n curves for $U > U_c$ show a double change of slope, so that the instability zone extends between two spinodal lines (black connected circles) both at finite doping from half-filling. The results are obtained using the Slave-spin approach in Ref. [21].

We choose the values of U such that all of them but one are above the critical value for the Mott transition at half-filling $n = N$ (where N is the number of orbitals), which for the present choice of parameters are $U_c^{N=2} = 1.96\,D$, $U_c^{N=3} = 1.52\,D$ and $U_c^{N=5} = 1.06\,D$. Therefore, for all these curves the starting half-filling point describes a Mott insulator. In each plot there is also a reference value of U below the Mott transition. In this latter metallic solution, coming from higher densities towards half-filing, the chemical potential decreases smoothly all the way down to the half-filling value $\mu = 0$. The compressibility is clearly positive for every density and the system is thermodynamically stable. The same behavior is found also for the other curves $U < U_c$ belonging to the metallic side, but they are omitted here due to redundancy.

The situation is completely different when $U > U_c$. Here the slope remains positive when we are far from the Mott insulator but, reducing the doping, we find, for every value of the orbital degeneracy N, a non monotonic behavior. The chemical potential increases when we

decrease the doping, which signals a negative compressibility and an unstable system. The change in slope obviously goes through a vanishing slope, which corresponds to a divergence of the compressibility. The divergence of the compressibility is marked with a black line.

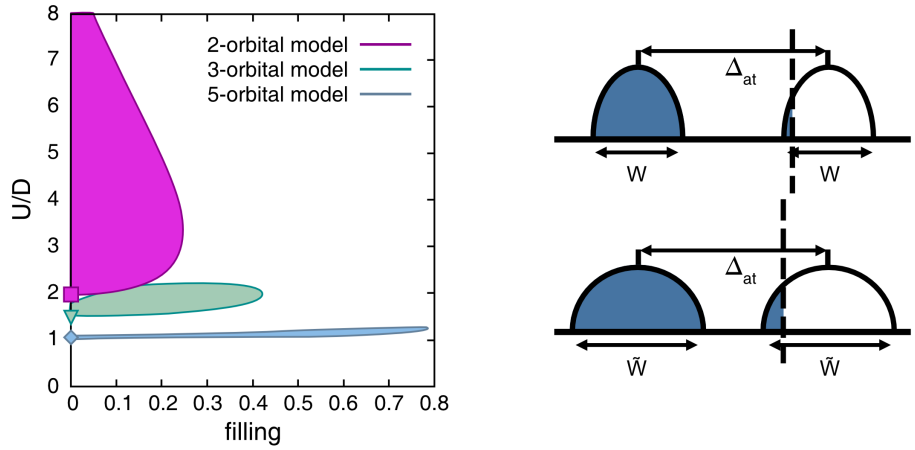

Figure 7.2: Left panel: Instability zones reported in the U-doping plane for the two-orbital (purple), three-orbital (green), and five-orbital (blue) models, with $J/U = 0.25$. The low-U frontier departs from the Mott transition point at half-filling (symbols). For growing number of orbitals N the unstable zone extends to larger value of doping, albeit narrowing in U. Right panel: A plausible mechanism for the charge instability cause by the presence of J. Seemingly, the Hund's rule coupling causes total quenching of orbital fluctuations at half-filling, reducing the width of the Hubbard bands. Upon doping the quenching is lifted and the Hubbard bands are expected to expand (going from $\sim W$ to some larger value $\tilde{W}$). This might cause a lower chemical potential at larger particle density, i.e. a charge instability [21].

From Fig. 7.1 it becomes immediately evident that, despite the common appearance of a divergent compressibility, the results for the two-orbital model present a qualitatively different trend with respect to other two, three- and five-orbital case. As we said above, the large doping region is apparently stable with a positive slope. Then one encounters one single minimum ("critical") point for which the slope vanishes, ie. $\frac{\mathrm{d}\mu}{\mathrm{d}n} = \kappa_{el}^{-1} = 0$, or in another words, a divergent compressibility. Moving further towards half-filling, the slope becomes negative and it remain negative for any doping smaller than the critical point where the compressibility diverges. Exactly at half-filling the chemical potential jumps at $\mu = 0$. This happens for all values of $U > U_c$. Therefore the phase separation is always between a half-filled Mott insulator and a doped metal. Indeed if we depict all the points of divergent compressibility in the phase diagram shown in Fig. 7.2, we find an instability zone which survives up to very large values of U (even if it shrinks as a function of doping in the very-large U region).

On the other hand, the behavior of the $\mu(n)$ curves is richer in the region of small dopings. For U slightly above the Mott transition we find a similar behavior with respect to $N = 2$, with an instability which extends down to half-filling. At some distance from the Mott insulator we find instead that the curvature turns back into positive for very small doping through a maximum (see for example the data for $1.9 < U < 2.2$ in the middle panel of Fig. 7.1). The maximum corresponds obvioulsy to a second line of divergent compressibility shown in the figure. This means that we can also have a phase separation between two metallic solutions with different densities. For larger interactions the region of phase separation shrinks and disappears, meaning that the system becomes stable again, in sharp contrast with the two-orbital model.

These results, as well as difference and analogies between models with different number of orbitals, are summarized in Fig. 7.2, where the boundaries corresponding to the divergence of the charge susceptibilities are compared. The two-orbital case shows a phase separation in the whole

region of $U > U_c$, but it is limited to a region of moderate doping which extends maximally for $U \simeq 3D$ and shrinks rather slowly, with a kind of "onion" shape. As we increase the number of the orbitals, the divergence is limited to a thinner and thinner region of interactions close to U_c, but at the same time it extends to larger and larger dopings. The shape qualitatively changes from an onion to a kind of "moustache", which gets more and more thin and extended in doping as the number of orbital grows. Interestingly for $N = 5$, which is relevant to iron-based superconductors, the region extends almost to $n = 6$, which is the stochiometric composition.

7.3 Gutzwiller approximation results

In this section we present a complete set of results using the rotation-invariant Gutzwiller formulation, which allows us to solve both the Ising version of the model and the full Kanamori interaction as written in Eq. (3.10), which was not accessible to the Slave-spin mean-field of Ref. [21]. This extension is particularly important because the study we just reviewed shows that the results are extremely sensitive to a change in the number of orbitals and it is not clear if the choice of the interaction Hamiltonian can have a similar effect. In the Supplementary material of Ref. [21] one can find a brief discussion of this comparison in the case of the two-orbital model (using RISB), which shows that the qualitative response remains similar, even if the inclusion of spin-flip and pair-hopping term appears to reduce the doping region where the instability takes place. However, we have already shown that the two-orbital case is peculiar, and a direct study of three and five orbitals is necessary to support these results and ultimately address the relevance of the compressibility divergence in multi-orbital models and possibly in iron-based superconductors.

7.3.1 Three-orbital Model

In this section we report the results of our intensive investigation of the phase separation boundary, which is mainly focused at understanding the importance of the full Kanamori interaction. In Fig. 7.3 we report the μ-n curves obtained using the Gutzwiller method for the Ising (left) and Kanamori (right) interactions and two different values of Hund's coupling, $J/U = 0.15$ and $J/U = 0.25$. These are just two examples taken among many data we have obtained, chosen to compare the value used in the previous section with a more realistic estimate for transition-metal oxides or the iron-based superconductors. Also in this case we choose one value of U below the Mott transition and several values for $U > U_c$ where the half-filled system is a Mott insulator.

The results show that, at least within this range, the phase separation instability is not strongly affected by the value of J/U and actually we find that the quantitative effect of reducing J/U is opposite in the Ising case (where a smaller J leads to a slightly smaller region of phase separation) and the Kanamori case (where reducing J leads to a very small increase of the phase separation region).

The most interesting feature of this plot is that the instability region indeed is present also in the Kanamori modeling, even if the details of the phenomenology are different from the Ising case. In particular, similarly to the two-orbital Ising model, the three-orbital Kanamori only displays one line of divergence and the compressibility is negative down to half-filling. In contrast with this case, however, the phase separation region closes if we increase U. It must be noted that the critical value for the Mott transition depends rather strongly on the used model.

We can indeed summarize the evolution and the change in position and shape of the instability region in a plane of density and U for the two models and different choices of J/U. The results

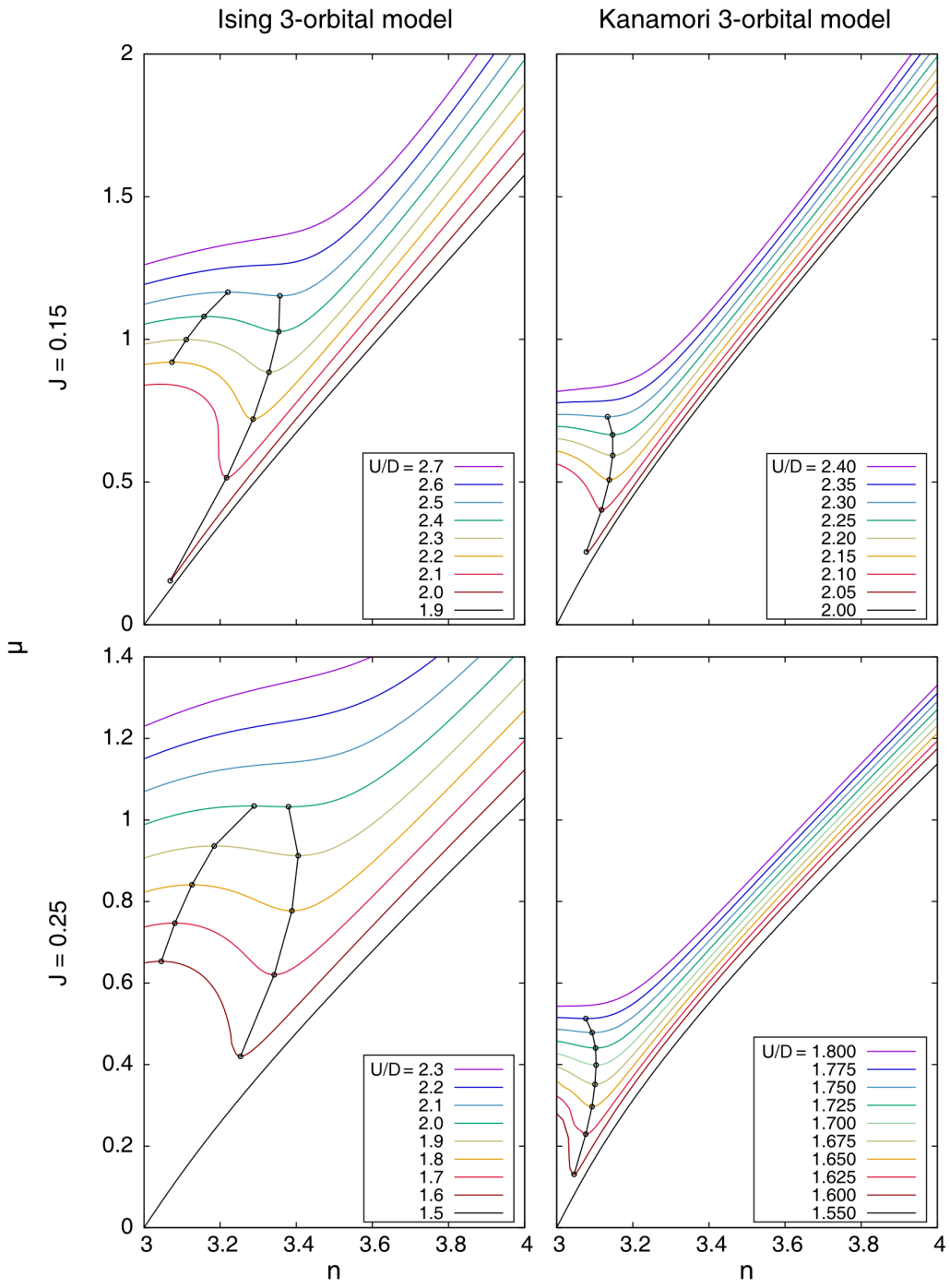

Figure 7.3: Chemical potential μ vs. total charge density n, for the degenerate three-orbital Hubbard model with semi-circular density of states of half-bandwidth D, and with Hund's coupling $J/U = 0.15$ (typical value) and $J/U = 0.25$ (value used in Ref. [21]). Left panel corresponds to the Ising-type of Hund's coupling, while the right one shows the full-Kanamori interaction. The curves are associated to different values of the interaction strength, where most of the $U > U_c$ curves show a double change of slope for the Ising model, a negative slope inside a spinodal line departing from the Mott transition that is marked with black connected circles, so that the instability zone extends between two spinodal lines (black connected circles) both at finite doping from half-filling. On another side, in the Kanamori model the slope remains negative up to the Mott transition. Moreover, one can note a significant reduction of the instability zone for this model. The results are obtained using the Gutzwiller approach.

are shown in Fig. 7.4, left panel representing the Ising solution, right - Kanamori. Indeed, while at $J = 0$ no divergent compressibility is found, thus the system appears to be always stable, already at small J/U a wide instability range opens in both cases. For both models the region of interactions where phase separation occurs is very large for small J/U and it becomes thinner and thinner as J/U grows. The areas of instability are also pushed down to smaller U simply because the critical U for the Mott transition is reduced by J. As we mentioned above, the extension in doping evolves differently as a function of J/U. For the Ising interaction, larger J/U implies a larger critical density, for the Kanamori interaction it is exactly the opposite and the doping range becomes indeed very small when J/U becomes very large.

For instance, $n_c \approx 3.41$ at $J/U = 0.3$ for Ising, while for the Kanamori model we have $n_c \approx 3.08$ for $J/U = 0.3$. These results show a non-trivial effect of the precise choice of interaction which partially contradicts the results for two orbitals reported in Ref. [21] (Supplement material). In the next section we will see how the scenario evolves moving to five orbitals.

We can add a very handwaving argument about this difference. The answer for this behavior might be explained by following: the main difference between the Ising and Kanamori Hamiltonian lies in the Hund's coupling contributions taken into account. Namely, while Ising model accounts only for the density-density term of Eq. (3.10), the Kanamori instead considers also the additional processes, such as spin-flip and pair-exchange. These processes give rise to magnetic fluctuations in the system, reducing somehow the impact of the Hund's interaction and favoring this way the metallic behavior.

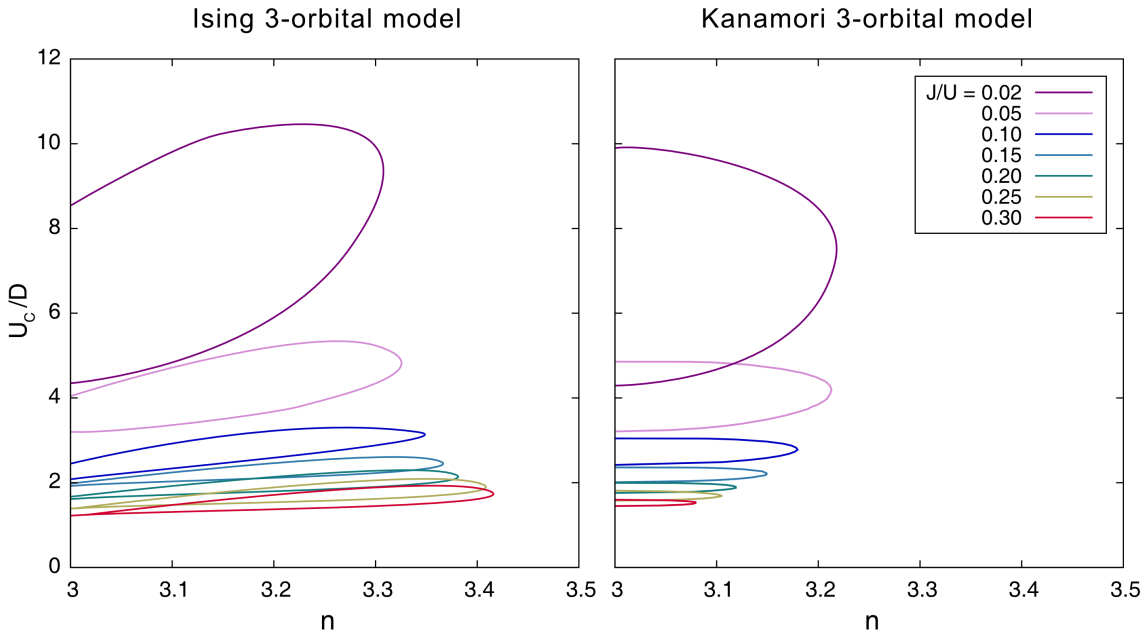

Figure 7.4: Evolution of the zone of instability (in the U-n plane) as a function of J/U in the three-orbital Hubbard model. At each value the system is unstable for densities between $n = 3$ and the corresponding frontier: left panel showing the Ising type, and right panel the Kanamori type of the Hund's interaction. The instability is absent at $J = 0$.

We have already noticed that region bounded by the divergence of the compressibility starts at the half-filled Mott transition, just like the region of Hund's metal, as we discussed in the Chapter 3. We now discuss the relationship between the enhancement of the compressibility and various observables which are sensitive to the Hund's metal crossover [20, 71, 77, 78, 84].

In particular, we consider two different dopings, chosen such that one falls into the instability region and is close enough to half-filling, and another right outside the instability region, as

reported in Fig. 7.5, both for Ising and Kanamori three-orbital model for $J/U = 0.25$ (therefore the actual values of the densities are different because of the different shape in the phase diagrams). In the four panels we show, the effective mass enhancement due to interaction (which does not depend on the orbital in the present model) that is given by $m^*/m = 1/Z$, the expectation value of the square of the total spin $\langle S_z^2 \rangle$, the inter-orbital charge correlation functions between two arbitrary orbitals C_{inter} and the inverse of the compressibility κ_{el}^{-1}. In the region of small U, where the system is safely in the metallic regime, all our observables do not depend on the chosen doping.

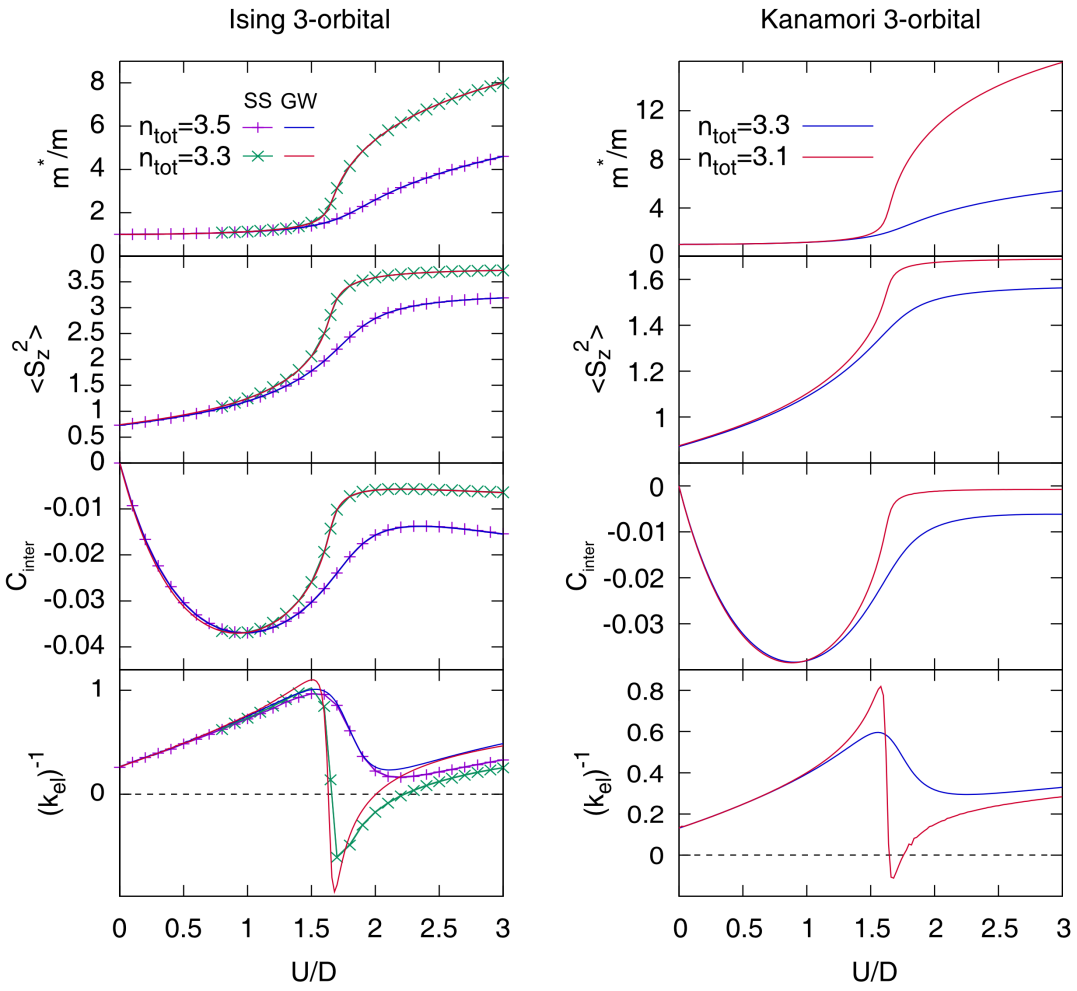

Figure 7.5: Main quantities highlighting the crossover from normal (small U/D) to Hund's metal (large U/D) in three-orbital Ising (left) and Kanamori (right) Hubbard model with Hund's rule coupling $J/U = 0.25$, solved within the Gutzwiller approach (labeled "GW") for two different dopings in proximity of half-filling: mass enhancement, total local spin-spin correlation function, inter-orbital charge correlation function and (inverse) electronic compressibility. The results obtained for the Ising model within Slave-spin mean-field (labeled "SS") are taken from Ref. [21] and replotted on top of our results. We can see the perfect overlap between all the quantities but the compressibility, implying that the difference between the two methods, Gutzwiller and Slave-spin, lie in differently estimated value of μ (see in the text).

We can observe that in metallic regime, for small enough U, while $U < U_c$ the two lines, corresponding to different dopings, coincides for all the quantities. Increasing the interaction, the observables for the smaller doping (closer to half-filling) display a rather abrupt crossover and they rapidly reach extreme values, while the same observables at a larger doping undergo a

smoother evolution and they reach intermediate values. In particular, the effective mass grows to a large value, the total spin reaches a saturated high-spin value (which is larger for the Ising model due to the neglect of quantum fluctuations), and the inter-orbital correlation vanishes signaling the orbital decoupling. The occurrance of a sharp crossover takes place at the same interaction strength where the compressibility diverges (zero of its inverse), which only happens for the small doping. The correspondence between the boundary of the Hund's crossover and the compressibility divergence is realized both in the Ising and the Kanamori models, suggesting that this result has a deep physical meaning. For the larger dopings we still observe some precursors of the phenomena happening at the crossover, with a relatively large compressibility and a milder crossover in the observables.

So far we have compared the results for different densities and the same model. If we, instead, contrast the behavior of the two models for the same density $n = 3.3$, we can see that for the same doping the effective mass of the Ising model is almost twice the value found for Kanamori model. This confirms that the Ising model drives system to a more correlated regime, favoring the Mott phase.

7.3.2 Five-orbital model

In this section we extend our analysis to the five-orbital degenerate model. In Fig. 7.6 we plot the same information of Fig. 7.3, comparing the Ising (left) and Kanamori (right) type of interaction for the same two values of $J/U = 0.15, 0.25$. The computational cost of the calculation is somewhat larger than for three orbitals, which limits a little our analysis in the small doping region.

For five orbitals we find a stronger dependence on J/U, especially for the Ising model, and all the four sets of data show a minimum and a maximum of $\mu(n)$, i.e., the phase separation region is limited to finite-doping slice and it does not extend down to half-filling.

In Fig. 7.6 one can notice a feature which we did not observed in the previous data, namely a sudden jump in μ for very small doping and for U-s which are just above U_c. This jump is not just a numerical artifact, and it arises by comparing the energies of two different solutions, obtained starting respectively from $n = N$ (in this case $n = 5$) and $n = N + 1$ (here $n = 6$) and moving slowly and carefully the density in the two opposite directions, as marked with the arrows in Fig. 7.7. In left panel of this plot we have indeed shown the two different solutions found depending on the choice of the direction in which we move in the phase diagram, and a coexistence region between them (shaded). If we, for instance, plot the quasiparticle weight Z as a function of doping, we can see the same feature. This gives us idea that we have the coexistence region between two distinct metals (whose energies we need to compare in order to get a transition point between the two). Indeed, the metal extended in larger values of doping corresponds to a normal metal arising from the non-interacting limit once the interactions included, whereas the one obtained for the values of doping close to $n = N$ is the metal obtained while doping the Mott insulator at half filling. Interestingly, this feature, which can connect the divergence of the compressibility with the coexistence of solutions which is characteristic of the Mott transition in DMFT, is realized only for five orbitals.

Finally, the evolution of the instability zone (see Fig. 7.8) reminds the one for the model with three-orbitals, but unlike expected in Ref. [21], the instability region does not increase in doping with the number of orbitals. This conclusion represents rather a drawback of the Ising treatment that does not take into account the full Hund's coupling. Kanamori treatment, on another side, fully accounts for the present quantum fluctuations and effect of J, limiting the instability region in quite reduced range of doping ($n \approx 5.3$ for $J/U = 0.25$, instead of $n \approx 5.85$ estimated with the Ising treatment of Hund's coupling).

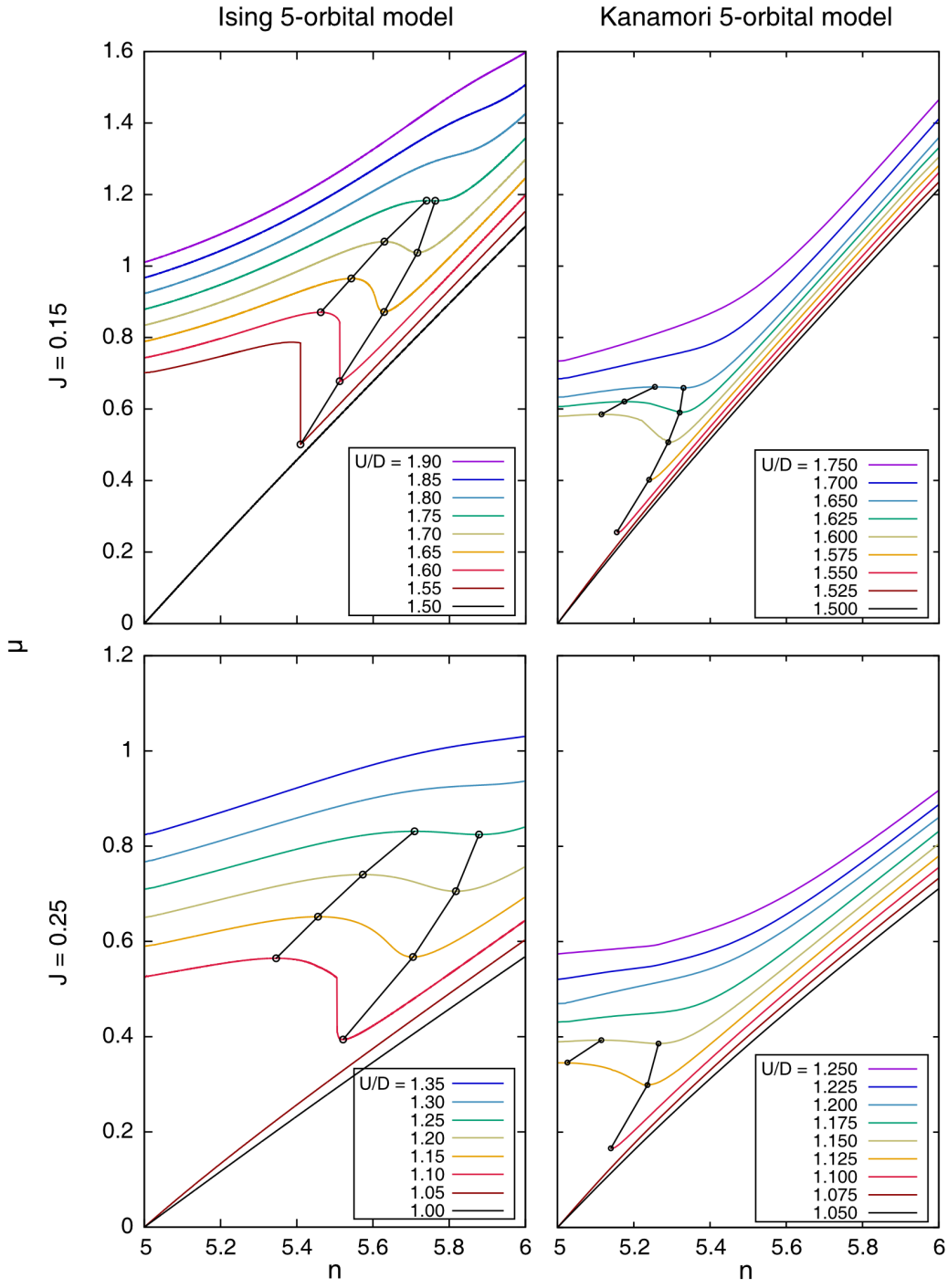

Figure 7.6: Chemical potential μ vs. total charge density n, for the degenerate five-orbital Hubbard model with semi-circular density of states of half-bandwidth D, and with Hund's coupling $J/U = 0.15$ (typical value) and $J/U = 0.25$ (value used in Ref. [21]). Left panel corresponds to the Ising-type of Hund's coupling, while the right one shows the full-Kanamori interaction. The curves are associated to different values of the interaction strength, where most of the $U > U_c$ curves show a double change of slope, a negative slope inside a spinodal line departing from the Mott transition that is marked with black connected circles, so that the instability zone extends between two spinodal lines (black connected circles) both at finite doping from half-filling. One can note a significant reduction of the instability zone for this model, pushed closer to the smaller values of doping. The results are obtained using the Gutzwiller approach.

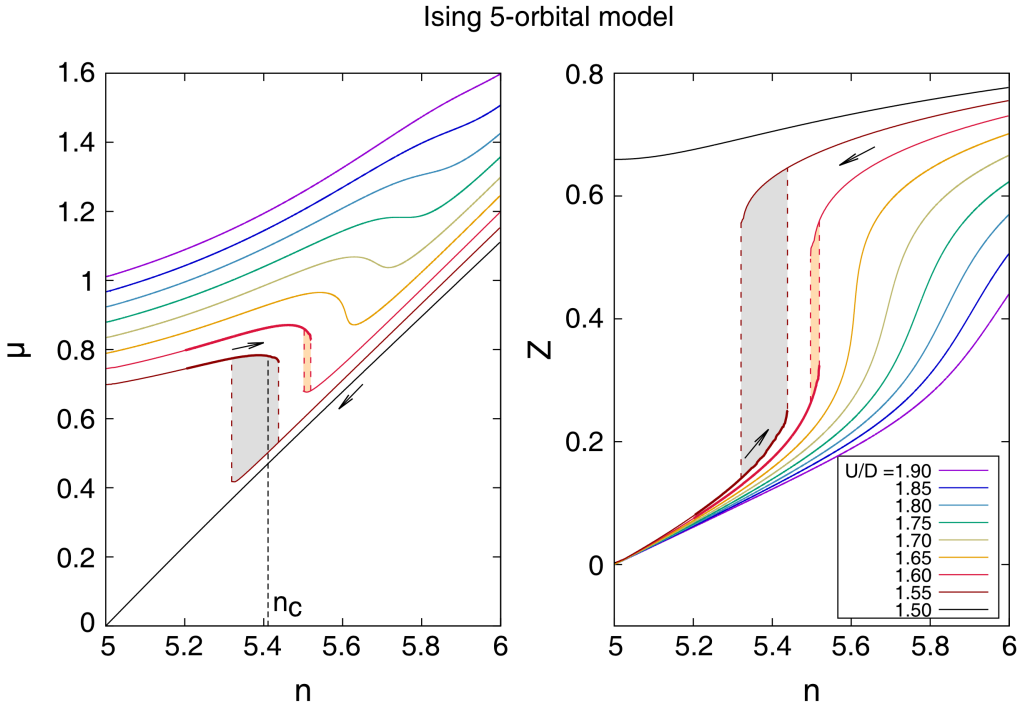

Figure 7.7: Coexistence of two metallic solutions at the zone of phase instability. An example is given for the five-orbital case, demonstrating the chemical potential μ and the quasiparticle weight Z as a function of doping n at $J/U = 0.15$ (for the Ising model).

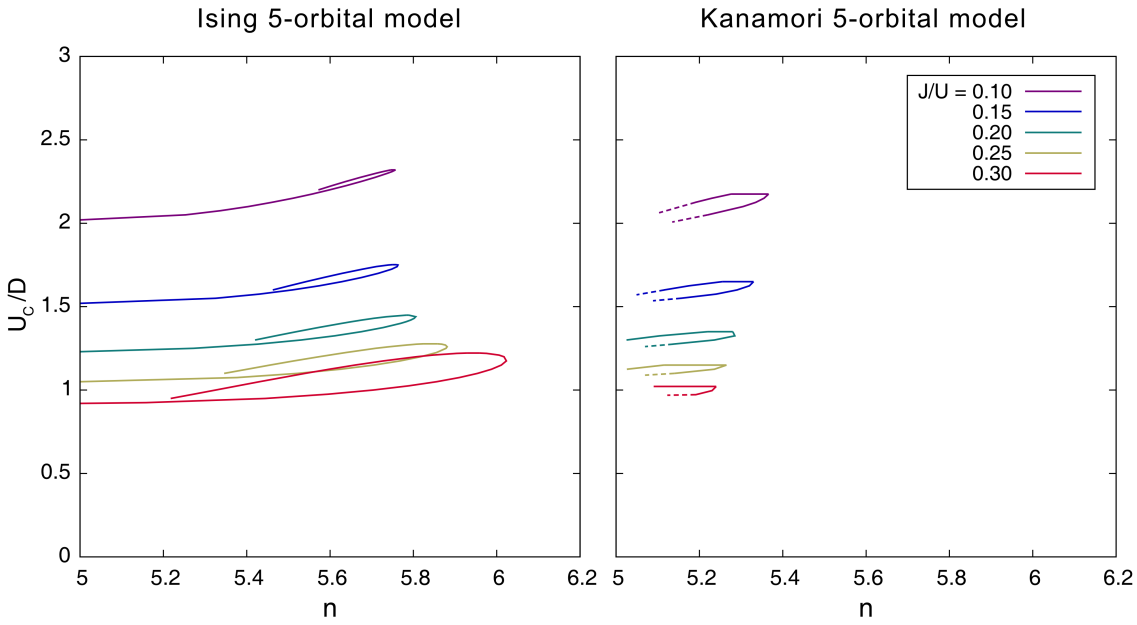

Figure 7.8: Evolution of the zone of instability (in the U-n plane) as a function of J/U in the five-orbital Hubbard model. At each value the system is unstable for densities between $n = 5$ and the corresponding frontier: left panel showing the Ising type, and right panel the Kanamori type of the Hund's interaction. The instability is absent at $J = 0$.

7.3.3 Discussion

We give now a brief qualitative discussion of the physical origin of a negative and divergent compressibility in the present calculations. We stress again that a similar instability is a rather counterintuitive phenomenon. When κ_{el} is positive, adding an electron to the system shifts the chemical potential to higher values. We can picture this process as filling a glass with water: as long as we pour water in the glass, the water lever will rise. Now, let us assume the charge compressibility has a negative value, as, indeed, we have seen in our data. This means that the chemical potential will drop down while adding more electrons in the system. Correspondingly, it would be as if the level of water in a glass would decrease while pouring water in it. Figuratively, this might have happened if the glass was able to change its shape in the presence of the water due to some feedback of the presence of water itself. In other words, a non-interacting picture (where the glass remains itself in the presence of water) can not explain any instability in which the compressibility is not simply positive.

Within the Gutzwiller approximation or the Slave-boson mean-field, the effects of correlations are relatively simple and they amount to introduce a quasiparticle renormalization Z and Lagrange multipliers which renormalize the chemical potential. In the models we have studied, where orbital degeneracy is not broken, Z and λ are orbital-independent and we have only two quantities to express the effect of the interactions. Therefore, our effective Hamiltonian can be written as

$$\hat{H} - \mu\hat{n} = \sum_{km\sigma} \left(Z\epsilon_{\mathbf{k}} + \lambda - \mu\right) f^{\dagger}_{km\sigma} f_{km\sigma} \,, \tag{7.3}$$

where $f^{\dagger}_{km\sigma}$ represents the creation operator of a quasiparticle, with defined momentum k, orbital m and spin σ index. Having in mind degenerate multi-orbital system, the bare electronic dispersion relation $\epsilon_{\mathbf{k}}$ is the same for each band as well as λ and Z. The number of quasiparticles should be equal to the particle density $n_f \equiv \sum_{km\sigma} \left\langle f^{\dagger}_{km\sigma} f_{km\sigma} \right\rangle = n$. Imposing the Luttinger theorem, that states that the volume of the interacting Fermi surface is proportional to the particle density, we can relate the chemical potential μ of the interacting model to the non-interacting one, μ_0, with the same density, or in another words:

$$n_f(U) = \int^{(\mu-\lambda)/Z} d\epsilon D(\epsilon) = \int^{\mu_0} d\epsilon D(\epsilon) = n(U=0) \,, \tag{7.4}$$

obtaining the relation (at zero temperature)

$$\mu_0 = \frac{\mu - \lambda}{Z} \,. \tag{7.5}$$

From Eq. (7.3) one can compute the compressibility and obtain a Fermi liquid-like expression where $D^*(E_F) = D(E_F)/Z$ as expected and

$$F^s_0 = D^*(E_F) \left(\mu_0 \frac{\partial Z}{\partial n} + \frac{\partial \lambda}{\partial n} \right) . \tag{7.6}$$

This implies that a divergence of the compressibility, which can only happen if $F^s_0 = -1$, can only arise from the two derivatives in Eq. (7.6). The first term is always positive because Z is always reduced when we approach the Mott insulator, which means that its derivative with respect to density has the same sign of μ_0. Therefore the only source of a negative Landau amplitude is a negative derivative of the Lagrange multiplier (obviously with a sufficiently large amplitude to overcome the positive contribution and to reach a value of -1).

Once again, a similar result is not expected in a rigid-band picture. λ basically acts as a correction to the chemical potential and it grows if the density grows. In particular, when we

dope a Mott insulator, it jumps towards the Hubbard bands, which are roughly at a distance $U/2 - \tilde{W}/2$ from the chemical potential of the Mott insulator, where $\tilde{W}$ is the effective width of the Hubbard bands. Then, further increasing the density would be expected to increase λ at least within a rigid-band picture. Our evidence clearly demonstrate that this is not the case and some collective effect must invert this trend. We can indeed give an argument, based on the concept of orbital decoupling.

We have briefly discussed that a sizable Hund's coupling leads to an effective decoupling between the orbitals, which makes the excitations orbital-diagonal. This has crucial consequences on the width of the Hubbard bands. So far it has been shown that the width of the Hubbard bands [36, 41] depends in general on the number of orbitals. In particular for zero or small J, $\tilde{W}$ typically scales with the number of orbitals N as $\sim \sqrt{N}W$ (where W is a bare bandwidth of a single-orbital model) [129]. However, the onset of Hund's coupling J tends to reduce this value to the bare one W [71], as a consequence of the orbital decoupling, which makes excitation within each orbital similar to those of a single-band model. As a consequence of quench of the orbital fluctuations, which is the strongest at half-filling, one finds the reduction of the hopping channel and lastly a decrease of the kinetic energy.

Apparently, this gives rise to the reduction of the width of the Hubbard bands. The described mechanism holds at half-filling, but it is expected to smoothly break down as we dope the system. It is somehow intuitive to expect that once an extra charge is brought to the system, the number of doubly occupied orbitals increases leading to an "unquenching" of the orbital degrees of freedom. This would cause again the widening of the Hubbard bands (up to the value $\sim \sqrt{N}W$). Therefore, if the Hubbard bands widen as the system is doped, one can have the counterintuitive effect that the effective chemical potential (controlled by λ) actually decreases when the density increases, as shown in the right panel of Fig. 7.2. This effect is the realization of the adaptive glass we mentioned in our intuitive picture.

This arguments show the crucial role of the Lagrange multiplier and its density dependence in the onset of the divergent compressibility. Therefore also the difference between Slave-spin and Gutzwiller results for the same model is most likely due to λ, also because Z does not show important differences.

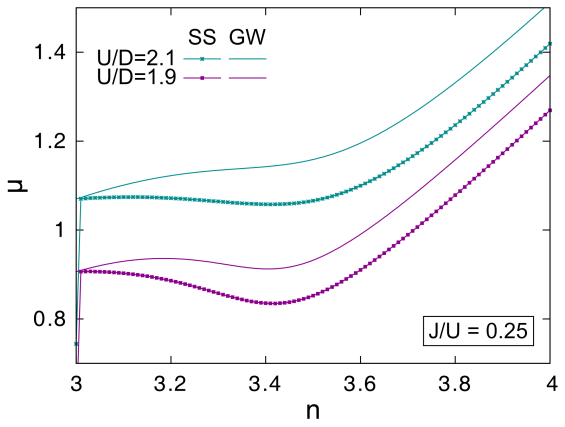

Figure 7.9: Robustness of the compressibility divergence with respect to the choice of numerical method: Slave-spin mean-field (labeled "SS") and present, Gutzwiller approach (labeled "GW"). Results for μ with respect to n curve in the three-orbital model with $J/U = 0.25$ for $U/D = 1.9, 2.1$ (from bottom to top) are displayed and show that the instability is robustly found in both methods. Both methods give the same estimation for μ close to half-filling. However, results slightly differ at larger U/D, due to the difference in the treatment of λ (contributing μ) in the two methods.

Either way, from Fig. 7.9 one can notice the same position of the chemical potential (and therefore λ) at half-filling, and then a shift that barely increases as a function of n, and consequently a slight discrepancy in κ_{el} vs. U curves. However, the difference is just quantitative, whereas the qualitative description holds and is not affected by different λ. Therefore, the found divergence and appearance of the frontier from the half-filled Mott transition point is a common, robust feature, independently of the chosen method.

7.4 Conclusions

In this chapter we have extended a previous analysis [21] of the charge compressibility of multi-orbital Hubbard models by comparing Ising and Kanamori type of Hund's coupling, at the same time confronting the two methods, Slave-spin mean-field and Gutzwiller approach for three- and five-orbital models.

We have confirmed that the main ideas related to the Ising type of interaction, discussed in Ref. [21], are robust and hold in general for multi-orbital systems, namely, that the presence of a diverging compressibility is connected with the crossover between the crossover from a regular metal to a Hund's metal, and that this feature is independent on the choice of the methods, at least at the level of these quasiparticle-based approaches. A slight difference can arise in some of the quantities, whereas the qualitative description remains unchanged in general. Moreover, the estimation of the lower frontier departing from the half-filled Mott transition is quite precise and coincides between the different methods.

However, in the particular case the Slave-spin method fails to treat in a proper way the full Kanamori interaction [71], therefore tends to an overestimation of the region of phase separation. We have shown that Kanamori treatment recovers qualitatively all the main ideas from Ref. [21], with the only difference that the instability zone is largely reduced and tends to drop further with the increase of the Hund's coupling.

In any case, the overall numerical results indicate that the enhancement of the charge compressibility associated with the phase separation does exist near the Mott transition at half filling. This result is of a huge interest owning to the connection between the instabilities arising with the phase separation that can give rise to the possible pairing mechanism important for the emergence of the high-T_c superconductivity. The remarkable point is that the instability phase arises at the crossover between conventional metallic phase, and the Hund's phase, characterized by the (orbitally) selective electronic correlation strength. This can also establish one further link with the cuprates [14], where phase separation has been widely discussed as a possible source of anomalies of the phase diagram including charge-density waves and some aspects of the superconductivity itself.

8 Conclusions

Undoped iron-based superconductors accommodate six electrons in the five d-orbitals belonging to Fe-atom. It is nowadays well established that a correlated model at this filling is characterized by a bad metallic state induced by a sizable value of the Hund's coupling J even when the Hubbard U becomes substantially larger than the bandwidth [12, 13, 19, 76]. Such systems are usually identified as Hund's metal [16]. This concept has been introduced to rationalize the observation that, in theoretical models of iron-based superconductors, ruthenates, and other materials, many relevant observables turn out to be remarkably dependent on Hund's coupling J rather than on the Hubbard interaction U.

In this thesis we gave some contributions to the understanding of this –still elusive– regime exploring different regimes of the incredibly rich physics of multi-orbital strongly correlated model.

The main theoretical tool used in this thesis has been the Gutzwiller approximation and correspondingly - the equivalent Rotationally-invariant slave-boson approach. These approaches provide a reliable description of the Mott transition starting from the metallic solution, for a relatively cheap numerical investigation of a wide range of model parameters. Moreover, the rotational invariance of this formalism gives possibility to treat all interacting terms on an equal footing. This allows us to explore the different effects arising in the presence of U and J in the multi-orbital Hund's metals, such as FeSC. Therefore, in spite of being limited only to the metallic solution of the problem, these methods reasonably captures all the physics of the strong correlated systems with bad-metallic behavior.

In the introductory chapters we summarized some relevant aspects of iron-based SC and of the relative models, supplemented by some original calculations used either to benchmark our approach comparing with previous results and to complement the physical picture in light of our original contributions. In particular, we focused on the difference between the so-called Kanamori modeling of the Hund's coupling which has rotational invariance in the orbital space and its Ising approximation, and we discussed the role of single-particle perturbations breaking the orbital symmetry via crystal-field splitting or assuming different hopping for different orbitals.

Particularly, we focused our research on three- and five-orbital models, since these usually represent the active orbitals in FeSC, and moreover, both show the same emerging effects in the presence of Hund's coupling. For obvious reasons of numerical cost, most of our studies have

been limited to the three-orbital model, but a number of examples in previous papers and in the present thesis suggest that the results for the three-orbital model share the same basic physics of the more expensive five-orbital version.

We have organized our original results in three chapters which focus respectively on different aspects of Hund's-induced strong electronic correlations, namely (i) the physical origin and the characterization of the Hund's metal and its resilience to large repulsions; (ii) the effect of anisotropic interactions in the orbital space in modifying the multi-orbital physics and (iii) The role of the Hund's coupling in driving a phase-separation instability at the crossover between a normal metal and a Hund's metal.

In Chapter 5 we have studied the origin of the Hund's metal phase by exploring the phase diagram of the Kanamori model in a wider than usual range of parameters. In the case of two electrons in three-orbitals, our analysis has shown that the correlation-resilient metal emerges from the competition between two distinct insulating states, namely a high-spin Mott and a charge disproportionation insulator, favored by the Hubbard repulsion U and the exchange coupling, respectively, and characterized by a different ionic valence. This competition results in an asymptotic mixed-valence metallic state, at arbitrarily large interaction strength, along a line of the phase diagram where the two parent insulators are degenerate. In this state, charge fluctuations and metallic behavior arise from the presence of hopping processes that connect the two degenerate insulators. The metallic properties are maximized when the system is exactly in the middle between the two insulators, in order to exploit as much as possible the charge fluctuations between the atomic state with different local occupation.

This observation also connects the Hund's metal behavior with the charge-disproportionation observed in some chromates, which have exactly the electronic configuration for which this physics is found. We notice that the charge-disproportionation of the insulator is a key ingredient for the appearance of the Hund's metal.

Considering other densities and even a different sign for the Hund's exchange, we have established a strong link between the existence of a Hund's metal (i.e., a metal which survives when the interactions are much larger than the bare kinetic energy) and the degeneracy between competing insulators. In particular, we find that for the standard Kanamori model the case $n = 3$ there is no competition between insulators and no Hund's metal state. On the other hand in a model with negative J (which can be seen as arising from Jahn-Teller coupling with some local phononic modes) we find a correlations-resilient metal (a Jahn-Teller metal, in this case) for $n = 3$, where two different insulators exist and become degenerate exactly where the metal is stabilized, and we do not find any special metallic state for $n = 2$, where there is only one insulating solution.

These findings clearly provide a new perspective on the Hund's metal, whose very existence appears associated to a mixed-valence state where the prevalence of the Hund's coupling leads to the population of different atomic states with different occupation, all with the highest spin.

In the following Chapter 6 we relaxed some of the approximations used in defining a Kanamori Hamiltonian, considering a more generic form of the interactions which takes into account a possible asymmetry between the orbitals which can arise from chemical or structural differences. Similar deviations between interaction parameters are indeed typical in realistic estimates of the U and J terms performed using, e.g., constrained-RPA. One immediately realizes that in principle one has a huge number of interaction terms even for three orbitals. For this reason we selected, with some arbitrariness, a parametrization in terms of two parameters, which we labeled α and β. Basically the former controls the ratio between intra-orbital and inter-orbital interactions, while the latter controls the ratio between the interaction in one of the three orbitals and in the others. We have studied the interplay between these two terms,

showing that the main outcome is the competition between a regime where the three orbitals remain coupled and a single Mott transition takes place with the same population for the three orbitals and a second regime with a pronounced orbital polarization where the most correlated orbital becomes empty and the system reduces to a two-orbital system which undergoes an independent Mott transition. However, the results also depend on the number of electrons and in the specific case of four electrons we find a regime of orbital-selective Mott transition. We also notice that, in the presence of deviations from the fully simmetric modeling the role of the Hund's coupling is reduced and the difference between a Kanamori modeling and an Ising approximation becomes much smaller. Roughly speaking, we can picture the breaking of the degeneracy between the interaction terms as leading to an effective crystal-field splitting which indeed competes with J.

These results suggest that the inclusion of minor orbital-dependence in the interaction parameters can lead to important changes in the physics including the onset of novel phenomena which are absent in the symmetric parametrization. In a general sense, this observation follows from the extreme sensitivity of these systems to perturbations which affect the orbital channel. This should be seriously taken into account in theoretical approaches where strong correlation effects are added to the realistic bandstructure.

In Chapter 7 we turn back to symmetric Kanamori and Ising models to address the issue of their stability with respect to phase separation and the relevance of the Mott insulator at half-filling in determining the full phase diagram as a function of the density. We have indeed shown that a recent claim [21] of a divergence of the compressibility in a region of the density-interaction phase diagram, which originates from the Mott transition, is robust with respect to the number of orbitals and the precise form of the interaction Hamiltonian. The emergence of the diverging compressibility close to the half-filled Mott transition is a common feature that can be put into connection with the crossover where the Hund's metal is established. Regardless the slight quantitative discrepancy between results, qualitative estimation of the lower frontier departing from the half-filled Mott transition is quite precise and coincides between different methods. On another hand, the Kanamori treatment of the problem reveals that the instability zone is reduced and tends to drop further with the increase of the Hund's coupling, comparing to the Ising approach in Ref. [21]. The answer for this behavior can be find in the fact that the Kanamori Hamiltonian, besides density-density Hund's coupling terms, includes also the hopping processes collected in the spin-flip and pair-exchange interaction (see Eq. (3.10)). Besides, this study also confirms the central role of the Mott transition at global half-filling in determining the degree of correlation in the full doping phase diagram, which appears as a completely general feature regardless of the number of orbitals and the precise nature of the interaction Hamiltonian.

The generic divergence of the compressibility can be closely related to very appearance of superconductivity or, in more general terms, to the enhancement of various instabilities, including superconductivity, nematic ordering and possible charge-ordered states. This last observation can link the results we discussed above on charge disproportionation with the present tendency towards phase separation, confirming a strong connection between Hund's metal and incipient charge instabilities.

These new results contribute to close the gaps in our understanding of Hund's metals and their role in real materials, and they also open new perspectives for future studies, among which we can foresee a thorough investigation of the effect of anisotropies of the interaction on the behavior of the compressibility and the charge instabilities, as well as a microscopic calculation aiming to link the enhancement of the compressibility with weak-coupling instabilities.

A

First appendix

A.1 Derivation of the multi-orbital Hubbard Hamiltonian

In this appendix we derive the multi-orbital form of the Hubbard model and corresponding Coulomb integrals. For that reason let us consider the second quantization many-body Hamiltonian for interacting electrons in a periodic potential, namely [28]

$$\hat{H} = \sum_{\sigma} \int d\mathbf{r}\, \Psi^{\dagger}_{\sigma}(\mathbf{r}) \left[-\frac{\hbar^2}{2m_e} \vec{\nabla}^2 + V(\mathbf{r}) \right] \Psi_{\sigma}(\mathbf{r}) + \\ + \sum_{\sigma\sigma'} \int d\mathbf{r}\, d\mathbf{r'}\, \Psi^{\dagger}_{\sigma'}(\mathbf{r})\, \Psi^{\dagger}_{\sigma}(\mathbf{r'})\, U(\mathbf{r}-\mathbf{r'})\, \Psi_{\sigma'}(\mathbf{r'})\, \Psi_{\sigma}(\mathbf{r}) \tag{A.1}$$

where m_e is the mass of an electron, $V(\mathbf{r}) = -\sum_i \frac{Z_i e^2}{|\mathbf{R}_i - \mathbf{r}|}$ and refers to the periodical potential, $U(\mathbf{r}-\mathbf{r'}) = \frac{1}{2}\frac{e^2}{|\mathbf{r}-\mathbf{r'}|}$ is the Coulomb interaction and $\Psi_{\sigma}(\mathbf{r})$ is a field operator that creates a particle with spin σ at position $\mathbf{r}$. Moreover, the first term of Eq. (A.1), that we may denote as $\hat{H}_0$, represents the single-particle term (or more precisely kinetic energy plus the periodic potential provided by the ions), whereas the second one, say $\hat{H}_{int}$, collects all the information about the electron-electron interactions.

Kinetic part of Hamiltonian $\hat{H}_0$ is diagonalized by Bloch wave-functions $\psi_{\mathbf{k}m\sigma}(\mathbf{r})$, which are delocalized in the solid. On another side, for setting up our problem, it is convenient to introduce a basis set of localized wave-functions, such as Wannier states, which are defined in terms of the Bloch wave-functions $\psi_{\mathbf{k}m\sigma}(\mathbf{R})$ (where $\mathbf{k}$ is a wave-vector), and have the form:

$$w_{im\sigma}(\mathbf{r}) = w_{m\sigma}(\mathbf{r}-\mathbf{R}_i) \equiv \frac{1}{\sqrt{N_s}} \sum_{k\in BZ} e^{-i\mathbf{k}\cdot\mathbf{R}_i}\, \psi_{\mathbf{k}m\sigma}(\mathbf{r}) \tag{A.2}$$

where N_s represents the number of sites, and BZ - Brillouin zone of the reciprocal $\mathbf{k}$-space. The Wannier wave-functions represent a convenient choice since they satisfy orthogonality and

completeness relations:

$$\int d\mathbf{r}\, w^*_{im\sigma}(\mathbf{r})\, w_{jm'\sigma'}(\mathbf{r}) = \delta_{ij}\,\delta_{mm'}\delta_{\sigma\sigma'}\,, \tag{A.3a}$$

$$\sum_{im\sigma} w^*_{im\sigma}(\mathbf{r})\, w_{im\sigma}(\mathbf{r'}) = \delta(\mathbf{r}-\mathbf{r'})\,. \tag{A.3b}$$

It is clear that the form of Wannier functions present in Eq. (A.2) is particularly useful when dealing with strongly correlated materials, since one assumes the density of the electrons concentrated mostly around the position of the ion.

At this point we are able to define the field operator in this basis as:

$$\Psi^\dagger_\sigma(\mathbf{r}) = \sum_i \sum_m w_{im\sigma}(\mathbf{r})\, c^\dagger_{im\sigma}\,. \tag{A.4}$$

Here $c^\dagger_{im\sigma}$ is an operator that creates an electron with the spin σ in the n-th Wannier orbital and position $\mathbf{R}_i$.

If we now apply the transformation defined with Eq. (A.4) to the field operators in the expression (A.1), the kinetic part reads:

$$\begin{aligned}
\hat{H}_0 &= \sum_\sigma \int d\mathbf{r}\, \Psi^\dagger_\sigma(\mathbf{r}) \left(-\frac{\hbar^2}{2m_e}\vec{\nabla}^2 + V(\mathbf{r})\right)\Psi_\sigma(\mathbf{r}) = \\
&= \sum_\sigma \sum_{mm'} \sum_{ij} \int d\mathbf{r}\, w^*_{im\sigma}(\mathbf{r})\, c^\dagger_{im\sigma} \left(-\frac{\hbar^2}{2m_e}\vec{\nabla}^2 + V(\mathbf{r})\right) w_{jm'\sigma}(\mathbf{r})\, c_{jm'\sigma} = \\
&= \sum_\sigma \sum_{mm'} \sum_{ij} t^{mm'}_{ij}\, c^\dagger_{im\sigma} c_{jm'\sigma}\,,
\end{aligned} \tag{A.5}$$

where the hopping matrix elements $t^{mm'}_{ij}$ correspond to:

$$\begin{aligned}
t^{mm'}_{ij} &= \int d\mathbf{r}\, w^*_{im\sigma}(\mathbf{r}) \left(-\frac{\hbar^2}{2m_e}\vec{\nabla}^2 + V(\mathbf{r})\right) w_{jm'\sigma}(\mathbf{r}) \\
&= \int d\mathbf{r} \left(\frac{\hbar^2}{2m_e}\left(\vec{\nabla} w^*_{im\sigma}(\mathbf{r})\right)\cdot\vec{\nabla} w_{jm'\sigma}(\mathbf{r}) + V(\mathbf{r})\, w^*_{im\sigma}(\mathbf{r})\, w_{jm'\sigma}(\mathbf{r})\right).
\end{aligned} \tag{A.6}$$

Since the Wannier orbitals are localized in space, the hopping amplitude $t^{mm'}_{ij}$ decays rapidly with the distance, so we can take into a consideration just the existence of the hoppings between the nearest neighbors. This is a valid approximation when dealing with highly localized d orbitals, as in our case. Moreover, $t^{mm'}_{ij}$ can always be rewritten in a proper basis via an unitary transformation, in order to get a diagonal form. However, within this work we were assuming just the intra-orbital hoppings, hence let us impose, due to simplicity, that $m = m'$. This way the kinetic energy becomes

$$\hat{H}_0 = \sum_{ij} \sum_m \sum_\sigma t^m_{ij}\, c^\dagger_{im\sigma}\, c_{jm\sigma}\,. \tag{A.7}$$

Accordingly, one can obtain the interacting part of the Hamiltonian (A.1), substituting the field operators with the new Wannier functions (A.4), such that

$$\hat{H}_{int} = \frac{1}{2} U_{ijkl}^{mm'm''m'''} \, c_{im\sigma}^{\dagger} \, c_{jm'\sigma'}^{\dagger} \, c_{km''\sigma'} \, c_{lm'''\sigma} \,, \tag{A.8}$$

with the interaction

$$U_{ijkl}^{mm'm''m'''} = \int d\mathbf{r} \, d\mathbf{r'} \, w_{im\sigma}^{*}(\mathbf{r}) \, w_{jm'\sigma}^{*}(\mathbf{r'}) \, U(\mathbf{r} - \mathbf{r'}) \, w_{km''\sigma'}(\mathbf{r'}) \, w_{lm'''\sigma}(\mathbf{r}). \tag{A.9}$$

In the following we will omit the spin index in the orbital wave-functions, since it is important only for the spin-orbit interaction that we will not be dealing with. Moreover, dealing with purely local interactions that decay rapidly with the distance between two sites, say i and j, means that all the site indices are equal, namely $i = j = k = l$, which further permits us to drop out the site index i.

The simplest realization is the on-site interaction between electrons in the same orbital, meaning that $m = m' = m'' = m'''$. which is nothing but the contribution to the interaction in the Hubbard model. The interaction matrix element is:

$$U^{m} = \frac{1}{2} \int d\mathbf{r} \, d\mathbf{r'} \, |w_m(\mathbf{r})|^2 \; U(\mathbf{r} - \mathbf{r'}) \; |w_m(\mathbf{r'})|^2 \tag{A.10}$$

whereas the corresponding contribution to the Hamiltonian is

$$\begin{aligned}
\hat{H}_{int}^{U} &= \frac{1}{2} \sum_{i} \sum_{m} \sum_{\sigma\sigma'} U^{m} c_{im\sigma}^{\dagger} \, c_{im\sigma'}^{\dagger} \, c_{im\sigma'} \, c_{im\sigma} = \\
&= \frac{1}{2} \sum_{i} \sum_{m} \sum_{\sigma\sigma'} U^{m} \left(c_{im\sigma}^{\dagger} \, c_{im\sigma} \, c_{im\sigma'}^{\dagger} \, c_{im\sigma'} - \delta_{\sigma\sigma'} c_{im\sigma}^{\dagger} \, c_{im\sigma'} \right) = \\
&= U^{m} \sum_{i} \sum_{m} \hat{n}_{im\uparrow} \hat{n}_{im\downarrow}.
\end{aligned} \tag{A.11}$$

Analogously, one can find the second contribution arising from the on-site interaction between electrons in different bands. Namely, if we impose in Eq. (A.9) that $m = m'$ and $m'' = m'''$, with $m \neq m''$, performing a change of variable label $m'' \rightarrow m'$, the so-called inter-orbital Coulomb interaction becomes:

$$U'^{mm'} = \frac{1}{2} \int d\mathbf{r} \, d\mathbf{r'} \, |w_m(\mathbf{r})|^2 \; U(\mathbf{r} - \mathbf{r'}) \; |w_{m'}(\mathbf{r'})|^2 \,, \tag{A.12}$$

giving the Hamiltonian

$$\begin{aligned}
\hat{H}_{int}^{U'} &= \frac{1}{2} \sum_{i} \sum_{mm'} \sum_{\sigma\sigma'} U'^{mm'} c_{im\sigma}^{\dagger} \, c_{im'\sigma'}^{\dagger} \, c_{im'\sigma'} \, c_{im\sigma} = \\
&= \frac{1}{2} \sum_{i} \sum_{mm'} \sum_{\sigma\sigma'} U'^{mm'} \hat{n}_{im\sigma} \, \hat{n}_{im'\sigma'} = \\
&= \frac{1}{2} \sum_{i} \sum_{\sigma} \sum_{mm'} U'^{mm'} \left(\hat{n}_{im\sigma} \, \hat{n}_{im'\sigma} + \hat{n}_{im\sigma} \, \hat{n}_{im'\bar{\sigma}} \right) = \\
&= U' \sum_{i} \sum_{\sigma\sigma'} \hat{n}_{im\sigma} \hat{n}_{im'\sigma'} \,.
\end{aligned} \tag{A.13}$$

We can have also the channels which are not diagonal in the occupation number. One of the possibilities is too impose $m = m'' \neq m' = m'''$, such that the exchange reads as

$$J^{mm'} = \frac{1}{2}\int d\mathbf{r}\, d\mathbf{r'}\, w^*_m(\mathbf{r})\, w^*_{m'}(\mathbf{r'})\, U(\mathbf{r}-\mathbf{r'})\, w_m(\mathbf{r'})\, w_{m'}(\mathbf{r})\,. \tag{A.14}$$

Further, we can write the corresponding Hamiltonian as

$$\begin{aligned}\hat{H}^J_{int} &= \frac{1}{2}\sum_i \sum_{mm'} \sum_{\sigma\sigma'} J^{mm'} c^\dagger_{im\sigma}\, c^\dagger_{im'\sigma'}\, c_{im\sigma'}\, c_{im'\sigma} = \\ &= J\sum_i \sum_{\sigma\sigma'} c^\dagger_{im\sigma} c^\dagger_{im'\sigma'} c_{im\sigma'} c_{im'\sigma}.\end{aligned} \tag{A.15}$$

The last contribution to the interacting Hamiltonian is the pair-exchange term, which arises for $m = m' \neq m'' = m'''$, and is written as

$$J'^{mm'} = \frac{1}{2}\int d\mathbf{r}\, d\mathbf{r'}\, w^*_m(\mathbf{r})\, w^*_m(\mathbf{r'})\, U(\mathbf{r}-\mathbf{r'})\, w_{m'}(\mathbf{r'})\, w_{m'}(\mathbf{r}), \tag{A.16}$$

whereas the Hamiltonian becomes

$$\begin{aligned}\hat{H}^{J'}_{int} &= \frac{1}{2}\sum_i \sum_{mm'} \sum_{\sigma\sigma'} J'^{mm'} c^\dagger_{im\sigma}\, c^\dagger_{im\sigma'}\, c_{im'\sigma'}\, c_{im'\sigma} = \\ &= \frac{1}{2}\sum_i \sum_{mm'} J'^{mm'} \left(c^\dagger_{im\uparrow}\, c^\dagger_{im\downarrow}\, c_{im'\downarrow}\, c_{im'\uparrow} + c^\dagger_{im\downarrow}\, c^\dagger_{im\uparrow}\, c_{im'\uparrow}\, c_{im'\downarrow}\right) = \\ &= -J'\sum_i \left(c^\dagger_{im\uparrow} c_{im\downarrow} c^\dagger_{im'\downarrow} c_{im'\uparrow} + \text{h.c.}\right).\end{aligned} \tag{A.17}$$

All these therms corresponding to the interacting Hamiltonian can be summed up and present in the Kanamori form (see Eq. (3.10) and Section 3.3), which is discussed within this thesis.

B

Second appendix

B.1 Contraction terms with two fermionic lines

In the following we will show why the expectation values on the Slater determinant of those terms having $\mathcal{P}_i^\dagger \mathcal{P}_i$ with two fermionic lines vanish by means of Gutzwiller constraints (4.6).

For that purpose, let us recall Wick's theorem[1], which can be used to evaluate the average values on $|\Psi_0\rangle$. Now let us rewrite the second constraint in Eq. (4.6)[2]:

$$\begin{aligned}\langle\Psi_0|\mathcal{P}_i^\dagger\mathcal{P}_i c_{ia}^\dagger c_{ib}|\Psi_0\rangle &= \overbrace{\langle\Psi_0|\mathcal{P}_i^\dagger\mathcal{P}_i|\Psi_0\rangle}^{=1}\langle\Psi_0|c_{ia}^\dagger c_{ib}|\Psi_0\rangle + \langle\Psi_0|\mathcal{P}_i^\dagger\mathcal{P}_i\, c_{ia}^\dagger c_{ib}|\Psi_0\rangle_{connected} \\ &\overset{\text{II cond.}}{=} \langle\Psi_0|c_{ia}^\dagger c_{ib}|\Psi_0\rangle + \cancelto{0}{\langle\Psi_0|\mathcal{P}_i^\dagger\mathcal{P}_i c_{ia}^\dagger c_{ib}|\Psi_0\rangle_{connected}} .\end{aligned} \tag{B.1}$$

The subscript "connected" refers to all possible contractions between $c_{ia}^\dagger c_{ib}$ and a pair of single fermion operators from $\mathcal{P}_i^\dagger\mathcal{P}_i$.

In Eq. (B.1) we have utilized constraints (4.6). Namely, this equation suggested us that the first disconnected term is the only one sufficient to satisfy the second condition, assuming at the same time the first condition. Therefore, we can conclude that the expectation values on the Slater determinant of any pair of single particle operators from $\mathcal{P}_i^\dagger\mathcal{P}_i$ will be equal to zero.

B.2 Contraction terms with four and more fermionic lines

We want to demonstrate that all those terms coming from the Wick's decoupling in eq. (4.7), and connecting the two sites, i and j, with four or more fermonic lines vanish in the limit of infinite dimensionality (lattice coordination number). For that aim, it is convenient to consider the following tight-binding Hamiltonian

[1] For Slater determinants Wick's theorem holds. This theorem states that expectation values of many-particle operators can be obtained by calculating all possible pairings of creation and annihilation operators.

[2] This is, in the following, derived only for single a and b index; one should, instead, do it for each pair.

$$\hat{H} = -\sum_{ij}\sum_{a,b=1}^{2M}\left(t_{ij}^{ab}c_{ia}^{\dagger}c_{jb} + h.c.\right) + \sum_{i}\hat{U}_i\,, \tag{B.2}$$

where creation (annihilation) operator $c_{ia}^{\dagger}(c_{jb})$ creates (annihilates) an electron at site $i\,(j)$, with the spin and M orbital denoted as $a\,(b)$, whereas t_{ij}^{ab} represents the hopping amplitude between the two nearest neighbors sites i and j, and $\hat{U}_i$ collecting all the local many-body terms. If we consider for a second the first term of Eq. (B.2), corresponding to the kinetic energy, we can notice that it scales as $\propto N_s\frac{Z}{2}$, where N_s is the number of sites in the crystal. In case where the coordination number goes as $Z \to \infty$, we need to normalize the hopping in the correct way. Therefore, t_{ij}^{ab} is normalized with respect to the coordination number such to give a finite average of the energy.

Indeed, Metzner and Vollhardt [48] stated that in the limit of infinite dimensionality the only way to obtain a Hubbard Mott with a non-trivial kinetic energy is to rescale the hopping amplitude as

$$t \propto \frac{\tilde{t}}{\sqrt{Z}}\,, \tag{B.3}$$

or in another words

$$t\sum_{\langle ij\rangle}\langle\Psi_0|c_{ia}^{\dagger}c_{ib}|\Psi_0\rangle \propto Zt\left\langle\langle\Psi_0|c_{ia}^{\dagger}c_{ib}|\Psi_0\rangle\right\rangle_j \propto \sqrt{Z}\tilde{t}\left\langle\langle\Psi_0|c_{ia}^{\dagger}c_{ib}|\Psi_0\rangle\right\rangle_j\,, \tag{B.4}$$

where $\left\langle\langle\Psi_0|c_{ia}^{\dagger}c_{ib}|\Psi_0\rangle\right\rangle_j$ is the average value of the hopping matrix element between nearest neighbors j[3].

From Eq. (B.4) one can find that, for large Z, the kinetic energy per site i is finite only for

$$\left\langle\langle\Psi_0|c_{ia}^{\dagger}c_{ib}|\Psi_0\rangle\right\rangle_j \propto \frac{1}{\sqrt{Z}}\,. \tag{B.5}$$

Therefore, multiplying four contraction terms of the Wick decoupling in Eq. (4.10) (or in more general expression (4.9)), where four fermionic lines join two sited i and j, one obtains a product of four terms of the kind (B.5), so that such connection term vanishes as $\propto \frac{1}{Z^2}$. Summing over all nearest neighbors j one finds a contribution of order $\frac{1}{Z}$ which vanishes in the limit of infinite Z. Clearly, contracting more than four fermionic lines vanishes even faster in the infinite coordination limit.

B.3 Derivation of the expectation values in the infinite lattice coordination

In the following we derive the expectation values of local and non-local operators presented in Chapter 4.

Local operator

The most general form of the local operator, expressed with Eq. (4.7), can be obtained as it follows:

[3] Apparently, including further neighboring sites one would have to substitute a scaling term $\sqrt{Z}$ with $\sqrt{d}$, where $d = N\frac{Z}{2}$ represents dimensionality.

$$
\begin{aligned}
\langle\Psi_G|\mathcal{O}_i|\Psi_G\rangle = \langle\mathcal{O}_i\rangle_{\Psi_G} &= \left(\langle\Psi_0|\prod_i \mathcal{P}_i^\dagger\right)\mathcal{O}_i\left(\prod_j \mathcal{P}_j|\Psi_0\rangle\right) = \left(\langle\Psi_0|\prod_{s\neq i}\mathcal{P}_s^\dagger\right)\mathcal{P}_i^\dagger\mathcal{O}_i\mathcal{P}_i\left(\prod_{j\neq i}\mathcal{P}_j|\Psi_0\rangle\right) \\
&\overset{s\to j}{=} \langle\Psi_0|\left(\prod_{j\neq i}\mathcal{P}_j^\dagger\mathcal{P}_j\right)\mathcal{P}_i^\dagger\mathcal{O}_i\mathcal{P}_i|\Psi_0\rangle \\
&= \underbrace{\langle\Psi_0|\prod_{j\neq i}\mathcal{P}_j^\dagger\mathcal{P}_j|\Psi_0\rangle}_{=1}\langle\Psi_0|\mathcal{P}_i^\dagger\mathcal{O}_i\mathcal{P}_i|\Psi_0\rangle + \cancelto{0}{\langle\Psi_0|\left(\prod_{j\neq i}\mathcal{P}_j^\dagger\mathcal{P}_j\right)\mathcal{P}_i^\dagger\mathcal{O}_i\mathcal{P}_i|\Psi_0\rangle_{connected}} \\
&\overset{Z\to\infty}{=} \langle\Psi_0|\mathcal{P}_i^\dagger\mathcal{O}_i\mathcal{P}_i|\Psi_0\rangle\ .
\end{aligned}
\tag{B.6}
$$

The label "connected" refers to all terms where operators at different sites are averaged together. Assuming Eqs. (4.6) and previous discussions in Sections B.1 and B.2, this term vanishes in the limit of infinite coordination.

Derivation of Eq. (4.8) follows straightforwardly from Eq. (B.6) just by substituting a general local operator $\mathcal{O}_i$ with $\mathcal{U}_i$ that contains all the interaction contributions.

Non-local operator

Accordingly, we apply the same procedure for deriving Eq. (4.9), namely

$$
\begin{aligned}
\langle\Psi_G|\mathcal{O}_{ij}|\Psi_G\rangle = \left\langle\mathcal{O}_{ij}\right\rangle_{\Psi_G} &= \left(\langle\Psi_0|\prod_i \mathcal{P}_i^\dagger\right)\mathcal{O}_{ij}\left(\prod_j \mathcal{P}_j|\Psi_0\rangle\right) = \left(\langle\Psi_0|\prod_{\substack{s\neq i\\ s\neq j}}\mathcal{P}_s^\dagger\right)\mathcal{P}_i^\dagger\mathcal{P}_j^\dagger\mathcal{O}_{ij}\mathcal{P}_i\mathcal{P}_j\left(\prod_{\substack{r\neq i\\ r\neq j}}\mathcal{P}_r|\Psi_0\rangle\right) \\
&\overset{r\to s}{=} \underbrace{\langle\Psi_0|\prod_{\substack{s\neq i\\ s\neq j}}\mathcal{P}_s^\dagger\mathcal{P}_s|\Psi_0\rangle}_{=1}\langle\Psi_0|\mathcal{P}_i^\dagger\mathcal{P}_j^\dagger\mathcal{O}_{ij}\mathcal{P}_i\mathcal{P}_j|\Psi_0\rangle\ .
\end{aligned}
\tag{B.7}
$$

The same holds when proving the result of Eq. (4.10), or more precisely (4.13):

$$
\begin{aligned}
\langle\Psi_G|c_{i\alpha}^\dagger c_{jm'}|\Psi_G\rangle = \left\langle c_{i\alpha}^\dagger c_{jm'}\right\rangle_{\Psi_G} &= \langle\Psi_0|\prod_{\substack{s\neq i\\ s\neq j}}\mathcal{P}_s^\dagger\mathcal{P}_s\mathcal{P}_i^\dagger c_{i\alpha}^\dagger\mathcal{P}_i\mathcal{P}_j^\dagger c_{jm'}\mathcal{P}_j|\Psi_0\rangle \\
&= \overbrace{\langle\Psi_0|\prod_{\substack{s\neq i\\ s\neq j}}\mathcal{P}_s^\dagger\mathcal{P}_s|\Psi_0\rangle}^{=1}\langle\Psi_0|\mathcal{P}_i^\dagger c_{i\alpha}^\dagger\mathcal{P}_i\mathcal{P}_j^\dagger c_{jm'}\mathcal{P}_j|\Psi_0\rangle \\
&= \langle\Psi_0|\mathcal{P}_i^\dagger\mathcal{P}_j^\dagger c_{i\alpha}^\dagger c_{jm'}\mathcal{P}_i\mathcal{P}_j|\Psi_0\rangle = \langle\Psi_0|\underbrace{\mathcal{P}_i^\dagger c_{i\alpha}^\dagger\mathcal{P}_i}_{\mathrm{I}}\underbrace{\mathcal{P}_j^\dagger c_{jm'}\mathcal{P}_j}_{\mathrm{II}}|\Psi_0\rangle \\
&= \begin{cases}\mathrm{I} = \sum_{m'} R_{iam'}^* c_{im'}^\dagger \\ \mathrm{II} = \sum_\alpha R_{jb\alpha} c_{j\alpha}\end{cases} \\
&= \sum_{\alpha m'} R_{iam'}^* R_{jb\alpha}\langle\Psi_0|c_{im'}^\dagger c_{j\alpha}|\Psi_0\rangle = \sum_{\alpha m'}\left(R_{i\beta a}^\dagger\right)^* R_{jb\alpha}\langle\Psi_0|c_{i\beta}^\dagger c_{j\alpha}|\Psi_0\rangle\ .
\end{aligned}
\tag{B.8}
$$

where we have expended the expectation value $\langle\Psi_0|\mathcal{P}_i^\dagger c_{i\alpha}^\dagger \mathcal{P}_i \mathcal{P}_j^\dagger c_{j\beta} \mathcal{P}_j|\Psi_0\rangle$ in Wick's products. By means of Wick's theorem, each contraction gives zero since we have the odd number of the operators. Hence the first term is the one where we can extract one line and it is the only one that survives (the next one will be the one with three lines - negligible, and so forth).
Apparently, taking the infinite coordination limit (see Sections B.1 and B.2) and imposing constraints defined in Eqs. (4.6) we have the cancellation of Gutzwiller projector contributions up to the expectation values. Therefore, it seems natural to follow the route $Z \to \infty$ such to have a controlled approximation [104, 105, 111].

C
Third appendix

C.1 Charge fluctuations in non-interacting and fully interacting limit

In this appendix we give a quick analytical check for the expected values of the charge fluctuations. Namely, we consider a trivial half-filling case, imposing $J = 0$, investigating two different limits, non-interacting and Mott insulating one.

For this purpose, let us write the expression for the charge fluctuations in the most general way, namely

$$\tilde{C}_{\alpha\beta} = \left\langle \hat{n}_\alpha \hat{n}_\beta \right\rangle - \langle \hat{n}_\alpha \rangle \left\langle \hat{n}_\beta \right\rangle . \tag{C.1}$$

Since $\hat{n}_{\alpha(\beta)} = \hat{n}_{\alpha(\beta)\uparrow} + \hat{n}_{\alpha(\beta)\downarrow}$, substituting it into Eq. (C.1), we get

$$\left\langle \hat{n}_\alpha \hat{n}_\beta \right\rangle = \left\langle (\hat{n}_{\alpha\uparrow} + \hat{n}_{\alpha\downarrow}) \left(\hat{n}_{\beta\uparrow} + \hat{n}_{\beta\downarrow} \right) \right\rangle = \left\langle \hat{n}_{\alpha\uparrow} \hat{n}_{\beta\uparrow} \right\rangle + \left\langle \hat{n}_{\alpha\downarrow} \hat{n}_{\beta\downarrow} \right\rangle + \left\langle \hat{n}_{\alpha\uparrow} \hat{n}_{\beta\downarrow} \right\rangle + \left\langle \hat{n}_{\alpha\downarrow} \hat{n}_{\beta\uparrow} \right\rangle \tag{C.2}$$

and

$$\langle \hat{n}_\alpha \rangle \left\langle \hat{n}_\beta \right\rangle = \langle (\hat{n}_{\alpha\uparrow} + \hat{n}_{\alpha\downarrow}) \rangle \left\langle \left(\hat{n}_{\beta\uparrow} + \hat{n}_{\beta\downarrow} \right) \right\rangle = \langle \hat{n}_{\alpha\uparrow} \rangle \left\langle \hat{n}_{\beta\uparrow} \right\rangle + \langle \hat{n}_{\alpha\downarrow} \rangle \left\langle \hat{n}_{\beta\downarrow} \right\rangle + \langle \hat{n}_{\alpha\uparrow} \rangle \left\langle \hat{n}_{\beta\downarrow} \right\rangle + \langle \hat{n}_{\alpha\downarrow} \rangle \left\langle \hat{n}_{\beta\uparrow} \right\rangle . \tag{C.3}$$

It is clear that assuming $\alpha = \beta$ we get

$$\begin{aligned}
&\langle \hat{n}_{\alpha\uparrow} \hat{n}_{\alpha\uparrow} \rangle = \langle \hat{n}_{\alpha\uparrow} \rangle \\
&\langle \hat{n}_{\alpha\downarrow} \hat{n}_{\alpha\downarrow} \rangle = \langle \hat{n}_{\alpha\downarrow} \rangle \\
&\langle \hat{n}_\alpha \hat{n}_\alpha \rangle = \langle \hat{n}_{\alpha\uparrow} \rangle + \langle \hat{n}_{\alpha\downarrow} \rangle + 2 \langle \hat{n}_{\alpha\uparrow} \rangle \langle \hat{n}_{\alpha\downarrow} \rangle \\
&\langle \hat{n}_\alpha \rangle \langle \hat{n}_\alpha \rangle = \langle \hat{n}_{\alpha\uparrow} \rangle^2 + \langle \hat{n}_{\alpha\downarrow} \rangle^2 + 2 \langle \hat{n}_{\alpha\uparrow} \rangle \langle \hat{n}_{\alpha\downarrow} \rangle ,
\end{aligned} \tag{C.4}$$

such that the expression for the intra-orbital charge fluctuations, once we substitute Eq. (C.4) into Eqs. (C.1), (C.2) and (C.3), becomes

$$\tilde{C}_{\alpha\alpha} = \tilde{C}_{intra} = \langle \hat{n}_{\alpha\uparrow} \rangle (1 - \langle \hat{n}_{\alpha\uparrow} \rangle) + \langle \hat{n}_{\alpha\downarrow} \rangle (1 - \langle \hat{n}_{\alpha\downarrow} \rangle) \,. \tag{C.5}$$

On another side, if $\alpha \neq \beta$, one finds

$$\begin{aligned} \left\langle \hat{n}_{\alpha\sigma} \hat{n}_{\beta\sigma'} \right\rangle &= \langle \hat{n}_{\alpha\sigma} \rangle \left\langle \hat{n}_{\beta\sigma'} \right\rangle \\ \left\langle \hat{n}_{\alpha} \hat{n}_{\beta} \right\rangle &= \langle \hat{n}_{\alpha} \rangle \left\langle \hat{n}_{\beta} \right\rangle \end{aligned} \tag{C.6}$$

which again, returning back to Eqs. (C.1), (C.2) and (C.3), gives us the inter-orbital fluctuations

$$\tilde{C}_{\alpha\beta} = \tilde{C}_{inter} = 0 \,. \tag{C.7}$$

It is useful to redefine Eq. (C.1), namely

$$C_{\alpha\beta} = \frac{\tilde{C}_{\alpha\beta}}{\langle \hat{n}_{\alpha} \rangle \left\langle \hat{n}_{\beta} \right\rangle} = \frac{\left\langle \hat{n}_{\alpha} \hat{n}_{\beta} \right\rangle}{\langle \hat{n}_{\alpha} \rangle \left\langle \hat{n}_{\beta} \right\rangle} - 1 \,, \tag{C.8}$$

such that in the non-interacting regime, when $U = 0$, we find:

$$C_{intra} = \frac{\langle \hat{n}_{\alpha\uparrow} \rangle + \langle \hat{n}_{\alpha\downarrow} \rangle + 2 \langle \hat{n}_{\alpha\uparrow} \rangle \langle \hat{n}_{\alpha\downarrow} \rangle}{\langle \hat{n}_{\alpha\uparrow} \rangle^2 + \langle \hat{n}_{\alpha\downarrow} \rangle^2 + 2 \langle \hat{n}_{\alpha\uparrow} \rangle \langle \hat{n}_{\alpha\downarrow} \rangle} \,,$$

$$C_{inter} = 0 \,.$$

On another side, entering the insulating regime is characterized by vanishing of the average $\left\langle \hat{n}_{\alpha} \hat{n}_{\beta} \right\rangle$, whereas the values $\langle \hat{n}_{\alpha} \rangle$ and $\left\langle \hat{n}_{\beta} \right\rangle$ remain finite. For this reason, one would expect to find

$$C_{inter} \approx -1 \,.$$

for the inter-orbital charge fluctuations. Further, interpolating the non-interacting and the fully interacting limit, we get that the inter-orbital correlation function should be negative.

At $U = 0$, zero-value of C_{inter} corresponds to the non-interacting limit and describes a situation where electrons fluctuate a lot. Introducing the correlations in the system, however, this value tends to drop down. Moreover, one can observe some additional changes in the behavior of C_{inter} once we allow $J \neq 0$, as described in Chapters 3 and 5.

References

References

[1] J. G. Bednorz, K. A. Müller, Zeitschrift fur Physik B Condensed Matter **64**, 189-193 (1986).

[2] E. Dagotto, Rev. Mod. Phys. **66**, 763 (1994).

[3] P. A. Lee, N. Nagaosa, X.-G. Wen, Rev. Mod. Phys. **78**, 17 (2006).

[4] Y. Kamihara, T. Watanabe, M. Hirano, H. Hosono, J. Am. Chem. Soc. **130**, 3296 (2008).

[5] P. Dai, Rev. Mod. Phys. **87**, 855 (2015).

[6] I. I. Mazin, Superconductivity gets an iron boost. Nat. Mater. **464**, 183-186 (2010).

[7] J. Paglione, R. L. Greene, Nat. Phys. **6**, 645-658 (2010).

[8] A. Tamai, A. Y. Ganin, E. Rozbicki, J. Bacsa, W. Meevasana, P. D. C. King, M. Caffio, R. Schaub, S. Margadonna, K. Prassides, M. J. Rosseinsky, F. Baumberger, Phys. Rev. Lett. **104**, 097002 (2010).

[9] Z. P. Yin, K. Haule, G. Kotliar, Nat. Mater. **10**, 932 (2011).

[10] M. Aichhorn, S. Biermann, T. Miyake, A. Georges, M. Imada, Phys. Rev. B **82**, 064504 (2010).

[11] H. Ishida, A. Liebsch, Phys. Rev. B **81**, 054513 (2010).

[12] A. Liebsch, H. Ishida, Phys. Rev. B **82**, 155106 (2010).

[13] R. Yu, Q. Si, Phys. Rev. B **86**, 085104 (2012).

[14] L. de' Medici, G. Giovannetti, M. Capone, Phys. Rev. Lett. **112**, 177001 (2014).

[15] A. Shorikov, M. Korotin, S. Streltsov, S. Skornyakov, D. Korotin, V. Anisimov, J. Exp. Theor. Phys. **108**, 121 (2009).

[16] K. Haule, G. Kotliar, New J. Phys. **11**, 025021 (2009).

[17] L. de' Medici, Weak and strong correlations in Fe-superconductors, Springer Series in Materials Science, **211**, 409-441 (2015).

[18] P. Hansmann, R. Arita, A. Toschi, S. Sakai, G. Sangiovanni, K. Held, Phys. Rev. Lett. **104**, 197002 (2010).

[19] P. Werner, E. Gull, M. Troyer, A. J. Millis, Phys. Rev. Lett. **101**, 166405 (2008).

[20] L. Fanfarillo, E. Bascones, Phys. Rev. B **92**, 075136 (2015).

[21] L. de' Medici, Phys. Rev. Lett. **118**, 167003 (2017).

[22] P. Werner, M. Casula, T. Miyake, F. Aryasetiawan, A. J. Millis, S. Biermann, Nat. Phys. **8**, 331 (2012).

[23] T. Misawa, K. Nakamura, M. Imada, Phys. Rev. Lett. **108**, 177007 (2012).

[24] L. de' Medici, S. R. Hassan, M. Capone, X. Dai, Phys. Rev. Lett. **102**, 126401 (2009).

[25] J. Wu, P. Phillips, A. Castro Neto, Phys. Rev. Lett. **101**, 126401 (2008).

[26] M. Capone, Nature Materials **17**, 855 (2018).

[27] R. Yu, Q. Si, Phys. Rev. Lett. **110**, 146402 (2013).

[28] N. W. Ashcroft, N. D. Mermin, Solid State Physics, Saunders, (1976).

[29] L. D. Landau, Sov. Phys. JETP 3, 920-925 (1957).

[30] L. D. Landau, E. M. Lifshitz, Statistical Physics, Part 2 (Pergamon, Oxford, 1980).

[31] D. Pines, P. Nozieres, The theory of quantum liquids, Vol.1 Normal Fermi liquids, Bejamin, New York (1966).

[32] A. A. Abrikosov, I. M. Khalatnikov, Rep. Progr. Phys. **22**, 329 (1959).

[33] J. H. de Boer, E. J. W. Verwey, Proc. Phys. Soc. **49**, 59 (1937).

[34] N. F. Mott, R. Peierls, Proc. Phys. Soc. London, Sect A **49**, 72 (1937).

[35] N. F. Mott, Proc. Phys. Soc. Sect. A **62**(7), 416 (1949).

[36] J. Hubbard, Proceedings of the Royal Society of London. Series A. Mathematical and Physical Sciences **276**, 238 (1963).

[37] M. Imada, A. Fujimori, Y. Tokura, Rev. Mod. Phys. **70**, 1039 (1998).

[38] N. F. Mott, Rev. Mod. Phys. **40**, 677 (1968).

[39] N. F. Mott, Metal–Insulator Transitions, 2nd edition, Taylor and Francis, London (1990).

[40] F. Gebhard, The Mott Metal-Insulator Transition, Springer, Berlin (1997).

[41] J. Hubbard, Proc. R. Soc. Lond. A **281**, 401 (1964).

[42] W. F. Brinkman, T. M. Rice, Phys. Rev. B **2**, 4302 (1970).

[43] D. Vollhardt, Rev. Mod. Phys. **56**, 99 (1984).

[44] A. Georges, G. Kotliar, W. Krauth, M. J. Rozenberg, Rev. Mod. Phys. **68**, 13 (1996).

[45] A. Georges, Strongly correlated electron materials: Dynamical mean-field theory and electronic structure. AIP Conf. Proc. 715(1), 3–74 (2004).

[46] D. Vollhardt, K. Byczuk, M. Kollar, Dynamical mean-field theory, Springer, Berlin, 203-236 (2012).

[47] G. Kotliar et al., Rev. Mod. Phys. **78**, 865 (2006).

[48] W. Metzner, D. Vollhardt, Phys, Rev. Lett. **62**, 324 (1989).

[49] E. Müller-Hartmann, Zeitschrift für Physik B Condensed Matter **74**, 507–512 (1989).

[50] E. Müller-Hartmann, Z. Phys. B **76**, 211 (1989).

[51] A. Georges, G. Kotliar, Hubbard model in infinite dimensions. Phys. Rev. B **45**, 6479–6483 (1992).

[52] A. Georges, W. Krauth, Phys. Rev. Lett. **69**, 1240–1243 (1992).

[53] T. Pruschke, M. Jarrell, J. K. Freericks, Advances in Physics **44**, 187–210 (1995).

[54] R. Bulla, Phys. Rev. Lett. **83**, 136 (1999).

[55] G. Kotliar, D. Vollhardt, Phys. Today **3**, 53 (2004).

[56] D. Vollhardt et al., J. Phys. Soc. Jpn. **74**, 136 (2005).

[57] A. I. Lichtenstein, M. I. Katsnelson, G. Kotliar Phys. Rev. Lett. **87**, 067205 (2001).

[58] S.-K. Mo, J. D. Denlinger, H.-D. Kim, J.-H. Park, J. W. Allen, A. Sekiyama, A. Yamasaki, K. Kadono, S. Suga, Y. Saitoh, T. Muro, P. Metcalf, G. Keller, K. Held, V. Eyert, V. I. Anisimov, D. Vollhardt, Phys. Rev. Lett. **90**, 186403 (2003).

[59] M. Jarrell, Phys. Rev. Lett. **69**, 168 (1992).

[60] M. J. Rozenberg, X. Y. Zhang, G. Kotliar, Phys. Rev. Lett. **69**, 1236 (1992).

[61] T. Maier, M. Jarrell, T. Pruschke, M. H. Hettler, Rev. Mod. Phys. **77**, 1027 (2005).

[62] E. Gull, A. J. Millis, A. I. Lichtenstein, A. N. Rubtsov, M. Troyer, P. Werner, Rev. Mod. Phys. **83**, 349 (2011).

[63] T. Pruschke, R. Bulla, Eur. Phys. J. B **44**, 217 (2005).

[64] R. Bulla, T. A. Costi, T. Pruschke, Rev. Mod. Phys. **80**, 395 (2008).

[65] W. Hofstetter, Phys. Rev. Lett. **85**, 1508 (2000).

[66] M. Caffarel, W. Krauth, Phys. Rev. Lett. **72**, 1545 (1994).

[67] J. P. Lu, Phys. Rev. B **49**, 5687 (1994).

[68] S. Florens, A. Georges, G. Kotliar, O. Parcollet, Phys. Rev. B **66** 205102 (2002).

[69] M. J. Rozenberg, Phys. Rev. B **55** (R)4855 (1997).

[70] P. Werner, E. Gull, A. Millis, Phys. Rev. B **79** 115119 (2009).

[71] L. de' Medici, M. Capone, Modeling Many-Body Physics with Slave-Spin Mean-Field: Mott and Hund's Physics in Fe-Superconductors, Springer International Publishing, Cham., 115–185 (2017).

[72] L. de' Medici, A. Georges, S. Biermann. Phys. Rev. B **72**, 205124 (2005).

[73] A. Koga, Y. Imai, N. Kawakami, Phys. Rev. B **66**, 165107 (2002).

[74] J. I. Facio, V. Vildosola, D. J. Garcia, P. S. Cornaglia, Phys. Rev. B **95**, 085119 (2017).

[75] F. Hund, Z. Phys. **33**, 345–371 (1925).

[76] L. de' Medici, J. Mravlje, A. Georges, Phys. Rev. Lett. **107** 256401 (2011).

[77] L. de' Medici, Phys. Rev. B **83**, 205112 (2011).

[78] A. Georges, L. de' Medici, J. Mravlje, Annual Rev. of Cond. Mat. Phys. **4**, 137 (2013).

[79] J. Kanamori, Prog. Theor. Phys. **30**, 275 (1963).

[80] F. Aryasetiawan, M. Imada, A. Georges, G. Kotliar, S. Biermann, A. I. Lichtenstein, Phys. Rev. B **70**, 195104 (2004).

[81] Y. Ono, M. Potthoff, R. Bulla, Phys. Rev. B **67**, 035119 (2003).

[82] K. Inaba, A. Koga, Phys. Rev. B **73**, 155106 (2006).

[83] F. Lechermann, A. Georges, G. Kotliar, O. Parcollet, Phys. Rev. B **76**, 155102 (2007).

[84] N. Lanatá, H. U. R. Strand, G. Giovannetti, B. Hellsing, L. de' Medici, M. Capone, Phys. Rev. B **87**, 045122 (2013).

[85] C. Piefke, F. Lechermann, Phys. Rev. B **97**, 125154 (2018).

[86] V. I. Anisimov, I. A. Nekrasov, D. E. Kondakov, T. M. Rice, M. Sigrist, Eur. Phys. J. B **25**, 191 (2002).

[87] A. Rüegg, M. Indergand, S. Pilgram et al. Eur. Phys. J. B **48**, 55-64 (2005).

[88] A. Liebsch, Phys. Rev. Lett. **91**, 226401 (2003).

[89] A. Liebsch, Phys. Rev. B **70**, 165103 (2004).

[90] A. Liebsch, Phys. Rev. Lett. **95**, 116402 (2005).

[91] A. Koga, N. Kawakami, T. M. Rice, M. Sigrist, Phys. Rev. Lett. **92**, 216402-1 (2004).

[92] A. Koga, N. Kawakami, T. M. Rice, M. Sigrist, Physica B **359**, 1366 (2005).

[93] A. Koga, N. Kawakami, T. M. Rice, M. Sigrist, Phys. Rev. B **72**, 045128 (2005).

[94] K. Inaba, A. Koga, S. I. Suga, N. Kawakami Phys. Rev. B **72**, 085112 (2005).

[95] M. Ferrero, F. Becca, M. Fabrizio, M. Capone, Phys. Rev. B **72**, 205126 (2005).

[96] P. Werner, A. Millis, Phys. Rev. Lett. **99**, 126405 (2007).

[97] A. I. Poteryaev, M. Ferrero, A. Georges, O. Parcollet, Phys. Rev. B **78**, 045115 (2008).

[98] L. Huang, L. Du, X. Dai, Phys. Rev. B **86**, 035150 (2012).

[99] M. C. Gutzwiller, Phys. Rev. Lett. **10**, 159 (1963).

[100] M. C. Gutzwiller, Phys. Rev. **134**, A923 (1964).

[101] M. C. Gutzwiller, Phys. Rev. **137**, A1726 (1965).

[102] W. Metzner, D. Vollhardt, Phys, Rev. Lett. **59**, 121 (1987).

[103] W. Metzner, D. Vollhardt, Phys, Rev. B **37**, 7382 (1988).

[104] J. Bünemann, F. Gebhard, W. Weber, J. Phys.: Condens. Matter **9**, 7343 (1997).

[105] J. Bünemann, W. Weber, F. Gebhard, Phys. Rev. B **57**, 6896 (1998).

[106] M. Fabrizio, Phys. Rev. B **76**, 165110 (2007).

[107] N. Lanatá, P. Barone, M. Fabrizio, Phys. Rev. B **78**, 155127 (2008).

[108] N. Lanatá, P. Barone, M. Fabrizio, Phys. Rev. B **80**, 224524 (2009).

[109] G. C. Wick, Phys. Rev. **80**, 268 (1950).

[110] J. J. Sakurai, Modern Quantum Mechanics, Addison-Wesley Publishing Company, (1994).

[111] C. Attaccalite, M. Fabrizio, Phys. Rev. B **68**, 155117 (2003).

[112] M. Capello, F. Becca, M. Fabrizio, S. Sorella, E. Tosatti, Phys. Rev. Lett. **94**, 026406 (2005).

[113] S. Sorella, Phys. Rev. B **71**, 241103(R) (2005).

[114] A. I. Liechtenstein, M. I. Katsnelson, Phys. Rev. B **62**, R9283 (2000).

[115] A. Isidori, M. Berovic, L. Fanfarillo, L. de' Medici, M. Fabrizio, M. Capone, arXiv:1810.01899

[116] H. U. R. Strand, Phys. Rev. B **90**, 155108 (2014).

[117] M. Capone, M. Fabrizio, P. Giannozzi, E. Tosatti, Phys. Rev. B **62**, 7619 (2000).

[118] M. Capone, M. Fabrizio, C. Castellani, E. Tosatti, Science **296**, 2364 (2002).

[119] M. Capone, M. Fabrizio, C. Castellani, E. Tosatti, Rev. Mod. Phys. **81**, 943 (2009).

[120] Y. Nomura, S. Sakai, M. Capone, R. Arita, Science Advances 1, e1500568 (2015).

[121] Y. Nomura, S. Sakai, M. Capone, R. Arita, J. Phys.: Condens. Matter (Topical Reviews) **28**, 153001 (2016).

[122] S. Hoshino, P. Werner, Phys. Rev. Lett. **118**, 177002 (2017).

[123] A. Isidori, M. Capone, Phys. Rev. B **80**, 115120 (2009).

[124] M. Keller, W. Metzner, U. Schollwöck, Phys. Rev. Lett. **86**, 4612 (2001).

[125] M. Capone, C. Castellani, M. Grilli, Phys. Rev. Lett. **88**, 126403 (2002).

[126] V. J. Emery, S. A. Kivelson, H. Q. Lin, Phys. Rev. Lett. **64**, 475 (1990); F. Becca, M. Capone, S. Sorella, S Phys. Rev. B **62**, 12700 (2000); S. Sorella Phys. Rev. B **91**, 241116(R) (2015).

[127] M. Capone, G. Sangiovanni, C. Castellani, C. Di Castro, M. Grilli, Phys. Rev. Lett. **92**, 106401 (2004).

[128] S. Caprara, C. Di Castro, G. Seibold, M. Grilli Phys. Rev. B **95**, 224511 (2017).

[129] O. Gunnarsson, E. Koch, R. M. Martin, Phys. Rev. B **56**, 1146 (1997).